Epithelial RIG-I inflammasome activation suppresses antiviral immunity and promotes inflammatory responses in virus-induced asthma exacerbations and COVID-19

Radzikowska, U [1,2,3], Eljaszewicz A [1,2,3], Tan G [1,4], Stocker N [1], Heider A [1], Westermann P [1], Steiner S [5,6,7], Dreher A [1,2], Wawrzyniak P [1,2,8], Rückert B [1], Rodriguez-Coira J [1,9], Zhakparov D [1], Huang M [1], Jakiela B [10], Sanak M [10,] Moniuszko M [3,11], O`Mahony L [1,12], Kebadze T [13], Jackson DJ [14]; Edwards MR [15]; Thiel V [5]; Johnston SL [16]; Akdis CA [1,2,&]; Sokolowska M [1,2,&,*]

&Senior Co-Authorship

* Corresponding Author

[1] Swiss Institute of Allergy and Asthma Research (SIAF), University of Zurich, Davos, Switzerland

[2] Christine Kühne – Center for Allergy Research and Education (CK-CARE), Davos, Switzerland

[3] Department of Regenerative Medicine and Immune Regulation, Medical University of Bialystok, Bialystok, Poland

[4] Functional Genomics Center Zurich, ETH Zurich/University of Zurich, Zurich, Switzerland

[5] Institute of Virology and Immunology (IVI), Bern, Switzerland

[6] Department of Infectious Diseases and Pathobiology, Vetsuisse Faculty, University of Bern, Bern, Switzerland

[7] Graduate School for Cellular and Biomedical Sciences, University of Bern, Bern, Switzerland

[8] Division of Clinical Chemistry and Biochemistry, University Children`s Hospital Zurich and Children`s Research Center, University Children`s Hospital Zurich, Zurich, Switzerland

[9] IMMA, Department of Basic Medical Sciences, Facultad de Medicina, Universidad San Pablo-CEU, CEU Universities Madrid, Spain; Centre for Metabolomics and Bioanalysis (CEMBIO), Department of Chemistry and Biochemistry, Facultad de Farmacia, Universidad San Pablo-CEU, CEU Universities Madrid, Spain

[10] Department of Internal Medicine, Jagiellonian University Medical College, Cracow, Poland

[11] Department of Allergology and Internal Medicine, Medical University of Bialystok, Bialystok, Poland

[12] Department of Medicine and School of Microbiology, APC Microbiome Ireland, University College Cork, Ireland

[13] National Heart and Lung Institute Imperial College London, United Kingdom; Asthma UK Centre in Allergic Mechanisms of Asthma, London, United Kingdom

[14] Guy's Severe Asthma Centre, School of Immunology & Microbial Sciences, King's College London, London, United Kingdom

[15] Guy's & St Thomas' NHS Trust SE1 9RT; GSTT & South Thames Asthma Network Guy's Severe Asthma Centre, Guy's Hospital; Faculty of Life Sciences & Medicine King's College London, London, United Kingdom

[16] National Heart and Lung Institute Imperial College, London, United Kingdom; Asthma UK Centre in Allergic Mechanisms of Asthma, London, United Kingdom; Imperial College Healthcare NHS Trust, London, United Kingdom

Correspondence:

Milena Sokolowska, MD, PhD

Head of Immune Metabolism

Swiss Institute of Allergy and Asthma Research (SIAF)

Herman-Burchard-Strasse 9

CH-7265 Davos Wolfgang

E-mail: milena.sokolowska@siaf.uzh.ch

Tel: +41 (0) 81 410 08 54

Abstract

Rhinoviruses (RV) and inhaled allergens, such as house dust mite (HDM) are the major agents responsible for asthma onset, its life-threatening exacerbations and progression to severe disease. The role of severe acute respiratory syndrome coronavirus (SARS-CoV-2) in exacerbations of asthma or the influence of preexisting viral or allergic airway inflammation on the development of coronavirus disease 2019 (COVID-19) is largely unknown. To address this, we compared molecular mechanisms of HDM, RV and SARS-CoV-2 interactions in experimental RV infection in patients with asthma and healthy individuals. RV infection was sensed via retinoic acid-inducible gene I (RIG-I) helicase, but not via NLR family pyrin domain containing 3 (NLRP3), which led to subsequent apoptosis-associated speck like protein containing a caspase recruitment domain (ASC) recruitment, oligomerization and RIG-I inflammasome activation. This phenomenon was augmented in bronchial epithelium in patients with asthma, especially upon pre-exposure to HDM, which itself induced a priming step, pro-IL-1β release and early inhibition of RIG-I/TANK binding kinase 1/IκB kinase ε /type I/III interferons (RIG-I/TBK1/IKKε/IFN-I/III) responses. Excessive activation of RIG-I inflammasomes was partially responsible for the alteration and persistence of type I/III IFN responses, prolonged viral clearance and unresolved inflammation in asthma. RV/HDM-induced sustained IFN I/III responses initially restricted SARS-CoV-2 replication in epithelium of patients with asthma, but even this limited infection with SARS-CoV-2 augmented RIG-I inflammasome activation. Timely inhibition of the epithelial RIG-I inflammasome and reduction of IL-1β signaling may lead to more efficient viral clearance and lower the burden of RV and SARS-CoV-2 infection.

Abbreviations

ACE2, angiotensin-converting enzyme 2; *AIM2*, absent in melanoma 2; *ARTN*, artemin; *ASC*, apoptosis-associated speck-like protein containing CARD; *BAL*, bronchoalveolar lavage; *CARD*, caspase-recruitment domain; *CCL*, C-C motif chemokine; *CDC*, carboxy-terminal domain; *CLRs*, C-type lectin receptors; *COVID-19*, coronavirus disease 2019; *CXCL*, C-X-C motif chemokine; *dsRNA*, double-stranded RNA; *EN-RAGE*, extracellular newly identified RAGE-binding protein; *FCεRI*, Fc epsilon receptor; *HBECs*, human bronchial epithelial cells; *IAV*, influenza A virus; *ICAM-1*, intracellular adhesin molecule-1; *IFN*, interferon; *IgE*, immunoglobulin E; *IKKε*, inhibitor-κB kinase epsilon; *IL*, interleukin; *IL-1R*, IL-1 receptor; *ISG*, interferon-stimulated genes; *MAPK*, mitogen-activated protein kinase; *MAVS*, mitochondrial antiviral-signaling protein; *MCP*, monocyte chemoattractant protein; *MDA5*, melanoma differentiation-associated protein 5; *MOI*, multiplicity of infection; *MX1*, MX dynamin like GTPase 1; *MyD88*, MyD88 innate immune signal transduction adaptor; *NL*, nasal lavage; *NFκB*, nuclear factor kappa-light-chain-enhancer of activated B cells; *NGS*, next generation sequencing; *NLRC5*, NOD-like receptor family CARD domain containing 5; *NLRP3*, NLR family pyrin domain containing 3; *Nsp*, non-structural proteins; *OAS1*, 2'-5'-Oligoadenylate Synthetase 1; *ORF*, open read frames; *PARs*, protease activating receptors; *RV*, rhinovirus; *RV-A16*, rhinovirus A16; *PRR,* patter recognition receptor; *RIG-I*, retinoic acid-inducible gene I; *ROS,* reactive oxygen species; *SARS-CoV-1,* severe acute respiratory syndrome virus 1; *SARS-CoV-2,* severe acute respiratory syndrome virus 2; *SLAMF1*, signaling lymphocytic activation molecule precursor; *ssRNA*, single-stranded RNA; *TBK1*, TANK binding kinase 1; *TLR*, toll-like receptor; *TNF*, tumor necrosis factor; *TNFRSF9*, TNF receptor superfamily member 9; *TRAF*, TNF receptor associated factors; *TRANCE*, TNF-related activation-induced cytokine; *UV-RV-A16*, UV-light-inactivated rhinovirus A16; *VSV*, vescicular stomatitis virus.

1. Introduction

Asthma is one of the most common chronic inflammatory lung diseases affecting more than 5% of the global population[1]. Its pathogenesis and clinical presentation is complex[2], with a common feature of susceptibility to exacerbations leading to loss of disease control, hospitalizations, and in some cases, progressive loss of lung function[3,4]. Exacerbations of asthma are most often caused by common respiratory viruses[5,6], with rhinoviruses (RV) responsible for up to 80% of asthma attacks[5]. RVs that have been initially considered as benign viruses, now are also linked to the early-life development of asthma, severe bronchiolitis in infants and fatal pneumonia in elderly and immunocompromised patients[7-10]. Likewise, human coronaviruses have not been strongly linked with asthma pathology[11]. However, the current pandemic of severe acute respiratory syndrome coronavirus (SARS-CoV-2) has been challenging this view, resulting in contradictory observations of asthma being considered a risk factor for SARS-CoV-2 infection and coronavirus disease 2019 (COVID-19) severity[12-14] or constituting a protection from the disease[15,16]. Another important factor for asthma development and exacerbations is exposure to inhaled allergens. House dust mite (HDM) is the most significant source of perennial allergens worldwide. HDM sensitization is found in around 50%-85% of patients with asthma, and HDM exposure correlates with asthma severity[17,18]. There are strong epidemiological links between RV infections, allergen exposure and sensitization on the risk of asthma development and the rates of exacerbations[9,19]. Children with early life RV-induced wheezing and aeroallergen sensitization have an extremely high incidence of asthma in later years[9]. Combination of virus detection in the airways with the high allergen exposure markedly increases the risk of hospital admission[20]. In line with this, HDM immunotherapy significantly reduces risk of asthma exacerbations[21]. It has been also recently suggested that allergen exposure might influence SARS-CoV-2 infection patterns in the general population[22,23]. However, the underlying mechanisms of these noxious, reciprocal allergen-virus effects in asthma are incompletely understood[24].

The host response to the RV infection encompasses its RNA recognition by the endosomal toll-like receptor 3 (TLR) 3, TLR7/8 and cytoplasmic RNA helicases: retinoic acid-inducible gene I (RIG-I) and melanoma-differentiation-associated gene 5 (MDA5)[25-27], whereas its capsid might interact with the cell surface TLR2 and initiate myeloid differentiation primary response 88 (MyD88)-dependent nuclear factor `kappa-light-chain-enhancer' of activated B cells (NF-kB) activation[26,28]. RIG-I in its monomeric form binds to the 5' end of viral RNA and undergoes conformational changes, oligomerizing and exposing the caspase activation and recruitment domains (CARD), enabling further CARD-CARD interactions with mitochondrial antiviral signaling protein (MAVS)[29]. MAVS recruits tumor necrosis factor receptor-associated factor 3 (TRAF3) to activate TRAF family member-associated nuclear factor kappa B activator (TANK)-binding kinase (TBK)-1 and IκB kinase ε (IKKε) complex. TBK1 complex mediates phosphorylation of interferon (IFN) response factors and subsequent induction of type I and type III (I/III) IFNs[30-32]. Interferons further signal via their respective receptors which leads to the broad expression of interferon-stimulated genes (ISGs)[30-33]. Epithelial antiviral response should be

sufficient to clear RV infection in healthy airways[34]. We and others demonstrated several alternations in RV-induced type I/III IFN responses and other antiviral mechanisms in asthma[35-39]. Despite increased understanding of IFN signaling, no preventive methods or treatments targeting these pathways are available for virus-induced asthma exacerbations, suggesting greater complexity than previously anticipated[40-42].

RV infection also leads to the release of proinflammatory cytokines, chemokines and growth factors via activation of MyD88/NF-kB pathway[26,27,43]. This response is likely beneficial in the early infection phase and necessary for effective viral clearance. However, when it is sustained and excessive, it might lead to tissue damage and unresolved inflammation[44]. HDM also induces expression of proinflammatory mediators in the airway epithelium[24] via activation of MyD88/NF-kB and other transcriptional pathways, leading to an increase in expression of proinflammatory proteins[45-47]. Expression and release of mature IL-1β needs to be tightly regulated, by the transcriptional activation of pro-IL-1β, called priming, followed by an activation of supramolecular complexes called inflammasomes and release of mature, active forms of IL-1β and/or proinflammatory cell death called pyroptosis[48]. Inflammasomes are composed of at least a sensor protein and caspase-1 and often the adaptor protein apoptosis-associated speck-like protein containing a CARD (ASC)[49]. ASC is recruited by receptors not containing CARD domains, like NLR family pyrin domain containing 3 (NLRP3), to start oligomerization and further recruitment and activation of pro-caspase 1, via CARD-CARD interactions[49]. In the case of RIG-I (containing two CARD domains), ASC is recruited to couple and enhance caspase-1 recruitment and mature IL-1β[50] production, whereas MAVS interaction with CARD9 is responsible for NF-kB activation and transcriptional priming of pro-IL-1β[50]. Activation of NLRP3 as well as RIG-I inflammasome has been demonstrated in the context of some respiratory RNA viruses, including RV[51-53], influenza A (IAV)[52,54,55], SARS-CoV-1[56,57] and most recently SARS-CoV-2[58,59] with major differences depending on the hematopoetic[50,51] or epithelial cellular origin[52] and their differentiation state[53]. It remains unclear whether activation of airway epithelial inflammasomes is necessary to clear infection or in contrast, whether it initiates mucosal hyperinflammation delaying virus clearance[60,61]. Additionally, an involvement of NLRP3 priming and/or inflammasome activation in HDM-models of asthma and in severe asthma in humans has been demonstrated, however data are conflicting and remain poorly understood[46,62-64]. Finally, little is known about the airway epithelial response in health or during the preexisting HDM-induced inflammation in asthma and combined infection with RV and SARS-CoV-2.

Therefore, in the current study, we investigated the effects of HDM, RV and SARS-CoV-2 on differentiated primary human bronchial epithelium in vitro and in experimental in vivo RV infection in healthy subjects and in patients with asthma. We identified that RV infection and replication activated the RIG-I/ASC, but not the NLRP3, inflammasome, which was further augmented in the presence of HDM. Activation of the RIG-I inflammasome was stronger in patients with asthma and was partially responsible for disturbed RIG-I-

dependent IFN signaling, enhanced and sustained inflammation and infection in those patients, especially upon HDM pre-exposure. Finally, we observed that preexisting RV infection and induction of IFNs in the epithelium of patients with asthma decreased SARS-CoV-2 infection, but the presence of both viruses and HDM further increased RIG-I inflammasome activation and release of proinflammatory mediators.

2. Results

2.1 House dust mite increased rhinovirus-induced inflammasome activation in fully differentiated human bronchial epithelium

First, we aimed to investigate mechanisms of the release of mature IL-1β in differentiated primary human bronchial epithelial cells (HBECs) upon rhinovirus A16 (RV-A16) infection with and without exposure to HDM in a dose and time-dependent manner (Fig. 1A-C, S1A-D). RV-A16 infection at a multiplicity of infection (MOI) 0.1, but not UV-inactivated RV-A16 (UV-RV-A16) or HDM alone, significantly induced secretion of mature IL-1β in patients with asthma 24h after infection (Fig. 1B-C, S1C-D). This increase was accompanied by a higher virus replication at this time point (Fig. S1E). Interestingly, RV-A16-induced IL-1β secretion was even further increased by HDM in patients with asthma or significantly induced in controls (Fig. 1B-C, S1B). Still, this effect was significantly more pronounced in patients with asthma (Fig. 1B-C). Next, we demonstrated that mature IL-1β came from inflammasome activation and formation of ASC specks in HBECs from control individuals and patients with asthma infected with RV-A16 (Fig. 1D, S1F). Complementary to IL-1β secretion, HDM prestimulation increased RV-A16-induced ASC specks formation in HBECs from controls and patients with asthma (Fig. S1G). We did not observe ASC-speck formation after HDM or UV-RV-A16 alone. Once we demonstrated that RV-A16-induced inflammasome activation is enhanced in patients with asthma, we also looked at the baseline status of IL-1β expression and the efficiency of the priming step in both groups. We observed higher expression of pro-IL-1β protein in HBECs from patients with asthma at baseline in vitro (Fig. 1C, S1H), as well as a moderate upregulation of IL-1β concentrations in bronchoalveolar lavage (BAL) fluid in vivo (Fig. S1I). RV-A16, UV-RV-A16 and HDM+RV-A16 stimulation further increased expression of pro-IL-1β mRNA and protein, especially in epithelium in asthma (Fig. 1C, E, F, S1H), suggesting combined effects of HDM and RV-A16-replication independent and dependent mechanisms on pro-IL-1β expression. HDM stimulation, RV-A16 infection alone, or combined with HDM stimulation did not affect protein expression of ASC or pro-caspase-1 (Fig. 1C and S1 J, K). HDM alone increased pro-IL-1β protein expression and release of non-cleaved, pro-IL-1β in control individuals and patients with asthma (Fig. 1C, F). Next, we observed significant inhibition of HDM+RV-A16-induced inflammasome activation upon caspase-1 inhibitor (YVAD) treatment (Fig. 1G), while it did not affect either inflammasome priming (Fig. 1H), nor RV-A16 infection (Fig. S1L). Finally, to investigate

whether active RV-A16 infection is necessary for inflammasome activation in HBECs, we blocked RV-A16 entry to the cells using monoclonal antibodies, blocking its receptor ICAM-1. Indeed, significantly diminished RV-A16 infection (Fig. S1M) led to decreased mature IL-1β secretion (Fig. 1I), with no effect on the priming step (Fig. 1J). In summary, we demonstrated here that RV-A16 infection led to the formation and activation of inflammasome in the differentiated primary HBECs, which was enhanced by the exposure to HDM, especially in patients with asthma, who already had higher pro-IL-1β expression at baseline.

2.2 Rhinovirus infection activated the RIG-I ASC inflammasome, but not NLRP3 or MDA5 inflammasomes in human airway epithelium

Next, we investigated which of the pattern recognition receptors (PRR) expressed in human epithelium is a sensor and activator of inflammasome assembly. We found extremely low expression of *NLRP3* mRNA in fully differentiated, mature bronchial epithelial cells from patients with asthma and control individuals at baseline (Fig. S2A) or after RV-A16 infection (Fig. S2B). In line with that, we did not detect the expression of NLRP3 protein in differentiated HBECs from controls and patients with asthma at baseline, after RV-A16 infection, HDM stimulation or both (Fig. 2A, B). Lastly, using a specific NLRP3 inflammasome inhibitor (MCC950), we demonstrated, that it did not affect the secretion of mature IL-1β in epithelium from patients with asthma or control individuals upon RV-A16 infection with or without HDM (Fig. 2C). Therefore, since we found that NLRP3 priming or inflammasome activation is not involved in the epithelial response to infection with RV-A16 or HDM stimulation, we analyzed another PRR – RIG-I (*DDX58*), which was shown previously to form inflammasome in response to RNA viruses either in hematopoietic cells[50,51] or in epithelium[52]. In contrast to *NLRP3*, *DDX58* (RIG-I) mRNA was expressed in HBECs from both controls and patients with asthma at baseline (Fig. S2C). We observed further increases in *DDX58* (RIG-I) mRNA (Fig. 2D, S2D) and RIG-I protein (Fig. 2E, F) expression in HBECs from control individuals and patients with asthma upon RV-A16 infection in the presence or absence of HDM stimulation. Interestingly, RV-A16-induced upregulation of *DDX58* (RIG-I) was more enhanced in asthma as compared to control (Fig. 2D). We observed formation of RIG-I speck-like structures upon RV-A16 infection in the confocal microscopy, which further increased in the presence of HDM (Fig. 2G), suggesting RIG-I inflammasome formation. Indeed, coprecipitation of ASC with RIG-I, confirmed RIG-I binding to ASC upon RV-A16 infection and HDM pre-stimulation (Fig. 2H). Notably, MDA5 was not bound to ASC upon RV-A16 infection (Fig. S2E). Since ASC specs and assembled inflammasome complexes are often released from the cells together with mature IL-1β[65], we analyzed RIG-I protein expression also in the supernatants of the cells. Accordingly, we found that activation of RIG-I inflammasome led to increased release of RIG-I protein from the epithelial cells (Fig. 2I). Thus, we showed here that infection of human bronchial epithelium with RV-A16 led to RIG-I inflammasome activation, which was strongly enhanced in the epithelium of patients with asthma,

especially in the presence of HDM exposure. NLRP3 and MDA5 inflammasomes were not involved in the responses to RV-A16 infection or HDM exposure in differentiated human primary bronchial epithelial cells.

2.3 RIG-I inflammasome- and IL-1β-mediated immune responses are augmented in asthma at an early time point after rhinovirus infection

To evaluate whether the enhanced epithelial RIG-I inflammasome activation in response to RV infection might have further implications on the overall inflammatory responses at the bronchus barrier sites in asthma, we investigated inflammasome- and IL-1β-mediated immune responses. Using targeted proteomics, we found that in addition to IL-1β, also IL-18, IL-1α, tumor necrosis factor (TNF) and TNF-related activation-induced cytokine (TRANCE) were released 24h after RV-A16 infection in HBECs from both control individuals and patients with asthma (Fig. 3A). Monocyte chemoattractant protein (MCP)-1 was significantly upregulated only in asthma, while MCP-3 was significantly upregulated only in controls, but overall, we observed rather similar changes in the expression of the analyzed proinflammatory proteins in HBECs from both patients with asthma and control individuals 24h after infection. Therefore, to evaluate if the enhanced IL-1β release and stronger RV-A16 infection in patients with asthma might influence an even broader range of responses, we analyzed publicly available next-generation sequencing (NGS) raw data of RV-A16-infected HBECs[66]. An unbiased analysis of pathways and ontologies, revealed upregulated interferon signaling and innate immune responses to RNA viral infections (Fig. 3B, Suppl. Table S1). We also noted a significant enrichment of inflammasome-mediated immune responses, in both – control and asthma samples, but it ranked slightly higher in patients with asthma (Fig. 3B). Accordingly, epithelium from both patients with asthma and control individuals showed increased inflammasome-mediated immune responses after RV-A16 infection (Fig. 3C, D), but the inflammasome-related molecules, cytokines and chemokines, such as *CASP1* (caspase-1), *IL6*, NLR family CARD domain containing 5 (*NLRC5)*, *CXCL1* and others were significantly more upregulated in asthma (Fig. 3E). In agreement with the NGS results, we also observed that infection with RV-A16 increased expression of *NLRC5* and *CASP1* (caspase-1), which was significantly more enhanced in patients with asthma than control individuals (Fig. 3F). In summary, we demonstrated here that early after RV-A16 infection, other inflammasome- and IL-1β-mediated immune responses are boosted in both groups, controls and patients with asthma, but in case of several inflammasome-related molecules, cytokines and chemokines this increase is much more pronounced in patients with asthma.

2.4 Sustained bronchial RIG-I inflammasome activation and inflammasome-mediated immune responses in asthma after rhinovirus infection in vivo in humans

Next, we analyzed samples from a previously reported[67] controlled, experimental RV-A16 infection study of patients with asthma and control individuals, including BAL fluid, bronchial biopsies and bronchial brushings taken two weeks before infection (d-14, baseline) and 4 days after infection (Fig. 4A). Both groups were seronegative for anti-RV-A16 antibodies prior to infection and only individuals without recent natural respiratory infection underwent the experimental infection, as described previously[67]. Quite strikingly, we found a strong upregulation of the same transcriptome profiles of inflammasome-mediated immune responses in bronchial brushings from patients with asthma, in a sharp contrast to the downregulation of similar genes in control individuals at the same time (4 days after infection) (Fig. 4B, C, S3A, B). We further validated the expression of IL-1β, caspase-1, and RIG-I proteins in bronchial biopsies from the same patients. In line with the results demonstrated above, we found higher expression of IL-1β in the epithelial area of the bronchial biopsies of patients with asthma at baseline as compared to healthy controls (Fig. 4D). In accordance with its gene expression in bronchial brushings, in healthy controls, we noted a decrease in IL-1β expression following RV-A16 infection (Fig. 4D). Additionally, we assessed concentrations of mature IL-1β protein secreted into the bronchoalveolar lavage fluid. In agreement with the epithelial mRNA and protein expression of IL-1β, we found significantly decreased IL-1β protein concentration in BAL fluid from control individuals 4 days after infection, whereas in patients with asthma IL-1β protein concentrations in BAL fluid tended to be increased, though this increase was not statistically significant (Fig. 4E). Likewise, we also noted downregulation of epithelial expression of caspase-1 in bronchial biopsies from healthy controls 4 days after infection, whereas it did not change in patients with asthma (Fig. 4F, S3C). Here we also noticed that in vivo RIG-I protein expression in bronchial biopsies at baseline was higher in healthy controls than in patients with asthma, confirming our above-demonstrated in vitro data (Fig. S3D). After RV-A16 infection, there was a trend towards an increase in RIG-I expression in bronchial biopsies from patients with asthma, and towards a decrease in controls, but those trends were not statistically significant. Next, we investigated the dynamics and relationship of inflammasome-mediated immune responses after in vitro, and in vivo RV-A16 infection in patients with asthma and control subjects. We observed a strong negative correlation between gene expression of inflammasome-mediated immune responses after infection at 24h in vitro and at 4 days in vivo in control individuals (Fig. 4G, left panel). Genes upregulated in vitro at 24h post infection, were downregulated or not changed anymore at 4 days after in vivo infection. In contrast, in patients with asthma there was a strong positive correlation between the expression of similar genes at 24h in vitro and 4 days in vivo (Fig. 4G, right panel) showing that genes already strongly upregulated in asthma at an early time point after infection, still stayed significantly upregulated in vivo 4 days after infection. Altogether, combining the data from in vivo and in vitro approaches in humans, we demonstrated that the RIG-I inflammasome is indeed activated in human bronchial epithelium after in vivo infection with RV-A16. Moreover, our data revealed that

RIG-I inflammasome-mediated inflammation in healthy individuals was either being actively suppressed or already resolved 4 days after infection, whereas it was still ongoing in asthma.

2.5 Sustained rhinovirus infection and activation of antiviral responses in bronchial epithelium of patients with asthma in vivo

Since the major function of RIG-I is recognition of RNA viruses[30], we also analyzed the status of antiviral genes and proteins involved in in vivo and in vitro responses to RV-A16 infection. In line with inflammasome-mediated immune responses, the majority of genes encoding antiviral pathways were still upregulated 4 days after in vivo RV-A16 infection in patients with asthma while they were either downregulated or not changed in healthy controls (Fig. 5A, B, Supplementary Table S2). These data suggest less effective resolution of RV-A16 infection and delayed clearance of the virus in asthma. Indeed, RV-A16 load in the bronchoalveolar lavage fluid in asthma was around 100-fold higher than in controls and the peak nasal lavage virus load was 25-fold higher in patients with asthma than in healthy controls[67], though this difference was not statistically significant (Fig. 5C, D). In vitro at 24h post infection, antiviral gene (Fig. 5E, F, Supplementary Table S2) and protein responses (Fig. 5G) were enhanced in HBECs from both patients with asthma and control individuals. Interestingly, virus load was already slightly higher in epithelium from patients with asthma at this time-point (Fig. S1E). Therefore, as in the case of inflammasome mediated-immune responses, due to different dynamics of infection and viral clearance, we found a significant negative correlation of antiviral gene expression in HBECs from controls 24h after in vitro, and in bronchial brushings 4 days after in vivo RV-A16 infection (Fig. 5H, left panel). In contrast, in asthma, the delayed viral clearance and sustained high viral load resulted in a very strong positive correlation between in vitro upregulation of antiviral genes at an early time point and their ongoing upregulation observed in vivo at 4 days post infection (Fig. 5H, right panel). Thus, we showed here that bronchial epithelium from healthy individuals can efficiently respond to RV-A16 infection which leads to rapid virus clearance and subsequent resolution of antiviral responses. In contrast, in asthma, the lack of resolution of antiviral responses and delayed virus clearance suggest that there is an ongoing process in epithelium, which impairs the effectiveness of RIG-I-induced antiviral mechanisms.

2.6 Activation of the RIG-I inflammasome impaired RIG-I dependent interferon signaling in bronchial epithelium of patients with asthma

Having demonstrated excessive RIG-I inflammasome activation and IL-1β secretion in epithelium of patients with asthma in response to RV-A16, we hypothesized that this could result in persistent, but less efficient anti-RV-A16 response in asthma. Therefore, we further studied whether RIG-I activation of MAVS/TBK1/IKKε and downstream interferon signaling inhibits RIG-I inflammasome activation and conversely if formation of RIG-I

inflammasome inhibits interferon signaling. First, we used BX795, a chemical inhibitor of TBK1 and IKKε. As expected, it blocked expression of *IFNL2/3* (IFN-λ) in HBECs of patients with asthma (Fig. 6A) and subsequently decreased expression of *DDX58* (RIG-I) (Fig. 6B). BX795 treatment also reduced expression of interferon-stimulated chemokines: CXCL10, CXCL11 and CCL3 (Fig. 6C). It also led to a trend to increased RV-A16 infection (Fig. 6D), as well as to significantly augmented inflammasome priming (Fig. 6E) and activation (Fig. 6F). Next, we blocked IL-1β processing by RIG-I inflammasome with the use of the caspase-1 inhibitor YVAD and investigated interferon signaling and RV-A16 infection in bronchial epithelium. Inhibition of RIG-I inflammasome activation and subsequent IL-1β signaling indeed led to trends of increasing expression of *IFNB* (IFN-β) (Fig. 6G) and *DDX58* (RIG-I) mRNA (Fig. 6H) and it further increased the production of CXCL10, CXCL11, CCL3, and CCL4 (Fig. 6I). However, it did not change the infection at the same early timepoint (Fig. S1L). In summary, these data suggest that increased RV-A16-dependent RIG-I inflammasome activation in bronchial epithelium disturbed the effectiveness of RIG-I dependent anti-RV-A16 responses in asthma. Therefore, a timely blockade of the excessive RIG-I inflammasome activation and IL-1β signaling may lead to more efficient viral clearance and lower burden of infection.

2.7 House dust mite impaired interferon responses in rhinovirus-infected bronchial epithelium of patients with asthma

Having demonstrated that HDM increased RV-A16-induced RIG-I inflammasome activation, we continued to explore the effect of HDM pre-exposure on the timing and strength of antiviral responses. We found that HDM pre-treatment decreased RV-A16-induced mRNA expression of *IFNB* (IFN-β) and *DDX58* (RIG-I) only in HBECS from patients with asthma 24h, but not 6h after RV-A16 infection in vitro (Fig. 7A, B, S4A, B). Accordingly, when we analyzed protein expression and enriched biological pathways by targeted proteomics in the same conditions, we observed decreased cell- and IFNs- mediated antiviral responses in HBECs from control individuals and patients with asthma at 24h post infection (Fig. 7C). In addition, HDM in the presence of RV-A16 stimulated the release of epithelial to mesenchymal transition factors such as interleukin 15 receptor subunit alpha (IL-15RA)[68,69], artemin (ARTN)[70], tolerance inducing TNF receptor superfamily member 9 (TNFRSF9)[71] (also called 4-1BB and CD137), extracellular newly identified RAGE-binding protein (EN-RAGE) alarmin[72] in both studied groups. However, only in asthma, complementary with all our previous data, HDM simultaneously increased the activation status and release of proinflammatory and pro-remodeling proteins, such as IL-1α, signaling lymphocytic activation molecule family member 1 (SLAMF1)[73], cluster of differentiation (CD) 40[74,75] and TRANCE (RANKL)[76,77] (Fig. 7C, Supplementary Table S3). Importantly, HDM pre-stimulation had a slightly additive effect to the antiviral RIG-I pathway inhibitor (BX795) and further reduced BX795-decreased protein expression of the ISGs: CXCL10, CXCL11, CCL3 and CCL4 (Fig. 7D). It all suggests that pre-exposure to

HDM, before RV-A16 infection decreases IFN type I response in a non-specific way in patients with asthma and control individuals. However, only in patients with asthma, HDM exposure contributes further to the enhanced inflammasome-mediated and other immune responses, and associated impairment of the effectiveness of antiviral responses.

2.8 Pre-existing rhinovirus infection attenuated SARS-CoV-2 infection, but augmented epithelial inflammation in asthma

Finally, facing the current pandemic and noting the contradictory results about asthma as a risk factor for COVID-19 in different populations[12-16], we investigated if RV-A16-induced RIG-I inflammasome activation and HDM-mediated decrease of IFN responses may affect SARS-CoV-2 infection. We first treated primary HBECs from healthy controls and patients with asthma with or without HDM, next after 24h we infected them with RV-A16, and after a further 24h we infected them with SARS-CoV-2 for 48h (Fig. 8A). We confirmed infection with SARS-CoV-2 by the detection of its nucleocapsid protein N (Fig. 8B) and the increase of SARS-CoV-2 viral RNA (Fig. 8C). In patients with asthma, but not in healthy controls, we observed lower infection with SARS-CoV-2 in samples pre-infected with RV-A16 (Fig. 8C). Individual samples with high RV-A16 virus loads (Fig. 8D) had lower SARS-CoV-2 infection, and vice versa. This effect was diminished upon HDM pre-stimulation in samples from patients with asthma, suggesting that HDM pre-stimulation tended to increase SARS-CoV-2 infection in RV-A16+SARS-CoV-2 infected epithelium in asthma (Fig. 8C). To understand these different patterns of infection, we analyzed the expression of *DDX58* (RIG-I), type I/III IFNs and *IL1B* (IL-1β). In line with our previous data, RV-A16 infection increased the expression of *DDX58* (RIG-I) (Fig. 8E, S5A), *IFNB* (IFN-β) (Fig. 8F, S5B), *IFNL1* (IFN-λ1) (Fig. 8G, S5C) and *IFIH1* (MDA5) (Fig. 8H, S5D). However, we noted that infection with SARS-CoV-2 alone did not induce expression of *DDX58* (RIG-I), *IFIH1* (MDA5), *IFNB* (IFN-β), *IFNL1* (IFN-λ1) (Fig. 8 E-H, S5 A-D) or secretion of proinflammatory proteins (Fig. 8 I-J, Suppl. Table S4) at this timepoint. In contrast, HDM prestimulation increased the release of IL-18 in SARS-CoV-2-infected HBECs from patients with asthma (Fig. 8 I-J). Importantly though, we observed that infection with SARS-CoV-2 on top of the infection with RV-A16 resulted in the tendency to increase IL-18 (Fig. 8 I-J, Suppl. Table S4) and *IL1B* (IL-1β) (Fig. 8K, S5E). Notably, HDM pre-stimulation resulted in an amplified secretion of proinflammatory proteins, such as TRAIL, IL-15, CXCL9, IL-17C and CCL8-only in epithelium of patients with asthma infected with both viruses, whereas these conditions induced IL-18 secretion both in patients with asthma and control individuals (Fig. 8 I-J, Suppl. Table S4). In summary, we found here that pre-existing RV-A16 infection restricted SARS-CoV-2 replication in asthma, but not in controls, which was in line with the sustained type I/III IFNs at this time-point, induced by RV-A16 in asthma. SARS-CoV-2 infection alone did not induce *DDX58* (RIG-I), *IFIH1* (MDA5), *IFNB* (IFN-β), *IFNL1* (IFN-λ1) at 48h after infection. However, especially in the presence of HDM, we observed enhanced

proinflammatory responses in patients with asthma after SARS-CoV-2 co-infection with RV-A16, in spite of the reduced viral load of SARS-CoV-2.

3. Discussion

In the current study, we investigated mechanisms, interactions and dynamics of inflammasomes, antiviral and proinflammatory responses in the airways of healthy controls and patients with asthma upon combined exposures with house dust mite, rhinovirus and SARS-CoV-2. We analyzed the direct in vivo responses in humans, paired with the experiments in patients` primary cells. We showed, that recognition of replicating RV in bronchial epithelial cells by RIG-I helicase led to ASC recruitment, ASC oligomerization, activation of caspase-1, processing and release of mature IL-1β, independently of NLRP3 inflammasome activation. The same mechanisms occurred both in healthy individuals and in patients with asthma, but they were significantly more pronounced in asthma, especially when preceded with HDM exposure. Overactivation of epithelial RIG-I inflammasome in asthma compromised the dynamics of RIG-I-dependent type I/III IFNs and ISG responses, leading to less effective virus clearance, as well as to sustained inflammasome-, and IFN-dependent airway inflammation. In addition to enhancing RV-dependent RIG-I inflammasome activation, HDM also partly inhibited early type I/III IFN responses. Interestingly, this sustained RV-induced antiviral response in HBECS from patients with asthma led to restrained SARS-CoV-2 replication, but augmented inflammasome activation and proinflammatory responses.

There are four main inflammasomes described to date to be involved in innate antiviral immunity against RNA viruses – the NLRP3, RIG-I and in some cases MDA5 and absent in melanoma 2 (AIM2) inflammasomes [50,55,78,79]. They are activated by several stimuli involved in the viral infection, such as viral nucleic acids, viroporins, RNA-modulating proteins, reactive oxygen species (ROS) and others[61]. Here, we found, that in vivo in humans and in fully differentiated primary human bronchial epithelium, infection with RV, a single stranded RNA virus, leads to increased priming of pro-IL-1β in a replication independent and dependent manner, and to assembly of RIG-I/ASC inflammasome, in a replication dependent manner. We did not see involvement of NLRP3 inflammasome upon RV infection or HDM exposure or even significant expression of NLRP3 in airway epithelium at baseline in any of our in vivo, in vitro or data mining approaches[66,80]. We also did not see MDA5 forming inflammasome. Other groups observed that infection of human peripheral blood mononuclear cells, human macrophages and mouse bone-marrow derived cells with other single stranded RNA viruses, vesicular stomatitis virus (VSV) and IAV, activates RIG-I/MAVS-dependent pro-IL-1β transcription and RIG-I/ASC-dependent, but NLRP3-independent, inflammasome activation and mature IL-1β and IL-18 production[50,81]. In contrast, in undifferentiated, submerged cultures of primary human airway epithelial cells infection with IAV

revealed RIG-I and NLRP3-inflammasome-dependent mature IL-1β release[52], while infection with RV in a similar model led to activation of NLRP3/NLRC5/ASC complexes and mature IL-1β release[53]. These differences might come from i) the undifferentiated state of the cells in the previous studies, as in non-differentiated epithelium, lacking ciliated cells, viral infection might engage different pathways than in human airways in vivo[82,83]; ii) from different expression of inflammasome components in undifferentiated and differentiated mature epithelium lining human airways, as we showed previously[84]; as well as iii) from the differences in the virus strains and serotypes[85]. Importantly, our in vitro and in vivo data consistently showed the same results that RIG-I is engaged as inflammasome in bronchial epithelium upon RV infection, which constitutes an important early time-point event, triggering subsequent airway inflammation. It is also possible, that in vivo in humans both inflammasomes are engaged in different cellular compartments: RIG-I/ASC in airway epithelium and NLRP3 in the infiltrating inflammatory cells in the airways. Indeed, RV infection in mice leads to partly macrophage-derived, NLRP3 inflammasome-dependent airway inflammation[51]. However, neither depletion of macrophages nor NLRP3 knockout leads to the complete blockade of mature caspase-1 and IL-1β processing upon RV infection, underlining that RV might induce other inflammasomes in airway bronchial epithelium[51].

An appropriate balance between activation of RIG-I epithelial inflammasome and subsequent IL-1β/IL-1 receptor (IL1R) signaling with RIG-I-dependent type I/III IFN responses should lead to the limitation of viral replication, efficient virus clearance and timely resolution of airway inflammation[52]. Indeed, we observed here that in the bronchial epithelium of healthy subjects at early time points during RV infection there was an activation of RIG-I inflammasome and inflammasome-mediated immune responses, together with efficient type I/III IFN and ISG-responses. Importantly all of these responses were actively inhibited or went back to the pre-infection state, already 4 days after in vivo infection. In contrast, in epithelium of patients with asthma, there was enhanced RIG-I inflammasome activation accompanied by augmented inflammasome/IL1R-mediated proinflammatory responses starting early after infection and still non-resolved in vivo 4 days after infection. Overactivation of epithelial RIG-I inflammasome and subsequent increases in mature IL-1β release might be at least partially responsible for the delayed and sustained type I/III IFN/ISG responses. We demonstrated this here by blocking caspase-1 with YVAD which led to an increase in IFN-β *(IFNB)* and RIG-I (*DDX58*) mRNA together with IFN-responsive chemokines such as CXCL10, CXCL11, CCL3, and CCL4. Our findings are in line with early observations showing that IL-1β is able to attenuate transcription and translation of type I IFNs and excessive IFNα/β-induced effects via proteasome-dependent mechanisms or by induction of prostaglandin E2[86-88]. Interestingly, we also noted here that this cross-talk between IL-1β and type I IFNs is reciprocal, as blocking phosphorylation of TBK1 and IKKε by their inhibitor BX795 and thus reducing RIG-I-induced type I interferons, significantly increased pro-IL-1β transcription and its processing by RIG-I

inflammasome in airway epithelium. This was previously elegantly demonstrated in the case of NLRP3 inflammasome[89] and in transcriptional IL-1β regulation in macrophages and other myeloid cells[90], but it has not been demonstrated for RIG-I inflammasome or considered to be important at the epithelial barrier.

There is a long-lasting discussion about the underlying origins and mechanisms of the frequent viral infections and exacerbations in patients with asthma, which gained a special weight during the current SARS-CoV-2 pandemic[16,91]. An impairment in epithelial type I/III IFN responses has been demonstrated in patients with uncontrolled and/or severe asthma, while it is less or not detectable in mild or well-controlled asthma[92-94]. More recently, it was suggested that this impairment might result from the unfitting grade (too high or too low), incorrect timing of initiation (delayed)[95] or resolution of the antiviral and inflammatory response (sustained) in bronchi of patients with asthma[96,97]. Treatment with nebulized IFN-β initiated early after development of common cold symptoms, did not provide improvement in comparison to placebo in the whole studied group including a majority of patients with mild asthma[42], however in those with moderate/severe asthma, improvements in symptoms and lung function were observed[42,98]. Indeed, adding INF-β in vitro to monocyte-derived macrophages and epithelial cells prior to, but not after infection with IAV drastically reduced the number of nucleoprotein-1 positive cells[97]. These data combined suggest that type I/III IFNs might be extremely important in the antiviral response in the very early phase of infection, whereas they might not be relevant or could be even detrimental in the latter stages. Interestingly, the phenomenon of the frequent and severe exacerbations appears in both atopic, type-2 asthma, as well as in non-atopic, type-2 low asthma, suggesting that there might be a common mechanistic link to it [44,99]. Here, we showed that RV infection in asthma leads to the simultaneous overactivation of RIG-I inflammasome in their airway epithelium and impaired early RIG-I-dependent type I/III IFNs, which overall led to sustained inflammation, but insufficient viral clearance as compared to healthy controls. In patients with asthma, partially due to the higher pro-IL-1β expression, but lower RIG-I expression at baseline, RV infection led to the strong stimulation of RIG-I transcription and translation, and overactivation of both RIG-I-induced pathways: inflammasome and type I IFN responses. Since RIG-I inflammasome is also induced in healthy individuals in the early phase of RV infection, it might provide a physiological mechanism to fight an infection, as shown in ferrets, where the N protein of H5N1 influenza inhibiting this mechanism, resulted in higher mortality[52]. However, its overactivation in patients with asthma, especially at the very early stage of the infection, might contribute rather to the damage of the infected ciliated epithelium than to the effective antiviral response. Such damage might occur via pyroptosis[100] and lead to the release of active IL-1β and RIG-I/ASC/caspase-1 inflammasome complexes to the extracellular space and subsequent barrier impairment[2,101], recruitment of macrophages and neutrophils[101], and as we also showed here, to the inhibition of a timely and functional antiviral response and delayed in vivo viral clearance.

Presence of other airway barrier-damaging and/or activating factors, such as exposure to allergens in addition to the viral infection, worsens the clinical outcomes, leads to a more severe exacerbation, hospitalization or respiratory failure[11]. Mechanistically, it might be connected with the multiplication of pathways activated in airway epithelium and in cells infiltrating the airways, and/or with the additive effects of different triggers on the same pathway[24,91]. HDM activates airway epithelium via, among others, TLR2/4, C-type lectins, and PARs in an allergen-non-specific way to initiate allergen sensitization, but also to perpetuate already developed allergic and probably non-allergic airway inflammation in the absence of the sufficiently developed inhibitory signals[45-47]. It is known that one of the strongest effects of HDM-specific immunotherapy and anti-immunoglobulin E (IgE) treatment is the reduction of the rate of asthma exacerbations. It might be at least partially connected to the fact that in sensitized individuals, allergen binding to specific IgE, captured by the Fc epsilon receptor (FcεRI) receptor on the surface of plasmacytoid dendritic cells (DCs) may lead to the additional impairment of antiviral responses[102]. However, it is not well understood if and how HDM-induced signaling in the airway epithelium interferes with the effectiveness of early antiviral response. Here, we found that HDM contributes significantly to RV-induced pathologic responses in human airway epithelium in patients with asthma by i) enhancement of priming and non-mature pro-IL-1β release, ii) overactivation of RIG-I inflammasome and subsequent release of mature caspase-1, mature IL-1β, and RIG-I , iii) inhibition of type I/III IFNs and ISG-responses and iv) activation of extra proinflammatory and pro-remodeling proteins, such as IL-1α, SLAMF1[73], CD40[74,75] and TRANCE (RANKL)[76,77]. In the presence of both HDM and RV, we noted that increased usage of RIG-I protein engaged in inflammasome formation and its subsequent expulsion is paired with HDM-dependent inhibition of RIG-I, type I/III IFNs and several ISGs on the mRNA and protein level. At an early stage of RV infection, it might explain disturbance of the antiviral response dynamics observed in asthma by us and others[103]. Due to this functional reduction of RIG-I availability, the following type I/III IFN-response is less effective, not able to quickly and efficiently clear the infection and thus it is sustained up to later time points, together with the enhanced inflammasome-related proinflammatory response, as we demonstrated here in vivo and in vitro.

Co-infections with two or more respiratory viruses occur often and likely acts as additional factors increasing airway epithelial damage. Patients with asthma are at a greater risk of developing respiratory failure as shown in the case of H1N1 influenza infection[104]. Thus, it has been somewhat surprising that so far during the current SARS-CoV-2 pandemic, epidemiological cohorts of COVID-19 patients from different geographical locations have resulted in partially contradictory observations that asthma is (USA, United Kingdom, Australia) or is not (Europe, China) a risk factor for SARS-CoV-2 infection and/or severity of COVID-19[15,105,106]. We and others demonstrated that the expression of angiotensin-converting enzyme 2 (ACE2), the main SARS-CoV-2 receptor

and other plausible points of entry, are not changed in patients with asthma, even though different types of airway inflammation or inhaled steroids might modulate their expression[107,108] and as such it seems unlikely that it would be the main reason for observed discrepancies. Different geographical locations might represent variable levels and quality of environmental exposures such as viruses or allergens, which may interfere with the rate of SARS-CoV-2 infections[23,109] and COVID-19 severity. SARS-CoV-2, an enveloped, positive-sense, ssRNA virus[110] has been shown to be sensed, depending on the cell type, by MDA5[111], RIG-I[111] and NLRP3[112,113]. However, due to several evasion properties and encoding by non-structural (Nsp) and accessory proteins, such as Nsp1,6,12,13[114], various open read frames (ORFs)[115], protein M[116], protein N[117] and others, which antagonize interferon pathways on many levels[118] , induction of IFNs by SARS-CoV-2 itself is reduced or delayed[114,119] with the augmented proinflammatory mediator release. Several in vitro and in vivo animal studies revealed that SARS-CoV-2, similarly to SARS-CoV-1, is very sensitive to pre-treatment with type I/III IFNs[120-122], which inhibit its replication. Patients with disrupted IFN gene expression and production or patients with autoantibodies against type I IFNs have been shown to be at a greater risk of severe COVID-19. In accordance with these studies, we observed here that infection of epithelium from patients with asthma at the moment of heightened and sustained IFNs type I/III response induced by RV, results in reduced SARS-CoV-2 viral load, in contrast to the healthy epithelium, where the RV-induced IFN-I/III response has been already actively resolved. However, even if restricted, SARS-CoV-2 infection in combination with RV and HDM led to an increase in activation of epithelial inflammasome and release of higher amounts of IL-18 and other proinflammatory cytokines. In context of timing and possible clinical relevance it may mean that patients with asthma with pre-existing RV-infection might have a slightly restricted SARS-CoV-2 infection at first, but due to excessive inflammasome-related damage and proinflammatory signaling, together with SARS-CoV-2-induced inhibition of type I/III IFNs, they may in fact succumb eventually to more severe COVID-19. Importantly, in the presence of HDM, these potentially adverse effects are further heightened, meaning that HDM reduces RV-induced IFN response, which leads to higher SARS-CoV-2 replication and it enhances RIG-I inflammasome activation, inflammation and tissue damage.

All in all, we showed here in vivo and in vitro that the lack of balance between activation of RIG-I inflammasome and the RIG-I-IFNs-axis in response to a common respiratory virus, is an important driving factor of epithelial damage, lack of viral clearance and sustained airway inflammation in patients with asthma. Timely targeting of this abnormal response by the yet-to-be developed early therapeutics or even prophylactic approaches might provide in the future a beneficial strategy to prevent RV-induced exacerbations of asthma and potentially severe COVID-19.

4. Material and Methods

Reagents

House dust mite (HDM) extract (HDM) (Allergopharma, Reinbek, Germany) and house dust mite extract B (HDM B) (Citeq, York, UK) were diluted in sterile 0.9% saline (NaCl) and stored in -20°C. The concentration of the HDM used for the experiments was calculated according to the total protein content. Detailed description of the HDM extracts including protein, main allergens and endotoxin content is presented in the Supplementary Table S5.

All commercially available antibodies and reagents used in the manuscript are described in the Supplementary Table S6.

Mouse IgG2a monoclonal anti-human ICAM-1 antibody (antibody R6.5) was produced from the hybridoma cells (ATCC HB-9580, mouse hybridoma). The hybridoma cells were expanded in RPMI 1640 medium supplemented with 10% (v/v) IgG depleted fetal bovine serum, 2 mM L-glutamine, 1.25 g/L D-(+)-Glucose, 1 mM Sodium Pyruvate, 10 mM HEPES, 100 U/mL Penicillin-Streptomycin at 37°C in 5% CO_2. The IgG in culture media were affinity purified from the cell culture supernatant using a 1 mL HiTrap™ Protein G HP column (GE Healthcare, 29-0485-81). Eluted fractions were immediately neutralized and buffer exchanged into PBS using dialysis. The antibody was then filtered through a 0.22 µm filter and stored at 4°C.

Viruses

Rhinovirus A16 (RV-A16) was purchased from Virapur (San Diego, USA). UV-light inactivated RV-A16 (UV-RV-A16) was used as a control after an exposure to UV-light of the 254 nm at a 2 cm distance for 60 min. Cells were infected with RV-A16 or UV-RV-A16 at the multiplicity of infection (MOI) 0.1, 0.01 and 0.001 as determined by plaque assay. Briefly, HeLa cells were infected with the virus serial dilutions from 10^{-2} to 10^{-8} in duplicates. Seven days after infection, cells were fixed with formaldehyde solution and stained with 1% crystal violet in 20% ethanol and dH_20. Visible plaques were counted under a microscope.

SARS-CoV-2 viral genome was generated from the synthetic DNA fragments produced by GenScript (Piscataway, USA) using the in-yeast transformation-associated recombination (TAR) cloning method, as previously described[123]. In-vitro transcription was performed for the linearized Yeast artificial chromosome (YAC), containing the cDNA of the SARS-CoV-2 genome, as well as a PCR amplified SARS-CoV-2 N gene using theT7 RiboMAX Large Scale RNA production system (Promega, Madison, USA) with m7G(5')ppp(5')G cap provided as described previously[124]. Transcribed, capped mRNA was subsequently electroporated into baby hamster kidney cells (BHK-21) expressing SARS-CoV N protein. Co-culture of electroporated BHK-21 cells with susceptible Vero E6 cells produced passage 0 of SARS-CoV-2 virus. Passage 0 was used to infect Vero E6 cells

to generate passage 1 working stocks, which were used for all experiments. Titers were determined using standard plaque assay, as described previously[123].

Patients groups and experimental in vivo RV-A16 infection in humans

Experimental in vivo rhinovirus infection in 11 control individuals and 28 patients with asthma was performed as reported previously[67]. Briefly, non-smoking, non-atopic control individuals, and non-smoking mild/moderate patients with asthma without any recent viral illness and without serum neutralizing antibodies towards RV-A16, who passed inclusion criteria, underwent infection on day 0 with RV-A16 at the dose of 100 $TCID_{50.}$ Bronchial brushings, bronchial biopsies and bronchoalveolar lavage (BAL) fluid were collected around 2 weeks before and at 4 days after RV-A16 infection. Additionally, nasal lavage (NL) samples at the peak of RV-A16 infection were collected to assess RV-A16 infection rates. Only subjects who had sufficient remaining samples to be analyzed in this study and/or subjects who had successful infection in the lungs, as assessed by viral RNA copies by qPCR, were included in the BAL, NL, and biopsies analyses (n=9 healthy control, n=19 patients with asthma), and bronchial brushing microarray analysis (n=7 healthy controls, n=17 patients with asthma). The study received ethical approval from the St. Mary`s Hospital Research Ethics Committee (09/H0712/59). All participants gave written, informed consent. The clinical characteristics of the 9 control and 19 asthma study participants who had sufficient remaining samples to be analyzed in this study is presented in Supplementary Table S7.

Control individuals and patients with asthma were enrolled in the ALL-MED Medical Research Institute, Wroclaw, Poland; the Pulmonary Division, University Hospital of Zurich, Switzerland (cohort SIBRO)[125], or at the University Hospital, Jagiellonian University Medical College, Cracow, Poland (cohort A)[126], as described previously. Briefly, bronchoscopy with epithelial cells brushings and BAL fluid collection was performed. The study was granted ethical permission from Switzerland and Poland (KEK-ZH-Nr. 20212-0043 – Kantonale Ethik-Kommission Zürich; KB-70/2013 and KB-567/2014 – Bioethical Committee, Wroclaw Medical University) or the Jagiellonian University Bioethics Committee (KBET/68/B/2008 and KBET/209/B/2011). Asthma diagnosis and severity were assessed according to the GINA guidelines[3]. All participants gave written, informed consent. Clinical characteristics of the study participants is presented in the Supplementary Table S7.

Primary Human Bronchial Epithelial cells (HBECs) were obtained from the above-listed cohorts or from the doctor-diagnosed asthma and control individuals from two independent commercial sources: Lonza (Basel, Switzerland), and Epithelix (Plan-les-Ouates, Switzerland). Characteristics of the HBECs used in the manuscript are presented in Supplementary Table S8.

Air-liquid interface (ALI) cultures of bronchial epithelium from control individuals and patients with asthma

HBECs from the control subjects and patients with asthma were cultured and differentiated in the air-liquid interface (ALI) conditions as described previously, with minor alterations of the previous protocol[126]. Briefly, cells from passage 2 were grown in 20 mL of bronchial epithelial basal medium (Lonza, Basel, Switzerland) supplemented with the SingleQuot Kit (Lonza, Basel, Switzerland) placed in 150cm^2 T-flask in humidified incubator at 37°C with 5% CO_2 for maximum 10 days, or until 80%-90% confluency. Next, cells were trypsinized (ThermoFisher Scientific, Waltham, USA) and seeded at a density of 1.5x10^5 cells/well on the 6.5-mm-diameter polyester membranes with the 0.4 μm pore size and growth area of 0.33 cm^2 (Costar, Corning, NY, USA; Oxyphen, Wetzikon, Switzerland) in 24-well culture plates. Bronchial Epithelial Growth Medium (BEGM) (Lonza, Basel, Switzerland) supplemented with the SingleQuot kit (Lonza, Basel, Switzerland), with an exception of the retinoic acid (ATRA, Sigma-Aldrich, St. Louis, USA) and triiodothyronine, was mixed in the 1:1 ratio with the Dulbecco modified Eagle medium (DMEM, Gibco, Thermofisher Scientific, Waltham, USA). Fresh all-trans ATRA (Sigma-Aldrich, Merck, Kenilworth, USA) was supplemented at a concentration of 15 ng/mL. Cells were grown submerged for 3-5 days in the apical medium and were in contact with the basolateral medium. After they obtained a full confluence, the apical medium was removed and cells were kept in the air-liquid interface (ALI) cultures for at least 21 days. BEGM/DMEM/ATRA medium was maintained only basolaterally to differentiate the HBECs. During the cell culture process, medium was exchanged every 2-3 days and, periodically, excess of produced mucus was removed from the wells. All experiments were performed on the fully differentiated HBECs from the same passage, between 21 and 28 days of ALI culture (Fig. S1A).

House dust mite stimulation and rhinovirus A16 in vitro infection model in the primary HBECs

House dust mite (HDM) stimulation, followed by rhinovirus A16 (RV-A16) infection experiments were performed in the OptiMEM medium (LifeTechnologies, ThermoFisher Scientific, Waltham, USA). ALI-differentiated HBECs from control individuals and patients with asthma were treated apically with the HDM extract (Allergopharma, Reinbek, Germany) at a dose of 200 μg/mL of the total protein in 200 μl OptiMEM on the apical side, and 600 μl of clear OptiMEM on the basolateral side (Fig. S1A), in the humidified incubator at 37°C with 5% CO_2. After 24h of HDM stimulation cells, were apically infected with RV-A16 at the MOI of 0.1 or as otherwise specified, or stimulated with UV-RV-A16 at the same MOI, and cultured in the humidified incubator at 34.5°C with 5% CO_2 for the next 24h (Fig. S1A). Next, cell supernatants (apical and basolateral), RNA, and protein cellular lysates were collected and stored in -80°C. Some cells were fixed with 4% PFA (Fluka/Sigma Aldrich Buch, Switzerland) and were stored wet at 4°C for 1-2 weeks before the subsequent confocal analyses. All doses and time-points used for the final experiments were based on the preliminary dose-dependent and time-course experiments. Briefly, two different HDM extracts: main HDM extract used

in the manuscript (Allergopharma, Reinbek, Germany) at the dose of 200 μg/mL, and HDM extract B (Citeq, York, UK) at the dose of 200 and 100 μg/ml were investigated (Fig. S1B, S4A-B). RV-A16-infection of HBECs from patients with asthma was performed in 6h and 24h time-points (Fig. S1C). Lastly, RV-A16 infection at the MOI 0.001, MOI 0.01, and MOI 0.1 was investigated (Fig. S1D). Based on the secretion of the mature IL-1β, HDM extract from the Allergopharma, Reinbek, Germany at the dose of 200 μg/mL, RV-A16 MOI 0.1 and the 24h time-point were chosen, and are presented through the manuscript, if not mentioned differently. For the experiments with inhibitors, 40 μM of the caspase-1 inhibitor: ac-YVAD-cmk (Acetyl-tyrosine-valine-alanine-aspartate-chloromethyl ketone, Invivogen, San Diego, USA), 1μM of the IKKε/TBK1 inhibitor: BX795 (N-[3-[[5-iodo-4-[[3-[(2-thienylcarbonyl)amino]propyl]amino]-2-pyrimidinyl]amino]phenyl]-1-Pyrrolidinecarboxamide hydrochloride, Sigma Aldrich, Merck, Kenilworth, USA), or 1μM of the NLRP3 inflammasome inhibitor: MCC950 (C20H23N2NaO5S, Avistron, Bude, UK) or appropriate vehicle controls were used apically and basolaterally, 24h prior RV-A16 infection. To block ICAM-1, a receptor responsible for RV-A16 infection of HBECs, anti-ICAM-1 antibodies were added to the apical and basolateral compartment, 3h prior RV-A16 infection at the dose of 10ug/mL (Fig. S1A).

Rhinovirus and severe acute respiratory syndrome coronavirus-2 (SARS-COV-2) in vitro co-infection model in primary HBECs from control individuals and patients with asthma

The ALI-differentiated MucilAir cultures (Epithelix, Plan-les-Ouates, Switzerland) from primary human bronchial epithelium obtained from 4 control individuals and 5 patients with asthma (Supplementary Table S8) were cultured for 7 days in the MucilAir Medium (Epithelix, Plan-les-Ouates, Switzerland) in ALI conditions, with basolateral medium changed every other day. At the day of the experiment, performed in a biosafety level 3 (BSL3) laboratory, cells were washed with warm PBS to remove an excess of mucus. The experiment was performed in the OptiMEM medium (LifeTechnologies, ThermoFisher Scientific, Waltham, USA) in the volume of 250 μl on the apical, and 600 μl on the basolateral side. Through the whole experiment cells were kept in the humidified incubator at 37°C with 5% CO_2. First, HBECs were stimulated apically with 200 μg/mL of protein content of HDM extract or vehicle. 24h after HDM stimulation, cells were apically infected with/without RV-A16 at the MOI of 0.1. After next 24h, HBECs were apically infected with/without SARS-CoV-2 at the MOI of 0.1. Finally, 48h after SAR-CoV-2 infection experiment was harvested (Fig. 8A). In order to inactivate SARS-CoV-2, all collected supernatants were treated with 65°C for 30 min. Cells were fixed in 4% PFA for at least 20 min. Inactivated supernatants were frozen in -80°C until further analyses. For RNA analyses, insert with the fixed cells were preserved in RNAlater (Qiagen, Hilden, Germany), left overnight in 4°C, and stored in -20°C in the new, dry tube. In order to perform confocal staining, inserts with the fixed cells were snap frozen in the Clear Frozen Section Compound (FSC22, Leica, Wetzlar, Germany).

THP-1 cell culture

THP-1-XBlue cells (Invivogen, San Diego, USA) were defrosted in 32 mL of RPMI-1640 medium (Sigma-Aldrich, St. Louis, USA) supplemented with the Penicillin/Streptomycin/Kanamycin, MEM vitamins, Na-Pyruvate/MEM Non-essential Amino Acid Solution and heat-inactivated FCS (cRPMI medium) in the 75cm^2 T-flask, and cultured for 1 day in the humidified incubator at 37°C with 5% CO_2. In the following day, cells were counted, checked for viability (98%) and transferred to the 12-well cell cultures plate (0.5 mio cells/well in 1 mL of cRPMI medium). Next day, cells were stimulated with LPS (100 ng/mL, Invivogen, San Diego, USA) or vehicle for 4h followed by 2 mM ATP or vehicle (Invivogen, San Diego, USA) for 20 min. Cytospins (250xg, 3 mins, Shandon Cytospin 2, Marshall Scientific, Hampton, USA) were prepared, and cells were immediately fixed with 4% PFA (Fluka/Sigma Aldrich, Buchs, Switzerland), and stored in wet chamber before the confocal staining.

Immunoassays

ELISA and MSD multiplex

Secreted IL-1β in majority of in vitro experiments was measured with the ELISA kit (R&D Systems, McKinley Place, USA), according to the manufacturers instruction. Detection limit for the kit is 3.91 pg/mL. IL-1β in BAL fluid from control individuals and patients with asthma was measured using mesoscale discovery platform (MSD, Kenilworth, USA) kits as described previously[125]. Additionally, BAL samples from controls and patients with asthma before and after experimental intranasal RV-A16 infection in vivo were analyzed with V-PLEX human IL-1β Kit (MSD, Kenilworth, USA), according to the manufacturer's instructions. V-PLEX IL-1β is presented as $\log_{10}$ arbitrary units (au) corresponding to percentage of total protein concentration measured by BCA (ThermoFisher Scientific, Waltham, USA) and multiplied by factor 1000000.

Proximity extension assay (PEA) targeted proteomics

Protein expression in the apical compartments of the HBECs were measured using the proximity extension assay targeted proteomics technology (Olink, Stockholm, Sweden). Targeted 96-proteins Inflammation (control and asthma), Immune Response and Immuno-Oncology (asthma) panels were used according to the manufacturer's instructions with the suggested adaptations to the cell cultures conditions. Apical compartments from RV-A16+SARS-CoV-2 model were analysed with the human Target 48 Cytokine Panel (Olink, Uppsala, Sweden). Final results for 96-plex assay are reported as Normalized Protein eXpression (NPX), an arbitrary unit in $\log_2$-scale. Results from the Target 48 Cytokine Panel are in pg/mL.

Western Blotting

Western Blotting experiments from the cell lysates and the apical supernatants were performed as previously described[126,127]. Briefly, cells were lysed in RIPA Lysis and Extraction buffer (ThermoFisher Scientific, Waltham,

USA) supplemented with the protease inhibitor (Roche, Merck, ThermoFisher Scientific, Waltham, USA) for 15 minutes on ice, centrifuged (15 min, full speed, 4°C), and debris-free protein lysates were frozen in -80°C for further analyses. Protein concentration was assessed with the BCA kit (ThermoFisher Scientific, Waltham, USA), according to the manufacturer's instructions. Protein from the apical supernatants was precipitated with 1 volume of methanol (Fisher Scientific, Reinach, Switzerland) and ¼ volume of chloroform (Merck Millipore, Burlington, USA) as described previously[127]. Equal amounts of cell lysate proteins (10-20μg) were loaded on the 4-20% Mini-PROTEAN TGX Gel (Bio-Rad, Hercules, USA) or 4-20% SuperPAGE gel (GenScript, Leiden, Netherlands) in Tris/Glycine/SDS buffer (Bio-Rad Lab, Hercules, USA) or MOPS buffer (GenScript, Leiden, Netherlands). After electrophoresis, the proteins were transferred to the nitrocellulose membranes (Bio-Rad, Hercules, USA or Advansta, San Jose USA) using the Trans-Blot Turbo Blotting System (Bio-Rad, Hercules, USA) or eBlot L1 Protein Transfer System (GenScript, Leiden, Nederlands). The membranes were blocked with 5% nonfat milk in 0.1% Tween20 PBS (PBST) for 1h, washed with 10x PBST, and incubated with the primary antibodies for overnight in 4°C. Dilutions of primary antibodies used for the analyses of the cell lysates: 1:100 IL-1β (R&D Systems, McKinley Place, USA), 1:200 RIG-I (Santa Cruz Biotechnology, Dallas, USA), 1:1000 ASC (Santa Cruz Biotechnology, Dallas, USA), 1:1000 caspase-1 (Cell Signaling, Danvers, USA), and 1:1000 NLRP3 (Adipogen, San Diego, USA). The membranes were subsequently washed in 10xPBST and incubated with an appropriate secondary antibody conjugated with the horseradish peroxidase (HRP) (1:10,000 dilution) (Jackson ImmunoResearch, West Grove, USA; Santa Cruz Biotechnology, Dallas, USA) for 1h at room temperature. β-actin expression was determined with HRP-conjugated antibodies in 1:25,000 dilution (Abcam, Cambridge, UK). Protein samples precipitated from the apical supernatants were analyzed with the use of goat anti-IL-1β antibodies (1:1000, R&D Systems, Minneapolis, USA), rabbit anti-caspase-1 (1:1000, Cell Signaling Technology, Danvers, USA), and HRP conjugated anti-goat (1:10,000, Santa Cruz Biotechnology, Santa Cruz, USA), and anti-rabbit (1:10,000, Jackson ImmunoResearch, West Grove, USA) antibodies. After washing with 10xPBST, the blots were developed with the SuperSignal West Femto Kit (ThermoFisher Scientific, Waltham USA) or WesternBright Quantum/Sirius HRP substrate (Advansta, San Jose, USA) and visualized on the Luminescent Image Analyzed LAS-1000 (Fujifilm, Tokyo, Japan) or the Fusion FX (Vilber, Collegien, France). To assess more than one protein, the membranes were stripped with the Restore PLUS Western Blot Stripping Buffer (ThermoFisher Scientific, Waltham, USA). Quantification of the protein expression was performed in Fiji Software. [128] Briefly, an area of the peak of the protein of interest was measured in triplicates, and average was used to calculate the ratio between expression of the protein of interest and β-actin (protein/β-actin). Protein/β-actin ratio from HBECs from control individuals and patients with asthma upon HDM stimulation, RV-A16 infection, or both was further normalized to the vehicle control condition from control individuals, and log transformed with Y=log(Y) function.

Co-immunoprecipitation

For co-immunoprecipitation cells were lysed with the Lysing Buffer (1μM DTT + 10% Triton X100 in ddH_20 supplemented with the protease inhibitor (Roche, Merck, ThermoFisher Scientific, Waltham, USA) for 15 minutes on ice, centrifuged (15 min, full speed, 4°C), and the debris-free protein lysates were frozen in -80°C for further analyses. Protein concentration was assessed with the BCA kit (ThermoFisher Scientific, Waltham, USA) according to the manufacturer's recommendation. 100 μg of the pooled protein was pre-cleared with 100 μl of Protein A beads (Bio-Rad, Hercules, USA), magnetized, and incubated with 10 μg of anti-ASC antibodies (Santa Cruz Biotechnology, Santa Cruz, USA) overnight at 4°C, followed by ASC immunoprecipitation with 100 μl of Protein A beads (Bio-Rad, Hercules, USA) for 2h in RT. Co-IP samples and input (protein not bound to the beads) were collected and together with the cell lysates were further analyzed with the Western Blot protocol with the use of mouse anti-human RIG-I antibodies (1:200, Santa Cruz Biotechnology, Santa Cruz, USA) or rabbit anti-human MDA5 antibodies (1:1000, Abcam, Cambridge, UK) and HRP conjugated anti-mouse or anti-rabbit antibodies (1:10,000, Jackson ImmunoResearch, West Grove, USA).

mRNA isolation and RT-PCR

HDM and RV-A16 model

Cells were lysed on ice with the RLT buffer (Qiagen, Hilden, Germany) supplemented with β-mercaptoetanol (Sigma-Aldrich, St. Louis, USA), and stored at -80°C until further analyses. mRNA isolation was performed with the RNeasy Micro Kit (Qiagen, Hilden, Germany) according to the manufacturer's instructions. Quality and quantity of isolated RNA was assessed by the Nanodrop 2000 (ThermoFisher Scientific, Waltham, USA). Reverse transcription was performed with RevertAid RT kit (ThermoFisher Scientific, Waltham, USA) with random hexamers, according to the manufacturer's recommendations. Gene expression (5-10 ng of cDNA/well) was assessed by RT-PCR using the SYBR Green/ROX qPCR Master Mix (ThermoFisher Scientific, Waltham, USA), performed on the QuantStudio 7 Flex Real-Time PCR System (ThermoFisher Scientific, Waltham, USA). The sequences of used primers (5μM) are summarized in the Supplementary Table S9. Gene expression was normalized to the housekeeping gene, elongation factor 1α (EEF1A), and presented as a relative quantification calculated with the ΔΔCt formula, as described previously[46]. Depending on the analyses, data were calibrated according to the vehicle condition from HBECs from control individuals, or vehicle condition calculated separately for control individuals and patients with asthma. Data are presented as $2^{-\Delta\Delta Ct}$ values, or percentage change normalized to the specified condition.

HDM, RV-A16 and SARS-CoV-2 model

Samples preserved in the RNAlater, as described above, were immersed in the increasing concentrations of ethanol (30% up to 100%, increasing every 10%). After this initial step, RNA was isolated with use of RecoverAll

kit (Invitrogen, Waltham, USA) according to the manufacturer's protocol. Isolated mRNA was concentrated with the use of SpeedVac (DNA Speed Vac, DNA110, Savant, Hayanis, USA) for 1h in the ambient temperature. Sample concentration did not affect its quality, as measured with use of NanoDrop One^{C} (ThermoFisher Scientific, Waltham, USA). Reverse transcription was performed with use of the SuperScript IV VILO Master Mix (Thermofisher Scientific, Waltham USA), according to the manufacturer's recommendations. Gene expression (5ng of cDNA/well) was assessed by RT-PCR using i) SYBR Green PCR Master Mix (ThermoFisher Scientific, Waltham, USA) for *DDX58*, *IFNB*, *IFNL1*, *IL1B*, *MDA5*, and ii) TaqMan assays for RV-A16 and SARS-CoV-2 *Protein N*, *Protein S*, *ORF1AB* detection (ThermoFisher Scientific, Waltham, USA) and was performed on the QuantStudio 7 Flex Real-Time PCR System (ThermoFisher Scientific, Waltham, USA). The sequences of used primers are summarized in the Supplementary Table S9. Gene expression was normalized to the elongation factor 1α (EEF1A) (SYBR Green analyses), or RNase P (TaqMan assays), and presented as a relative quantification calculated with -$\Delta\Delta$Ct formula, compared to the vehicle condition separately for controls and patients with asthma, as described previously[46]. SARS-CoV-2 viral RNA in presented as $2^{-\Delta\Delta Ct}$ values averaged from the expression of *N protein*, *S protein* and *ORF1AB* in each condition.

Rhinovirus infection quantification in the nasal and bronchoalveolar lavage fluid in humans

Rhinovirus infection in control individuals and patients with asthma after experimental RV-A16 infection in vivo was performed in the nasal lavages (peak of infection) and BAL fluid (4 days post infection) with use of qPCR, as previously described. [67] Results are presented as $\log_{10}$ of viral RNA copies in 1 mL.

Confocal microscopy

Cells were fixed on the inserts with 4% paraformaldehyde (Fluka/Sigma Aldrich, Buch, Switzerland) for 10 minutes, permeabilized with detergent (PBS + 0.1% TritonX100 + 0.02% SDS) for 5 minutes and blocked with 10% goat serum (Dako, Agilent, Santa Clara, USA) in 1% BSA/PBS for 60 min at room temperature (RT). All antibodies were diluted in 4% goat serum + 1% BSA/PBS, and cells were stained from apical and basolateral sides with 100 µl of antibodies working solution. Samples were stained for ASC (2µg/mL, mouse anti-ASC, Santa Cruz Biotechnology, Santa Cruz, USA), IL-1β (10µg/mL, mouse anti- IL-1β, Abcam, Cambridge, UK), and RIG-I (2µg/mL, mouse anti-RIG-I, Santa Cruz Biotechnology, Santa Cruz, USA) for 60 minutes at RT. Proper mouse isotype controls, in the corresponding concentrations were used to control for unspecific binding. (Dako, Agilent, Santa Clara, USA). Subsequently, samples were incubated with the goat anti-mouse Alexa Fluor 488 (for ASC), and the goat anti-mouse Alexa Fluor 546 (for IL-1β and RIG-I) secondary antibodies at the concentrations of 1:2000 (Invitrogen, Waltham, USA) for 60 minutes at RT. Samples were mounted in the ProLong Gold mounting medium containing DAPI (Life Technologies, Carlsbad, USA) according to the manufacturer's instructions, analyzed with a Zeiss LSM780 confocal microscope (Zeiss, Oberkochen, Germany)

and Zen Software (Zeiss, Oberkochen, Germany). All pictures were taken at the 40x magnification and are presented as maximal projection (orthogonal projection) from z-stacks (3-22 for ASC, 4 for IL-1β and RIG-I). ¼ of the original picture is shown on the figures, with appropriate scale bar and further magnification of the area of interest. Additionally, to quantify ASC speck formation specks from 3-5 pictures per condition were counted in duplicates and averaged.

Differentiated HBECs upon HDM+ RV-A16 stimulation and THP-1 cells stimulated with LPS+ATP were used for NLRP3 and Occludin visualization, whereas HBECs from RV-A16+SARS-CoV-2 model were used for ACE2 and SARS-CoV-2 Protein N staining. Following fixation in 4% (wt/vol) PFA in PBS (Fluka, Fluka/Sigma Aldrich, Buchs, Switzerland), THP-1 cytospins were lined with the PAP pen (Sigma Aldrich, St. Louis, USA), HBECs were stained on the insert, whereas ¼ of the ALI insert from RV-A16+SARS-CoV-2 model were prepared for cryosections by freezing in Clear Frozen Section Compound (FSC22, Leica, Wetzlar, Germany), cut at 6 µm in a cryostat (LEICA CM3050S, Leica Microsystems, Wetzlar, Germany) and mounted on *SuperFrost Plus™* glass slides (Menzel, ThermoFisher, Waltham, USA). Samples were incubated in the blocking solution (10% normal goat serum, 1% bovine serum albumin and 0.2% TritonX-100 in PBS) (Dako, Agilent, Santa Clara, USA) for 1h at RT. Primary antibodies for NLRP3 (5 µg/mL, mouse anti-NLRP3, Adipogen, San Diego, USA), Occludin (2.5 µg/mL, mouse anti-Occludin, ThermoFisher, Waltham, USA), ACE-2 (2 µg/mL, rabbit anti-ACE2, Abcam, Cambridge, UK), and SARS-CoV-2 Protein N (1 µg/mL, mouse anti-Protein N, ThermoFisher, Waltham, USA) diluted in blocking solution (1:1 in PBS) and incubated at 4°C overnight. Proper isotype controls, in the concentrations corresponding to the antibodies, were used (Dako, Agilent, Santa Clara, USA). Following three washing steps in 0.05% Tween20 in PBS, secondary antibodies with DAPI (1 µg/mL, Sigma Aldrich, St. Louis, USA) in diluted blocking solution (1:1 in PBS) were applied for 2h at RT in the dark. Sections have been washed three times in 0.05%Tween20 in PBS before mounting with Fluoromount (Sigma Aldrich, St. Louis, USA). Image acquisition was performed with Zeiss LSM780 (Zeiss, Oberkochen, Germany), by using 40x objective and ZEN software (Zeiss, Oberkochen, Germany). ImageJ/Fiji[128] was used for tale scan stitching and image analysis.

Bronchial biopsies were collected from the control individuals and patients with asthma at baseline and 4 days after in vivo RV-A16 infection. Biopsies were fixed and embedded in the paraffin blocks, sections were cut, and placed on the glass slides as described previously[96]. Prepared slides were baked 30 minutes in 65°C, followed by the deparaffinization with xylol (2x10 min), graded isopropanol (2x3 mins 100%, 2x3 mins 96% and 3 mins 70%), and rehydration (2x5 mins in H_20_2). Samples were boiled in the sodium citrate buffer (10mM sodium citrate with 0.05% Tween 20 in PBS at pH6) in the pressure cooker for 4 mins, as described previously[129]. Samples were permeabilized and blocked with the Perm/Block Buffer (1%BSA+0.2%TritonX100+10% goat serum in PBS) for 25 minutes in RT. All antibodies were diluted in 4% goat

serum + 0.05% Tween20 in PBS, and 50 μl of antibodies per sample were used. Primary antibodies for IL-1β (10 μg/mL, mouse anti-IL1β, Abcam, Cambridge, UK), caspase-1 (1:50, rabbit anti-caspase 1, Cell Signaling, Danvers, USA), and RIG-I (1:250, mouse anti RIG-I, Santa Cruz Biotechnology, Santa Cruz, USA) were incubated in the wet chamber overnight at 4°C. Appropriate mouse and rabbit isotype controls, in the concentrations corresponding to the antibodies, were used (Dako, Agilent, Santa Clara, USA). Subsequently, samples were incubated with the goat anti-rabbit Alexa Fluor 488 (for caspase-1), and the goat anti-mouse Alexa Fluor 546 (for IL-1β and RIG-I) secondary antibodies for 60 minutes in RT in the concentration of 1:1000 (Invitrogen, Waltham, USA). After 3 minutes' incubation in 1% PFA in room temperature, samples were mounted in the ProLong Gold mounting medium containing DAPI (Life Technologies, Carlsbad, USA) according to the manufacturer's instructions, analyzed with a Zeiss LSM780 (Zeiss, Oberkochen, Germany) and Zen Software (Zeiss, Oberkochen, Germany). All pictures were taken at the 40x magnification and are presented as the maximal projection (orthogonal projection) from 4 z-stacks, with appropriate scale bar. For the quantification, 10 equal squares from epithelial areas of the tissue (assessed using Haematoxylin and Eosin staining of the adjacent slice) from stained and isotype control samples were measured for signal intensity and averaged. Isotype control signal was further subtracted from the intensity of the stained samples, and values from 10 squares per sample were presented as the mean fluorescent intensity (MFI) of the protein expression.

Transcriptome analyses

Next generation sequencing (NGS) from the differentiated human bronchial epithelial cells (HBECs) from control individuals and patients with asthma (cohort A) was performed as previously described[107]. Briefly, total RNA was isolated with a RNeasy Plus Micro Kit (Qiagen, Hilden, Germany). Library was prepared with the TruSeq Stranded mRNA Sample Prep Kit (Illumina, San Diego, USA), and sequenced on the Illumina HiSeq 4000 platform. Description of the study subjects is presented in the Supplementary Table S7.

HBECs from 6 control individuals and 6 patients with asthma, infected with RV-A16 in the MOI 10 for 24h were harvested and sequenced with the use of Illumina HiSeq 2000 platform, as described previously[66]. The mRNA expression data are publicly available at the Gene Expression Omnibus platform (https://www.ncbi.nlm.nih.gov/) under the accession number: GSE61141[66].

Bronchial brushings from control individuals and patients with asthma before and after experimental RV-A16 infection in vivo were analyzed by Affymetrix HuGene 1.0 array according to the manufacturer's instructions and Transcriptome Analysis Console v4.0 (Santa Clara, United States).

Data analysis

Distribution (normality) of the data was assessed with Shapiro-Wilk test. One-way ANOVA (Kruskal-Wallis test), RM one-way ANOVA (Friedman test) or mixed-effects model tests were performed for more than three groups comparisons depending on the data relation (paired/not-paired) and distribution (normal/not-normal). Two-tailed paired/not-paired t-test or Wilcoxon/U-Mann-Whitney tests were performed for two groups comparisons depending on the data relation and distribution. The data are presented as the mean ± SEM, with the number of samples in each experiment indicated in the figure description. IL-1β expression in BAL fluid from cohort SIBRO was analyzed with the Welsh`s test. Correlations regarding inflammasome and antiviral signatures between in vitro and in vivo RV-A16-infection models were calculated with Pearson`s correlation coefficient, or Spearman`s rank correlation coefficient (depending on data distribution) between genes significant both in vivo and in vitro (red) and gene significant in at least one type of experiment (black). All differences were considered significant when p≤0.05 and defined as *p-value≤0.05, **p-value≤0.01, ***p-value≤0.001, ****p-value≤0.0001. Statistical analysis was performed with the Prism 9 software (Redmond, USA).

Transcriptome data were processed with the workflow available at https://github.com/uzh/ezRun, with the significance threshold for differentially expressed genes set to p-value<.05 calculated for the entire gene lists in each project using the edgeR R package[130]. Microarray data was analyzed by the following Bioconductor microarray analysis workflow https://www.bioconductor.org/packages/release/workflows/vignettes/arrays/inst/doc/arrays.html. Differentially expressed probe was identified by the limma R package with empirical Bayes estimation. Threshold for significance for transcriptome data presented on the figures are as follows: p-value: *<0.05; **<0.005; ***<0.0005, ****<0.00005. Heatmaps display normalized gene expression across the gene in the groups (row normalization). Additionally, top 100 genes upregulated after RV-A16 infection in the HBECs from control individuals and patients with asthma from GSE61141[66] were analyzed for the enriched pathways using Metacore software version 20.3.70200 (Thomson Reuters, Toronto, Canada) (Supplementary Table S1). Inflammasome-mediated immune responses and antiviral responses gene sets were curated from GSEA and MSigDB Database (Broad Institute, Massachusetts Institute of Technology, and Reagent of the University of California, USA). Full sets of analyzed genes are described in the Supplementary Table S10.

Proximity Extension Assay (PEA) normalizes protein expression (NPX) data were analyzed with the use of the internal Shiny App Olink data analysis toolkit http://46.14.201.130:3838/OlinkR_shinyApp .The statistical comparison of protein expression between groups was performed with the Bioconductor limma package[131]. The fold change and p-value were estimated by fitting a linear model for each protein. Proteins with p-value<0.05 were considered significant. Additionally, for Target 96 Inflammation panel data are presented as:

i) heatmaps of curated signatures of inflammasome-mediated immune responses and antiviral responses (Supplementary Table S10) and ii) protein interactions and pathways analysis prepared using the STRING (version 11.0)[132], and further processed with the Cytoscape software (version 3.8.2)[133] (Supplementary Table S3). The list of all proteins available for PEA measurements at the moment of the current analysis, that were used as a background reference for STRING analyses for targeted proteomics data is presented in Supplementary Table S11.

5. Data availability

Transcriptome data from bronchial brushings from control individuals and patients with asthma experimentally infected with RV-A16 has been submitted to the NCBI GEO: GSE185658 and will be publicly available at the time of publication. All other data are included in the Online Supplement or are available from the corresponding author upon request.

6. Code availability

The codes for transcriptome data analysis are available here: https://github.com/uzh/ezRun (NGS), https://github.com/ge11232002/p1688-Ula (microarray). Code for Proximity Extension Assay data analysis is available from the corresponding author upon request. All codes will be publicly available at the time of publication.

7. Acknowledgements

The Authors are grateful to all patients, clinicians and research staff involved in securing and processing patients samples. We would like to thank David Mirer for rhinovirus plaque assay analyses. HDM extract was a gift from Allergopharma AG. This work was supported by the Swiss National Science Foundation (SNSF) grant nr 310030_189334/1, European Respiratory Society Long-term research fellowships, European Academy of Allergy and Clinical Immunology long-term research fellowship and GSK research grant (to MS), and the SNF grant nr 320030_176190 and GSK (to CA). The in vivo work was supported by the European Research Council (ERC FP7 grant number 233015); a Chair from Asthma UK (CH11SJ); the Medical Research Council Centre (grant number G1000758); National Institute of Health Research (NIHR) Biomedical Research Centre (grant number P26095); Predicta FP7 Collaborative Project (grant number 260895); and the NIHR Biomedical Research Centre at Imperial College London. SLJ is an Emeritus NIHR Senior Investigator. The in vivo transcriptome work was supported by GSK. UR, AE and MM were supported from funds from the Leading National Research Centre

(KNOW) in Bialystok, Poland. JRC was supported by an FPI-CEU predoctoral fellowship and the Swiss-European Mobility Programme.

8. Authors contributions

Concept design: MiSo. Data collection: UR, AE, MiSo, NS, AH, PaWe, SS, AD, PaWa, BR, JRC, DZ, MH, JB, MaSa, LOM, DJJ, MRE, TK. Analysis/interpretation of data: UR, AE, MiSo, GT, CA. Write/intellectual contribution: UR, AE, MiSo, CA, MM, TV, SJ. All authors approved the final version of the manuscript.

9. Ethics declaration

CA reports research grants from Allergopharma, Idorsia, Swiss National Science Foundation, Christine Kühne-Center for Allergy Research and Education, European Commission's Horison's 2020 Framework Programme "Cure", Novartis Research Institutes, Astrazeneca, SciBase, Stanford University SEAN Parker Asthma and Allergy Center; advisory board of Sanofi/Regeneron, GSK and Novartis, consulting fees from Novartis; Editor-in-Chief Allergy, Co-Chair EAACI Environmental Science in Allergic Diseases and Asthma Guidelines. AE reports National Science Centre Grant No. 2020/37/N/NZ5/04144, National Centre for Research and Development No. STRATEGMED2/269807/14/NCBR/2015, National Centre for Research and Development (POLTUR3/MT-REMOD/2/2019). DJJ reports advisory board and speaker fees from AstraZeneca, GSK and Sanofi and research grants from AstraZeneca. SLJ reports grants/contracts from European Research Council ERC FP7 grant number 233015, Chair from Asthma UK CH11SJ, Medical Research Council Centre grant number G1000758, NIHR Biomedical Research Centre grant number P26095, Predicta FP7 Collaborative Project grant number 260895, NIHR Emeritus NIHR Senior Investigator; consulting fees from Lallemand Pharma, Bioforce, resTORbio, Gerson Lehrman Group, Boehringer Ingelheim, Novartis, Bayer, Myelo Therapeutics GmbH; patents issued/licensed: Wark PA, Johnston SL, Holgate ST, Davies DE. Anti-virus therapy for respiratory diseases. UK patent application No. GB 0405634.7, 12March 2004. Wark PA, Johnston SL, Holgate ST, Davies DE. Interferon-Beta for Anti-Virus Therapy for Respiratory Diseases. International Patent Application No. PCT/GB05/50031, 12 March 2004. Davies DE, Wark PA, Holgate ST, JohnstonSL. Interferon Lambda therapy for the treatment of respiratory disease. UK patent application No. 6779645.9, granted15th August 2012; Participation on a data safety monitory board or advisory board: Enanta Chair of DSMB, Virtus Respiratory Research Board membership. MM reports personal payments from Astra Zeneca, GSK, Berlin-Chemie/Menarini, Lek-AM, Takeda, Celon and support for attending meetings from Astra Zeneca, GSK, Berlin-Biochemie/Menarini. UR reports board secretary position of Working Group of Genomics and Proteomics of the European Academy of Allergy and Clinical Immunology (EAACI). JRC reports Pre-doctoral grant FPI from Universidad CEU San Pablo, Swiss European Mobility Program grant from University of Zurich, EAACI Mid-term Fellowship. MiSo reports research grants from Swiss National Science Foundation, GSK, Novartis and speakers fee from AstraZeneca and board secretary position of the Basic and Clinical Immunology Section of the European Academy of Allergy and Clinical Immunology (EAACI). SS reports funding from National Center of Competence in Research (NCCR) on RNA and Disease to VT (https://nccr-rna-and-disease.ch/). VT reports grant from Swiss National Science Foundation. All other authors report no conflict of interest regarding this work.

10. References

1. Devereux, G. The increase in the prevalence of asthma and allergy: food for thought. *Nat Rev Immunol* **6**, 869-874 (2006).
2. Akdis, C.A. Does the epithelial barrier hypothesis explain the increase in allergy, autoimmunity and other chronic conditions? *Nat Rev Immunol* (2021).
3. Global Initiative for Asthma. Global Strategy for Asthma Management and Prevention, 2020. Available from: www.ginasthma.org. (2020).
4. Chung, K.F.*, et al.* International ERS/ATS guidelines on definition, evaluation and treatment of severe asthma. *The European respiratory journal* **43**, 343-373 (2014).
5. Papadopoulos, N.G.*, et al.* Viruses and bacteria in acute asthma exacerbations--a GA(2) LEN-DARE systematic review. *Allergy* **66**, 458-468 (2011).
6. Kim, C.K., Callaway, Z. & Gern, J.E. Viral Infections and Associated Factors That Promote Acute Exacerbations of Asthma. *Allergy, asthma & immunology research* **10**, 12-17 (2018).
7. Hai le, T.*, et al.* Fatal respiratory infections associated with rhinovirus outbreak, Vietnam. *Emerging infectious diseases* **18**, 1886-1888 (2012).
8. Kiang, D.*, et al.* Molecular characterization of a variant rhinovirus from an outbreak associated with uncommonly high mortality. *Journal of clinical virology : the official publication of the Pan American Society for Clinical Virology* **38**, 227-237 (2007).
9. Rubner, F.J.*, et al.* Early life rhinovirus wheezing, allergic sensitization, and asthma risk at adolescence. *J Allergy Clin Immunol* **139**, 501-507 (2017).
10. Lee, W.M.*, et al.* Human rhinovirus species and season of infection determine illness severity. *Am J Respir Crit Care Med* **186**, 886-891 (2012).
11. Jartti, T., Bønnelykke, K., Elenius, V. & Feleszko, W. Role of viruses in asthma. *Seminars in immunopathology* **42**, 61-74 (2020).
12. Schultze, A.*, et al.* Risk of COVID-19-related death among patients with chronic obstructive pulmonary disease or asthma prescribed inhaled corticosteroids: an observational cohort study using the OpenSAFELY platform. *The Lancet Respiratory Medicine* **8**, 1106-1120 (2020).
13. Williamson, E.J.*, et al.* Factors associated with COVID-19-related death using OpenSAFELY. *Nature* **584**, 430-436 (2020).
14. Bloom, C.I.*, et al.* Risk of adverse outcomes in patients with underlying respiratory conditions admitted to hospital with COVID-19: a national, multicentre prospective cohort study using the ISARIC WHO Clinical Characterisation Protocol UK. *The Lancet. Respiratory medicine* **9**, 699-711 (2021).
15. Skevaki, C.*, et al.* SARS-CoV-2 infection and COVID-19 in asthmatics: a complex relationship. *Nat Rev Immunol* **21**, 202-203 (2021).
16. Skevaki, C., Karsonova, A., Karaulov, A., Xie, M. & Renz, H. Asthma-associated risk for COVID-19 development. *J Allergy Clin Immunol* **146**, 1295-1301 (2020).
17. Sánchez-Borges, M.*, et al.* International consensus (ICON) on: clinical consequences of mite hypersensitivity, a global problem. *The World Allergy Organization journal* **10**, 14 (2017).
18. Smith, A.M.*, et al.* Repetitive aeroallergen challenges elucidate maladaptive epithelial and inflammatory traits that underpin allergic airway diseases. *J Allergy Clin Immunol* (2021).
19. Soto-Quiros, M.*, et al.* High titers of IgE antibody to dust mite allergen and risk for wheezing among asthmatic children infected with rhinovirus. *J Allergy Clin Immunol* **129**, 1499-1505.e1495 (2012).

20. Murray, C.S*., et al.* Study of modifiable risk factors for asthma exacerbations: virus infection and allergen exposure increase the risk of asthma hospital admissions in children. *Thorax* **61**, 376-382 (2006).
21. Virchow, J.C*., et al.* Efficacy of a House Dust Mite Sublingual Allergen Immunotherapy Tablet in Adults With Allergic Asthma: A Randomized Clinical Trial. *Jama* **315**, 1715-1725 (2016).
22. Balz, K*., et al.* Homologies between SARS-CoV-2 and allergen proteins may direct T cell-mediated heterologous immune responses. *Scientific reports* **11**, 4792 (2021).
23. Damialis, A*., et al.* Higher airborne pollen concentrations correlated with increased SARS-CoV-2 infection rates, as evidenced from 31 countries across the globe. *Proc Natl Acad Sci U S A* **118**(2021).
24. Harker, J.A. & Lloyd, C.M. Overlapping and distinct features of viral and allergen immunity in the human lung. *Immunity* **54**, 617-631 (2021).
25. Slater, L*., et al.* Co-ordinated role of TLR3, RIG-I and MDA5 in the innate response to rhinovirus in bronchial epithelium. *PLoS Pathog* **6**, e1001178 (2010).
26. Triantafilou, K*., et al.* Human rhinovirus recognition in non-immune cells is mediated by Toll-like receptors and MDA-5, which trigger a synergetic pro-inflammatory immune response. *Virulence* **2**, 22-29 (2011).
27. Wang, Q*., et al.* Role of double-stranded RNA pattern recognition receptors in rhinovirus-induced airway epithelial cell responses. *J Immunol* **183**, 6989-6997 (2009).
28. Xander, N*., et al.* Rhinovirus-Induced SIRT-1 via TLR2 Regulates Subsequent Type I and Type III IFN Responses in Airway Epithelial Cells. *J Immunol* **203**, 2508-2519 (2019).
29. Wu, B. & Hur, S. How RIG-I like receptors activate MAVS. *Current opinion in virology* **12**, 91-98 (2015).
30. Rehwinkel, J. & Gack, M.U. RIG-I-like receptors: their regulation and roles in RNA sensing. *Nature Reviews Immunology* **20**, 537-551 (2020).
31. Wu, W*., et al.* RIG-I and TLR3 are both required for maximum interferon induction by influenza virus in human lung alveolar epithelial cells. *Virology* **482**, 181-188 (2015).
32. Crotta, S*., et al.* Type I and type III interferons drive redundant amplification loops to induce a transcriptional signature in influenza-infected airway epithelia. *PLoS Pathog* **9**, e1003773 (2013).
33. Schoggins, J.W. & Rice, C.M. Interferon-stimulated genes and their antiviral effector functions. *Current opinion in virology* **1**, 519-525 (2011).
34. Warner, S.M., Wiehler, S., Michi, A.N. & Proud, D. Rhinovirus replication and innate immunity in highly differentiated human airway epithelial cells. *Respir Res* **20**, 150 (2019).
35. Contoli, M*., et al.* Th2 cytokines impair innate immune responses to rhinovirus in respiratory epithelial cells. *Allergy* **70**, 910-920 (2015).
36. Patel, D.A*., et al.* Interferon response and respiratory virus control are preserved in bronchial epithelial cells in asthma. *J Allergy Clin Immunol* **134**, 1402-1412 e1407 (2014).
37. Edwards, M.R*., et al.* Impaired innate interferon induction in severe therapy resistant atopic asthmatic children. *Mucosal Immunol* **6**, 797-806 (2013).
38. Sokolowska, M*., et al.* Dysregulation of lipidomic profile and antiviral immunity in response to hyaluronan in patients with severe asthma. *J Allergy Clin Immunol* **139**, 1379-1383 (2017).
39. Jansen, K*., et al.* Loss of regulatory capacity in T regulatory cells upon rhinovirus infection. *J Allergy Clin Immunol* (2021).
40. Silkoff, P.E*., et al.* Toll-like receptor 3 blockade in rhinovirus-induced experimental asthma exacerbations: A randomized controlled study. *J Allergy Clin Immunol* **141**, 1220-1230 (2018).

41. Johnston, S.L. IFN Therapy in Airway Disease: Is Prophylaxis a New Approach in Exacerbation Prevention? *Am J Respir Crit Care Med* **201**, 9-11 (2020).
42. Djukanovic, R.*, et al.* The Effect of Inhaled Interferon-beta on Worsening of Asthma Symptoms Caused by Viral Infections: a Randomised Trial. *Am J Respir Crit Care Med* (2014).
43. Tan, K.S.*, et al.* In Vitro Model of Fully Differentiated Human Nasal Epithelial Cells Infected With Rhinovirus Reveals Epithelium-Initiated Immune Responses. *The Journal of infectious diseases* **217**, 906-915 (2018).
44. Custovic, A.*, et al.* Cytokine Responses to Rhinovirus and Development of Asthma, Allergic Sensitization, and Respiratory Infections during Childhood. *Am J Respir Crit Care Med* **197**, 1265-1274 (2018).
45. Hammad, H.*, et al.* House dust mite allergen induces asthma via Toll-like receptor 4 triggering of airway structural cells. *Nat Med* **15**, 410-416 (2009).
46. Tan, H.T.*, et al.* Tight junction, mucin, and inflammasome-related molecules are differentially expressed in eosinophilic, mixed, and neutrophilic experimental asthma in mice. *Allergy* **74**, 294-307 (2019).
47. Schuijs, M.J.*, et al.* Farm dust and endotoxin protect against allergy through A20 induction in lung epithelial cells. *Science* **349**, 1106-1110 (2015).
48. Strowig, T., Henao-Mejia, J., Elinav, E. & Flavell, R. Inflammasomes in health and disease. *Nature* **481**, 278-286 (2012).
49. Lu, A.*, et al.* Unified polymerization mechanism for the assembly of ASC-dependent inflammasomes. *Cell* **156**, 1193-1206 (2014).
50. Poeck, H.*, et al.* Recognition of RNA virus by RIG-I results in activation of CARD9 and inflammasome signaling for interleukin 1 beta production. *Nature immunology* **11**, 63-69 (2010).
51. Han, M.*, et al.* Inflammasome activation is required for human rhinovirus-induced airway inflammation in naive and allergen-sensitized mice. *Mucosal Immunol* **12**, 958-968 (2019).
52. Pothlichet, J.*, et al.* Type I IFN triggers RIG-I/TLR3/NLRP3-dependent inflammasome activation in influenza A virus infected cells. *PLoS Pathog* **9**, e1003256 (2013).
53. Triantafilou, K., Kar, S., van Kuppeveld, F.J. & Triantafilou, M. Rhinovirus-induced calcium flux triggers NLRP3 and NLRC5 activation in bronchial cells. *Am J Respir Cell Mol Biol* **49**, 923-934 (2013).
54. Ichinohe, T., Pang, I.K. & Iwasaki, A. Influenza virus activates inflammasomes via its intracellular M2 ion channel. *Nat Immunol* **11**, 404-410 (2010).
55. Allen, I.C.*, et al.* The NLRP3 inflammasome mediates in vivo innate immunity to influenza A virus through recognition of viral RNA. *Immunity* **30**, 556-565 (2009).
56. Siu, K.L.*, et al.* Severe acute respiratory syndrome coronavirus ORF3a protein activates the NLRP3 inflammasome by promoting TRAF3-dependent ubiquitination of ASC. *FASEB journal : official publication of the Federation of American Societies for Experimental Biology* **33**, 8865-8877 (2019).
57. Chen, I.Y., Moriyama, M., Chang, M.F. & Ichinohe, T. Severe Acute Respiratory Syndrome Coronavirus Viroporin 3a Activates the NLRP3 Inflammasome. *Frontiers in microbiology* **10**, 50 (2019).
58. Campbell, G.R., To, R.K., Hanna, J. & Spector, S.A. SARS-CoV-2, SARS-CoV-1, and HIV-1 derived ssRNA sequences activate the NLRP3 inflammasome in human macrophages through a non-classical pathway. *iScience* **24**, 102295 (2021).

59. Junqueira, C.*, et al.* SARS-CoV-2 infects blood monocytes to activate NLRP3 and AIM2 inflammasomes, pyroptosis and cytokine release. *medRxiv : the preprint server for health sciences* (2021).
60. Lupfer, C.*, et al.* Receptor interacting protein kinase 2-mediated mitophagy regulates inflammasome activation during virus infection. *Nat Immunol* **14**, 480-488 (2013).
61. Spel, L. & Martinon, F. Detection of viruses by inflammasomes. *Current opinion in virology* **46**, 59-64 (2021).
62. Eisenbarth, S.C., Colegio, O.R., O'Connor, W., Sutterwala, F.S. & Flavell, R.A. Crucial role for the Nalp3 inflammasome in the immunostimulatory properties of aluminium adjuvants. *Nature* **453**, 1122-1126 (2008).
63. Allen, I.C.*, et al.* Analysis of NLRP3 in the development of allergic airway disease in mice. *J Immunol* **188**, 2884-2893 (2012).
64. Rossios, C.*, et al.* Sputum transcriptomics reveal upregulation of IL-1 receptor family members in patients with severe asthma. *J Allergy Clin Immunol* **141**, 560-570 (2018).
65. Tzeng, T.C.*, et al.* A Fluorescent Reporter Mouse for Inflammasome Assembly Demonstrates an Important Role for Cell-Bound and Free ASC Specks during In Vivo Infection. *Cell Rep* **16**, 571-582 (2016).
66. Bai, J.*, et al.* Phenotypic responses of differentiated asthmatic human airway epithelial cultures to rhinovirus. *PLoS One* **10**, e0118286 (2015).
67. Jackson, D.J.*, et al.* IL-33-dependent type 2 inflammation during rhinovirus-induced asthma exacerbations in vivo. *Am J Respir Crit Care Med* **190**, 1373-1382 (2014).
68. Zhu, X.*, et al.* Interleukin-15 expression is increased in human eosinophilic esophagitis and mediates pathogenesis in mice. *Gastroenterology* **139**, 182-193.e187 (2010).
69. Yuan, H.*, et al.* Transmembrane-Bound IL-15-Promoted Epithelial-Mesenchymal Transition in Renal Cancer Cells Requires the Src-Dependent Akt/GSK-3β/β-Catenin Pathway. *Neoplasia (New York, N.Y.)* **17**, 410-420 (2015).
70. Zhang, M.*, et al.* Artemin is hypoxia responsive and promotes oncogenicity and increased tumor initiating capacity in hepatocellular carcinoma. *Oncotarget* **7**, 3267-3282 (2016).
71. Park, S.J., Kim, H.J., Lee, J.S., Cho, H.R. & Kwon, B. Reverse signaling through the co-stimulatory ligand, CD137L, as a critical mediator of sterile inflammation. *Molecules and cells* **33**, 533-537 (2012).
72. Hofmann, M.A.*, et al.* RAGE mediates a novel proinflammatory axis: a central cell surface receptor for S100/calgranulin polypeptides. *Cell* **97**, 889-901 (1999).
73. Mühlebach, M.D.*, et al.* Adherens junction protein nectin-4 is the epithelial receptor for measles virus. *Nature* **480**, 530-533 (2011).
74. Cagnoni, F.*, et al.* CD40 on Adult Human Airway Epithelial Cells: Expression and Proinflammatory Effects. *The Journal of Immunology* **172**, 3205-3214 (2004).
75. Dugger, K., Lowder, T.W., Tucker, T.A. & Schwiebert, L.M. Epithelial cells as immune effector cells: the role of CD40. *Seminars in immunology* **21**, 289-292 (2009).
76. Infante, M.*, et al.* RANKL/RANK/OPG system beyond bone remodeling: involvement in breast cancer and clinical perspectives. *Journal of experimental & clinical cancer research : CR* **38**, 12 (2019).
77. Loser, K.*, et al.* Epidermal RANKL controls regulatory T-cell numbers via activation of dendritic cells. *Nat Med* **12**, 1372-1379 (2006).
78. Mitoma, H.*, et al.* The DHX33 RNA helicase senses cytosolic RNA and activates the NLRP3 inflammasome. *Immunity* **39**, 123-135 (2013).

79. Delaloye, J.*, et al.* Innate immune sensing of modified vaccinia virus Ankara (MVA) is mediated by TLR2-TLR6, MDA-5 and the NALP3 inflammasome. *PLoS Pathog* **5**, e1000480 (2009).
80. Kummer, J.A.*, et al.* Inflammasome components NALP 1 and 3 show distinct but separate expression profiles in human tissues suggesting a site-specific role in the inflammatory response. *J Histochem Cytochem* **55**, 443-452 (2007).
81. Rintahaka, J., Wiik, D., Kovanen, P.E., Alenius, H. & Matikainen, S. Cytosolic antiviral RNA recognition pathway activates caspases 1 and 3. *J Immunol* **180**, 1749-1757 (2008).
82. Lopez-Souza, N.*, et al.* Resistance of differentiated human airway epithelium to infection by rhinovirus. *American journal of physiology. Lung cellular and molecular physiology* **286**, L373-381 (2004).
83. Jakiela, B.*, et al.* Remodeling of bronchial epithelium caused by asthmatic inflammation affects its response to rhinovirus infection. *Scientific reports* **11**, 12821 (2021).
84. Martinez-Anton, A.*, et al.* Changes in microRNA and mRNA expression with differentiation of human bronchial epithelial cells. *Am J Respir Cell Mol Biol* **49**, 384-395 (2013).
85. Lewis-Rogers, N., Seger, J. & Adler, F.R. Human Rhinovirus Diversity and Evolution: How Strange the Change from Major to Minor. *J Virol* **91**(2017).
86. Tian, Z., Shen, X., Feng, H. & Gao, B. IL-1 beta attenuates IFN-alpha beta-induced antiviral activity and STAT1 activation in the liver: involvement of proteasome-dependent pathway. *J Immunol* **165**, 3959-3965 (2000).
87. Kohase, M.*, et al.* Interleukin-1 can inhibit interferon-beta synthesis and its antiviral action: comparison with tumor necrosis factor. *Journal of interferon research* **8**, 559-570 (1988).
88. Mayer-Barber, K.D.*, et al.* Host-directed therapy of tuberculosis based on interleukin-1 and type I interferon crosstalk. *Nature* **511**, 99-103 (2014).
89. Guarda, G.*, et al.* Type I interferon inhibits interleukin-1 production and inflammasome activation. *Immunity* **34**, 213-223 (2011).
90. Novikov, A.*, et al.* Mycobacterium tuberculosis triggers host type I IFN signaling to regulate IL-1β production in human macrophages. *J Immunol* **187**, 2540-2547 (2011).
91. Padayachee, Y., Faiez, T.S., Singanayagam, A., Mallia, P. & Johnston, S.L. Asthma and viruses: A focus on rhinoviruses and SARS-CoV-2. *The Journal of allergy and clinical immunology* **147**, 1648-1651 (2021).
92. Contoli, M.*, et al.* Role of deficient type III interferon-lambda production in asthma exacerbations. *Nat Med* **12**, 1023-1026 (2006).
93. Sykes, A.*, et al.* Rhinovirus-induced interferon production is not deficient in well controlled asthma. *Thorax* **69**, 240-246 (2014).
94. Wark, P.A.*, et al.* Asthmatic bronchial epithelial cells have a deficient innate immune response to infection with rhinovirus. *J Exp Med* **201**, 937-947 (2005).
95. Veerati, P.C.*, et al.* Airway Epithelial Cell Immunity Is Delayed During Rhinovirus Infection in Asthma and COPD. *Front Immunol* **11**, 974 (2020).
96. Zhu, J.*, et al.* Bronchial mucosal IFN-alpha/beta and pattern recognition receptor expression in patients with experimental rhinovirus-induced asthma exacerbations. *J Allergy Clin Immunol* **143**, 114-125 e114 (2019).
97. Watson, A.*, et al.* Dynamics of IFN-β Responses during Respiratory Viral Infection. Insights for Therapeutic Strategies. *American journal of respiratory and critical care medicine* **201**, 83-94 (2020).
98. McCrae, C.*, et al.* INEXAS: A Phase 2 Randomized Trial of On-demand Inhaled Interferon Beta-1a in Severe Asthmatics. *Clin Exp Allergy* **51**, 273-283 (2021).

99. Kupczyk, M., *et al.* Detection of exacerbations in asthma based on electronic diary data: results from the 1-year prospective BIOAIR study. *Thorax* **68**, 611-618 (2013).
100. Panganiban, R.A., *et al.* A functional splice variant associated with decreased asthma risk abolishes the ability of gasdermin B to induce epithelial cell pyroptosis. *J Allergy Clin Immunol* **142**, 1469-1478 e1462 (2018).
101. Jacobs, S.E., Lamson, D.M., St George, K. & Walsh, T.J. Human rhinoviruses. *Clin Microbiol Rev* **26**, 135-162 (2013).
102. Gill, M.A., *et al.* Enhanced plasmacytoid dendritic cell antiviral responses after omalizumab. *J Allergy Clin Immunol* **141**, 1735-1743 e1739 (2018).
103. Akbarshahi, H., *et al.* House dust mite impairs antiviral response in asthma exacerbation models through its effects on TLR3. *Allergy* **73**, 1053-1063 (2018).
104. Kloepfer, K.M., *et al.* Increased H1N1 infection rate in children with asthma. *Am J Respir Crit Care Med* **185**, 1275-1279 (2012).
105. Zhang, J.-j., *et al.* Clinical characteristics of 140 patients infected with SARS-CoV-2 in Wuhan, China. *Allergy* **75**, 1730-1741 (2020).
106. Zhu, Z., *et al.* Association of asthma and its genetic predisposition with the risk of severe COVID-19. *J Allergy Clin Immunol* **146**, 327-329 e324 (2020).
107. Radzikowska, U., *et al.* Distribution of ACE2, CD147, CD26, and other SARS-CoV-2 associated molecules in tissues and immune cells in health and in asthma, COPD, obesity, hypertension, and COVID-19 risk factors. *Allergy* **75**, 2829-2845 (2020).
108. Bradding, P., *et al.* ACE2, TMPRSS2, and furin gene expression in the airways of people with asthma-implications for COVID-19. *J Allergy Clin Immunol* **146**, 208-211 (2020).
109. Dee, K., *et al.* Human Rhinovirus Infection Blocks Severe Acute Respiratory Syndrome Coronavirus 2 Replication Within the Respiratory Epithelium: Implications for COVID-19 Epidemiology. *The Journal of infectious diseases* **224**, 31-38 (2021).
110. Gordon, D.E., *et al.* A SARS-CoV-2-Human Protein-Protein Interaction Map Reveals Drug Targets and Potential Drug-Repurposing. *bioRxiv* (2020).
111. Thorne, L.G., *et al.* SARS-CoV-2 sensing by RIG-I and MDA5 links epithelial infection to macrophage inflammation. *EMBO J* **40**, e107826 (2021).
112. Rodrigues, T.S., *et al.* Inflammasomes are activated in response to SARS-CoV-2 infection and are associated with COVID-19 severity in patients. *J Exp Med* **218**(2021).
113. Ferreira, A.C., *et al.* SARS-CoV-2 engages inflammasome and pyroptosis in human primary monocytes. *Cell Death Discov* **7**, 43 (2021).
114. Lei, X., *et al.* Activation and evasion of type I interferon responses by SARS-CoV-2. *Nat Commun* **11**, 3810 (2020).
115. Wu, J., *et al.* SARS-CoV-2 ORF9b inhibits RIG-I-MAVS antiviral signaling by interrupting K63-linked ubiquitination of NEMO. *Cell Rep* **34**, 108761 (2021).
116. Zheng, M., *et al.* TLR2 senses the SARS-CoV-2 envelope protein to produce inflammatory cytokines. *Nat Immunol* **22**, 829-838 (2021).
117. Mu, J., *et al.* SARS-CoV-2 N protein antagonizes type I interferon signaling by suppressing phosphorylation and nuclear translocation of STAT1 and STAT2. *Cell Discov* **6**, 65 (2020).
118. Lowery, S.A., Sariol, A. & Perlman, S. Innate immune and inflammatory responses to SARS-CoV-2: Implications for COVID-19. *Cell Host Microbe* **29**, 1052-1062 (2021).
119. Blanco-Melo, D., *et al.* Imbalanced Host Response to SARS-CoV-2 Drives Development of COVID-19. *Cell* **181**, 1036-1045 e1039 (2020).

120. Katsura, H.*, et al.* Human Lung Stem Cell-Based Alveolospheres Provide Insights into SARS-CoV-2-Mediated Interferon Responses and Pneumocyte Dysfunction. *Cell Stem Cell* **27**, 890-904 e898 (2020).
121. Lokugamage, K.G.*, et al.* Type I Interferon Susceptibility Distinguishes SARS-CoV-2 from SARS-CoV. *J Virol* **94**(2020).
122. Miorin, L.*, et al.* SARS-CoV-2 Orf6 hijacks Nup98 to block STAT nuclear import and antagonize interferon signaling. *Proc Natl Acad Sci U S A* **117**, 28344-28354 (2020).
123. Thi Nhu Thao, T.*, et al.* Rapid reconstruction of SARS-CoV-2 using a synthetic genomics platform. *Nature* **582**, 561-565 (2020).
124. Thiel, V., Herold, J., Schelle, B. & Siddell, S.G. Infectious RNA transcribed in vitro from a cDNA copy of the human coronavirus genome cloned in vaccinia virus. *Journal of General Virology* **82**, 1273-1281 (2001).
125. Michalovich, D.*, et al.* Obesity and disease severity magnify disturbed microbiome-immune interactions in asthma patients. *Nat Commun* **10**, 5711 (2019).
126. Wawrzyniak, P.*, et al.* Regulation of bronchial epithelial barrier integrity by type 2 cytokines and histone deacetylases in asthmatic patients. *J Allergy Clin Immunol* **139**, 93-103 (2017).
127. Sokolowska, M.*, et al.* Prostaglandin E2 Inhibits NLRP3 Inflammasome Activation through EP4 Receptor and Intracellular Cyclic AMP in Human Macrophages. *J Immunol* **194**, 5472-5487 (2015).
128. Schindelin, J.*, et al.* Fiji: an open-source platform for biological-image analysis. *Nature Methods* **9**, 676-682 (2012).
129. van de Veen, W.*, et al.* A novel proangiogenic B cell subset is increased in cancer and chronic inflammation. *Sci Adv* **6**, eaaz3559 (2020).
130. Robinson, M.D., McCarthy, D.J. & Smyth, G.K. edgeR: a Bioconductor package for differential expression analysis of digital gene expression data. *Bioinformatics* **26**, 139-140 (2010).
131. Ritchie, M.E.*, et al.* limma powers differential expression analyses for RNA-sequencing and microarray studies. *Nucleic Acids Research* **43**, e47-e47 (2015).
132. Szklarczyk, D.*, et al.* The STRING database in 2021: customizable protein-protein networks, and functional characterization of user-uploaded gene/measurement sets. *Nucleic Acids Res* **49**, D605-D612 (2021).
133. Shannon, P.*, et al.* Cytoscape: a software environment for integrated models of biomolecular interaction networks. *Genome Res* **13**, 2498-2504 (2003).

Figure 1

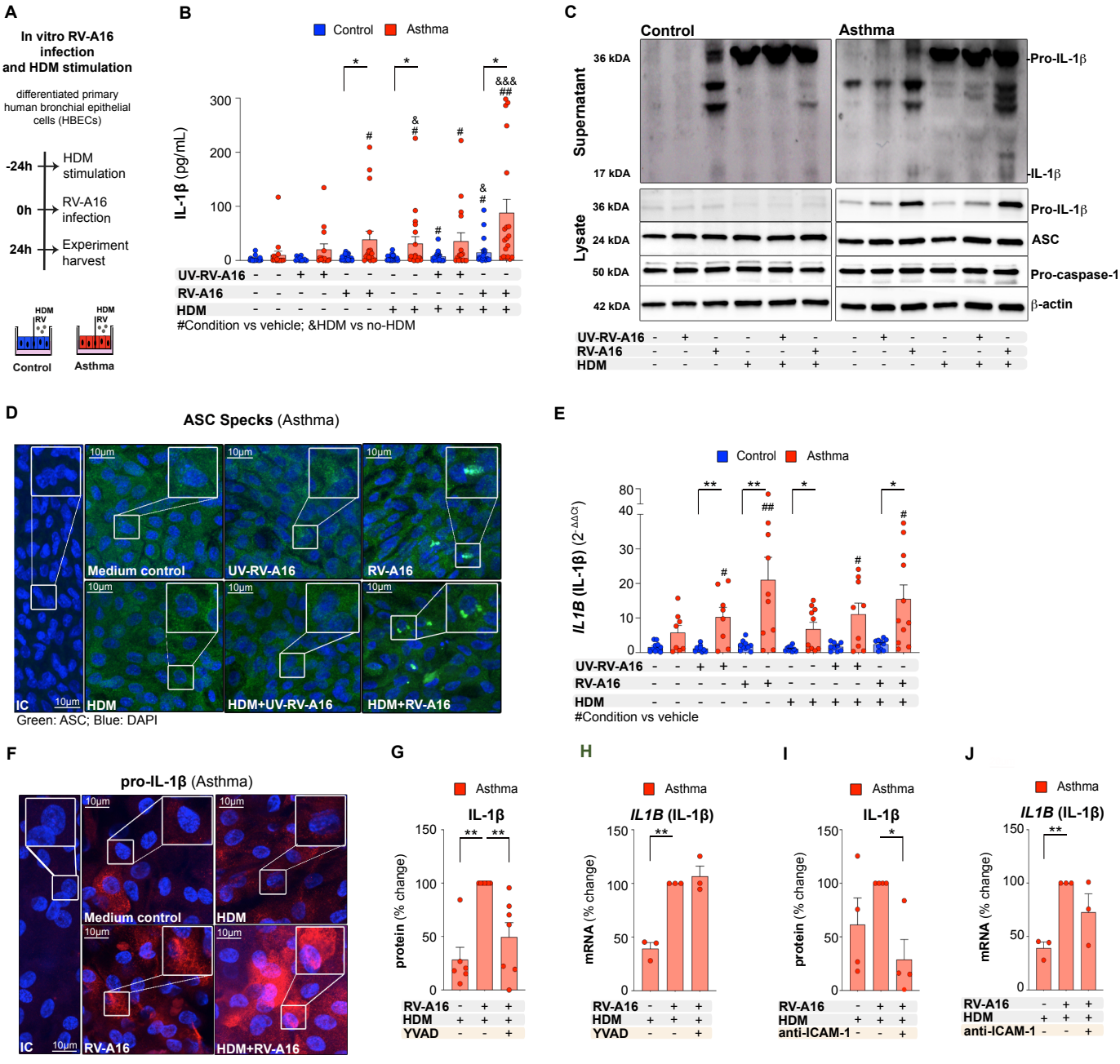
A
In vitro RV-A16 infection and HDM stimulation
differentiated primary human bronchial epithelial cells (HBECs)
-24h
HDM stimulation
0h
RV-A16 infection
24h
Experiment harvest
HDM
RV
Control
Asthma
B
Control
Asthma
IL-1β (pg/mL)
UV-RV-A16
RV-A16
HDM
#Condition vs vehicle; &HDM vs no-HDM
C
Control
Asthma
36 kDa
17 kDa
Supernatant
Pro-IL-1β
IL-1β
Lysate
36 kDa
24 kDa
50 kDa
42 kDa
Pro-IL-1β
ASC
Pro-caspase-1
β-actin
UV-RV-A16
RV-A16
HDM
D
ASC Specks (Asthma)
10μm
Medium control
UV-RV-A16
RV-A16
IC
HDM
HDM+UV-RV-A16
HDM+RV-A16
Green: ASC; Blue: DAPI
E
Control
Asthma
IL1B (IL-1β) (2-ΔΔCt)
UV-RV-A16
RV-A16
HDM
#Condition vs vehicle
F
pro-IL-1β (Asthma)
10μm
Medium control
HDM
IC
RV-A16
HDM+RV-A16
G
Asthma
IL-1β
protein (% change)
RV-A16
HDM
YVAD
H
Asthma
IL1B (IL-1β)
mRNA (% change)
RV-A16
HDM
YVAD
I
Asthma
IL-1β
protein (% change)
RV-A16
HDM
anti-ICAM-1
J
Asthma
IL1B (IL-1β)
mRNA (% change)
RV-A16
HDM
anti-ICAM-1

Figure 1

House dust mite increased rhinovirus-induced inflammasome activation in human bronchial epithelium in asthma

A) Experimental model overview. Primary air liquid interface (ALI)-differentiated human bronchial epithelial cells (HBECs) from control individuals and patients with asthma were treated with house dust mite (HDM) (200 μg/mL) or vehicle for 24h, followed by an infection with rhinovirus A16 (RV-A16) or UV-treated (UV)-RV-A16 in the multiplicity of infection (MOI) 0.1 for 24h. **B)** IL-1β release to the apical compartment assessed by ELISA (control n=14-22; asthma n=14-17). **C)** Representative Western Blot images of secreted IL-1β (apical compartment), and pro-IL-1β, ASC, pro-caspase-1 and β-actin (cell lysates) from HBECs from control subjects (left panel) and patients with asthma (right panel) **D)** Representative confocal images of ASC speck formation in HBECs from patients with asthma (n=3); scale bars: 10μm. **E)** mRNA expression of *IL1B* (IL1β) was assessed using RT-PCR, and presented as a relative quantification ($RQ=2^{-\Delta\Delta Ct}$) compared to the vehicle from the controls (control n=9-10, asthma n=8-10). **F)** Representative confocal images of IL-1β in HBECs from patients with asthma (n=3); scale bars: 10μm **G)** IL-1β release to the apical compartment assessed by ELISA (n=6-7), and **H)** mRNA expression of *IL1B* (IL1β) (n=3), in HBECs from patients with asthma in the presence or absence of caspase-1 inhibitor (YVAD). Data are presented as the percentage of the response after HDM+RV-A16 treatment. **I)** IL-1β release to the apical supernatants assessed by ELISA (n=4), and **J)** mRNA expression of *IL1B* (IL1β) in HBECs (n=3) from patients with asthma in the presence or absence of anti-ICAM-1 combined with HDM+RV-A16 stimulation. Data are presented as the percentage of the response after HDM+RV-A16 treatment. HBECs from patients with asthma are presented in red, HBECs from control individuals are presented in blue. (*) represents a significant difference as indicated. (#) represents a significant difference of the designated condition as compared to the vehicle from the same group. (&) represents a significant difference upon HDM treatment as compared to the corresponding condition without HDM. Bar graph data show mean ± SEM analyzed with one-way ANOVA (Kruskal-Wallis test), RM one-way ANOVA (Friedman test) or mixed-effects model, as appropriate, depending on the data relation (paired or unpaired) and distribution, *p-value≤0.05, **p-value≤0.01, ***p-value≤0.001. *ALI*; Air-liquid interface cultures; *anti-ICAM-1*, anti-ICAM-1 antibody; *IC*; Isotype control; *HDM*, house dust mite; *RV-A16*, rhinovirus A16; *UV-RV-A16*, UV-treated rhinovirus A16; *YVAD*, ac-YVAD-cmk (caspase-1 inhibitor); *MOI*, multiplicity of infection.

Figure 2

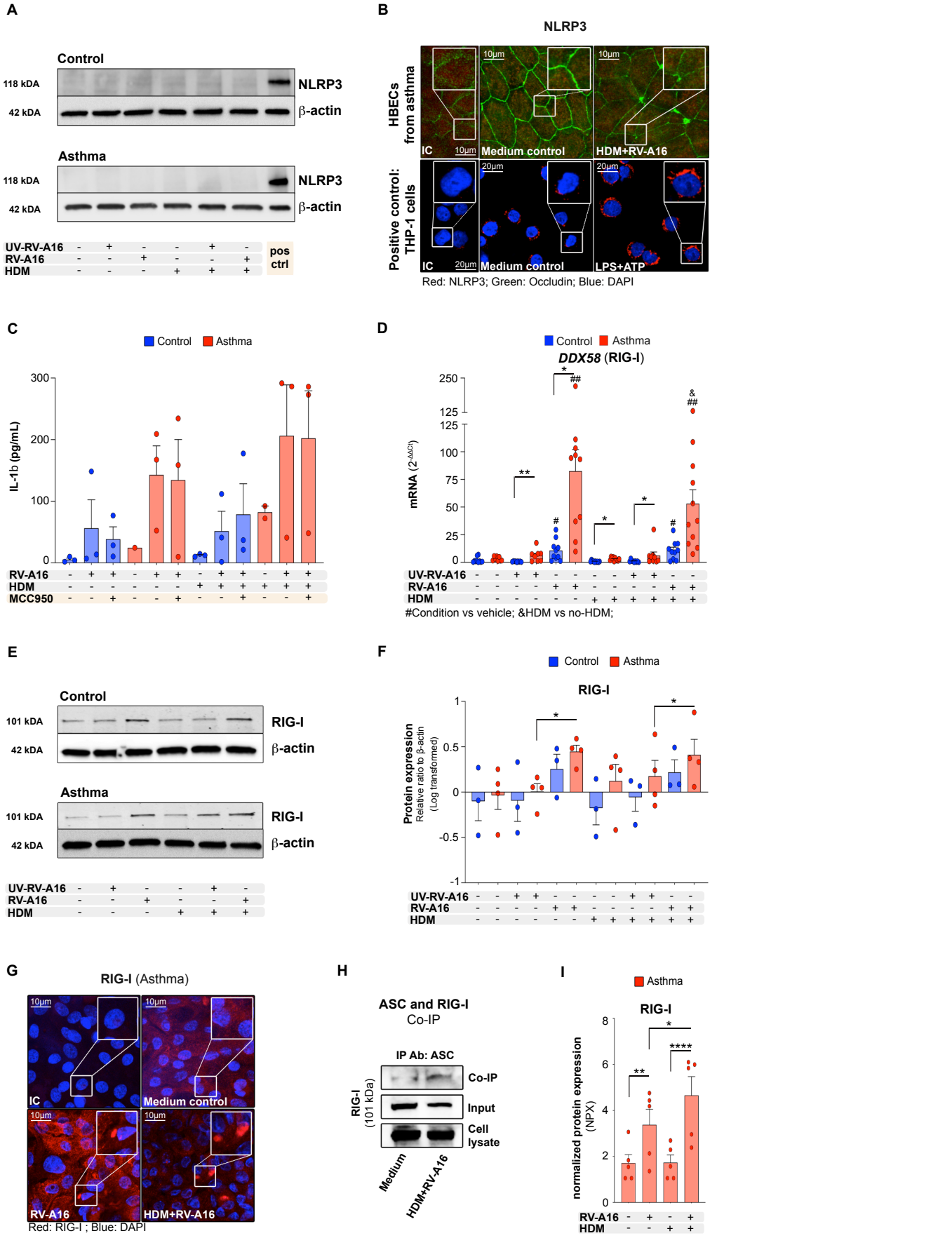
A
Control
118 kDA
42 kDA
NLRP3
β-actin
Asthma
118 kDA
42 kDA
NLRP3
β-actin
UV-RV-A16 - + - - + -
RV-A16 - - + - - +
HDM - - - + + +
pos ctrl
B
NLRP3
HBECs from asthma
10μm
IC
Medium control
HDM+RV-A16
Positive control: THP-1 cells
20μm
IC
Medium control
LPS+ATP
Red: NLRP3; Green: Occludin; Blue: DAPI
C
Control
Asthma
IL-1b (pg/mL)
300
200
100
0
RV-A16 - + + - + + - + + - + +
HDM - - - - - - + + + + + +
MCC950 - - + - - + - - + - - +
D
Control
Asthma
DDX58 (RIG-I)
mRNA (2^-ΔΔCt)
250
125
125
100
75
50
25
0
UV-RV-A16 - - + + - - - - + + - -
RV-A16 - - - - + + - - - - + +
HDM - - - - - - + + + + + +
#Condition vs vehicle; &HDM vs no-HDM;
E
Control
101 kDA
42 kDA
RIG-I
β-actin
Asthma
101 kDA
42 kDA
RIG-I
β-actin
UV-RV-A16 - + - - + -
RV-A16 - - + - - +
HDM - - - + + +
F
Control
Asthma
RIG-I
Protein expression
Relative ratio to β-actin
(Log transformed)
1
0.5
0
-0.5
-1
UV-RV-A16 - + + - - - - + + - -
RV-A16 - - - - + + - - - + + +
HDM - - - - - - + + + + + +
G
RIG-I (Asthma)
10μm
IC
Medium control
RV-A16
HDM+RV-A16
Red: RIG-I ; Blue: DAPI
H
ASC and RIG-I
Co-IP
IP Ab: ASC
RIG-I
(101 kDa)
Co-IP
Input
Cell lysate
Medium
HDM+RV-A16
I
Asthma
RIG-I
normalized protein expression
(NPX)
8
6
4
2
0
RV-A16 - + - +
HDM - - + +

Figure 2

Rhinovirus infection activated the RIG-I ASC inflammasome, but not NLRP3 or MDA5 inflammasomes in human airway epithelium

A) Representative Western Blot images of NLRP3 protein in the HBECs from control subjects (upper panel) and patients with asthma (lower panel) in all analyzed conditions, showed next to the positive control of lipopolysaccharide (LPS)-stimulated monocytes. Control n=3, asthma n=4, LPS-stimulated primary human monocytes n=7. **B)** Representative confocal images of NLRP3 and Occludin in HBECs from patients with asthma (n=3, upper panels); and in THP-1 cells used as positive controls: (n=2); scale bars: 10μm and 20μm, respectively. **C)** IL-1β release to the apical compartment with/without HDM, RV-A16 and NLRP3 inflammasome inhibitor (MCC950) (control n=3, asthma n=3). **D)** mRNA expression of *DDX58* (RIG-I) was assessed using RT-PCR and presented as a relative quantification ($RQ=2^{-\Delta\Delta Ct}$) as compared to the vehicle condition in HBECs from control subjects (control n=9-10, asthma n=9-10). **E)** Representative Western Blot images of RIG-I protein expression in HBECs from control subjects (upper panel) and patients with asthma (lower panel) (control n=4, asthma n=4). **F)** Quantification of densitometry of RIG-I protein expression, presented as a log-transformed ratio relative to β-actin and normalized to the vehicle condition in HBECs from control subjects (control n=3, asthma n=4). **G)** Representative confocal images of RIG-I in HBECs (n=3) from patients with asthma; scale bars: 10μm. **H)** Co-immunoprecipitation (co-IP) of ASC/RIG-I complex using anti-ASC antibodies followed by RIG-I detection (n=4). **I)** RIG-I release to the apical compartment assessed by the Proximity Extension Assay proteomics (PEA) in HBECs from patients with asthma (n=5). Data are presented as normalized protein expression (NPX). HBECs from patients with asthma are presented in red, HBECs from control individuals are presented in blue. (*) represents a significant difference as indicated. (#) represents a significant difference of indicated condition as compared to the vehicle from the same group. (&) represents a significant difference upon HDM treatment as compared to the corresponding condition without HDM. Bar graph data present mean ± SEM analyzed with one-way ANOVA (Kruskal-Wallis test), RM one-way ANOVA (Friedman test) or mixed-effects model, as appropriate, depending on the data relation and distribution, p-value: *<0.05; **<0.005; ***<0.0005; ****<0.00005. *IC*; Isotype control; *HBECs*, differentiated human bronchial epithelial cells; *HDM*, house dust mite; *RV-A16*, rhinovirus A16; *UV-RV-A16*, UV-treated rhinovirus A16; *pos ctrl*, positive control; *LPS*, lipopolysaccharide; *ATP*, adenosine triphosphate; *NPX*, normalized protein expression; *MCC950*, NLRP3 inflammasome inhibitor; *Co-IP*, Co-immunoprecipitation; *IP Ab*, antibodies used for co-precipitation.

Figure 3

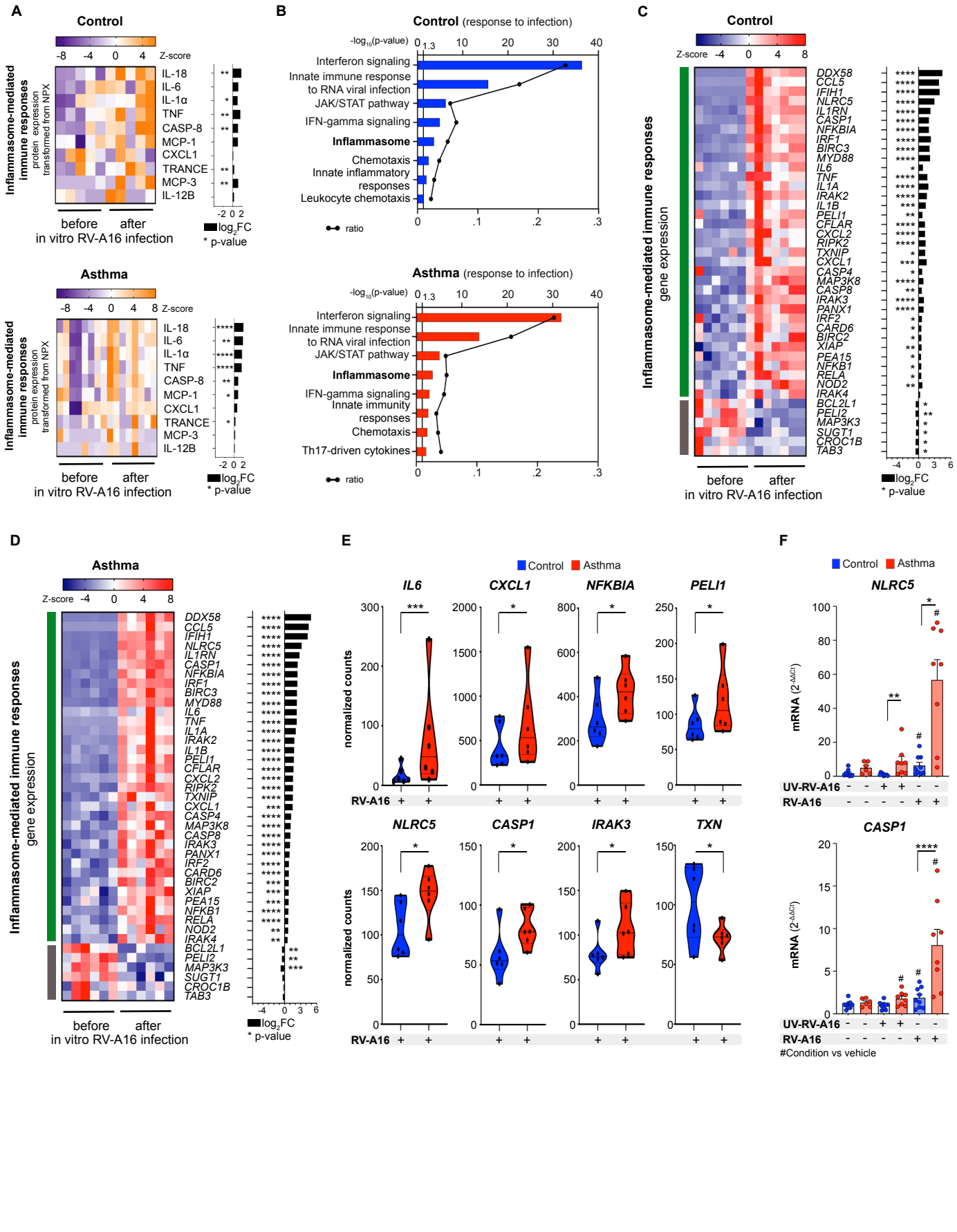
A
Control
Z-score
Inflammasome-mediated immune responses
protein expression transformed from NPX
IL-18
IL-6
IL-1α
TNF
CASP-8
MCP-1
CXCL1
TRANCE
MCP-3
IL-12B
before
after
in vitro RV-A16 infection
log2FC
* p-value
Asthma
B
Control (response to infection)
-log10(p-value)
Interferon signaling
Innate immune response to RNA viral infection
JAK/STAT pathway
IFN-gamma signaling
Inflammasome
Chemotaxis
Innate inflammatory responses
Leukocyte chemotaxis
ratio
Asthma (response to infection)
Innate immunity responses
Th17-driven cytokines
C
Control
Inflammasome-mediated immune responses
gene expression
DDX58
CCL5
IFIH1
NLRC5
IL1RN
CASP1
NFKBIA
IRF1
BIRC3
MYD88
IL6
TNF
IL1A
IRAK2
IL1B
PELI1
CFLAR
CXCL2
RIPK2
TXNIP
CXCL1
CASP4
MAP3K8
CASP8
IRAK3
PANX1
IRF2
CARD6
BIRC2
XIAP
PEA15
NFKB1
RELA
NOD2
IRAK4
BCL2L1
PELI2
MAP3K3
SUGT1
CROC1B
TAB3
D
Asthma
E
Control
Asthma
IL6
CXCL1
NFKBIA
PELI1
NLRC5
CASP1
IRAK3
TXN
normalized counts
RV-A16
F
Control
Asthma
NLRC5
CASP1
mRNA (2-ΔΔCt)
UV-RV-A16
RV-A16
#Condition vs vehicle

Figure 3

RIG-I inflammasome- and IL-1β-mediated immune responses are augmented in patients with asthma at an early time point after infection with rhinovirus

A) Heatmap of proteins associated with the inflammasome-mediated immune responses after in vitro RV-A16 infection in HBECs from control individuals (upper panel) and patients with asthma (lower panel) analyzed with the Proximity Extension Assay (PEA) proteomics, transformed from the normalized protein expression (NPX), and presented together with the $\log_2$ fold change (FC) (black bars) (control n=5, asthma n=8). Proteins were measured in the apical compartment of the ALI cultures. **B)** Top significantly enriched pathways within 100 most significantly upregulated genes in HBECs from controls (upper panel) and patients with asthma (lower panel) after RV-A16 infection in vitro (control n=6, asthma n=6; from GSE61141). Black line represents a ratio of genes in the experiment over the whole pathway set. **C-D)** Heatmap of genes encoding inflammasome-mediated immune responses in HBECS from **C)** control individuals and **D)** patients with asthma after in vitro RV-A16 infection presented together with the corresponding $\log_2$ fold change (FC) (control n=6, asthma n=6; GSE61141). Green and grey left side color bars represent genes upregulated or downregulated, respectively. **E)** Genes encoding inflammasome-mediated immune responses significantly different between control individuals and patients with asthma after in vitro RV-A16 infection (control n=6, asthma n=6; fromGSE61141). **F)** *NLRC5* (NLRC5, upper panel), and *CASP1* (caspase-1, lower panel) mRNA expression, assessed using RT-PCR in all analyzed conditions (control n=9, blue; asthma n=6-9, red). (*) represents a significant difference as indicated. (#) represents a significant difference of designated condition as compared to the vehicle from the same group. Bar graph data present mean ± SEM analyzed with one-way ANOVA (Kruskal-Wallis test), RM one-way ANOVA (Friedman test) or mixed-effects model, as appropriate, depending on the data relation and distribution, p-value: *<0.05; **<0.005; ***<0.0005, ****<0.00005. Heatmap displays normalized gene expression across the groups (row normalization). Inflammasome-mediated immune responses gene set was curated based on databases and ontologies listed in the Molecular Signatures Database (MSigDB, Broad Institute, Cambridge). *HBECs*, differentiated human bronchial epithelial cells; *RV-A16*, rhinovirus A16; *UV-RV-A16*, UV-treated rhinovirus A16; *NPX*, normalized protein expression.

Figure 4

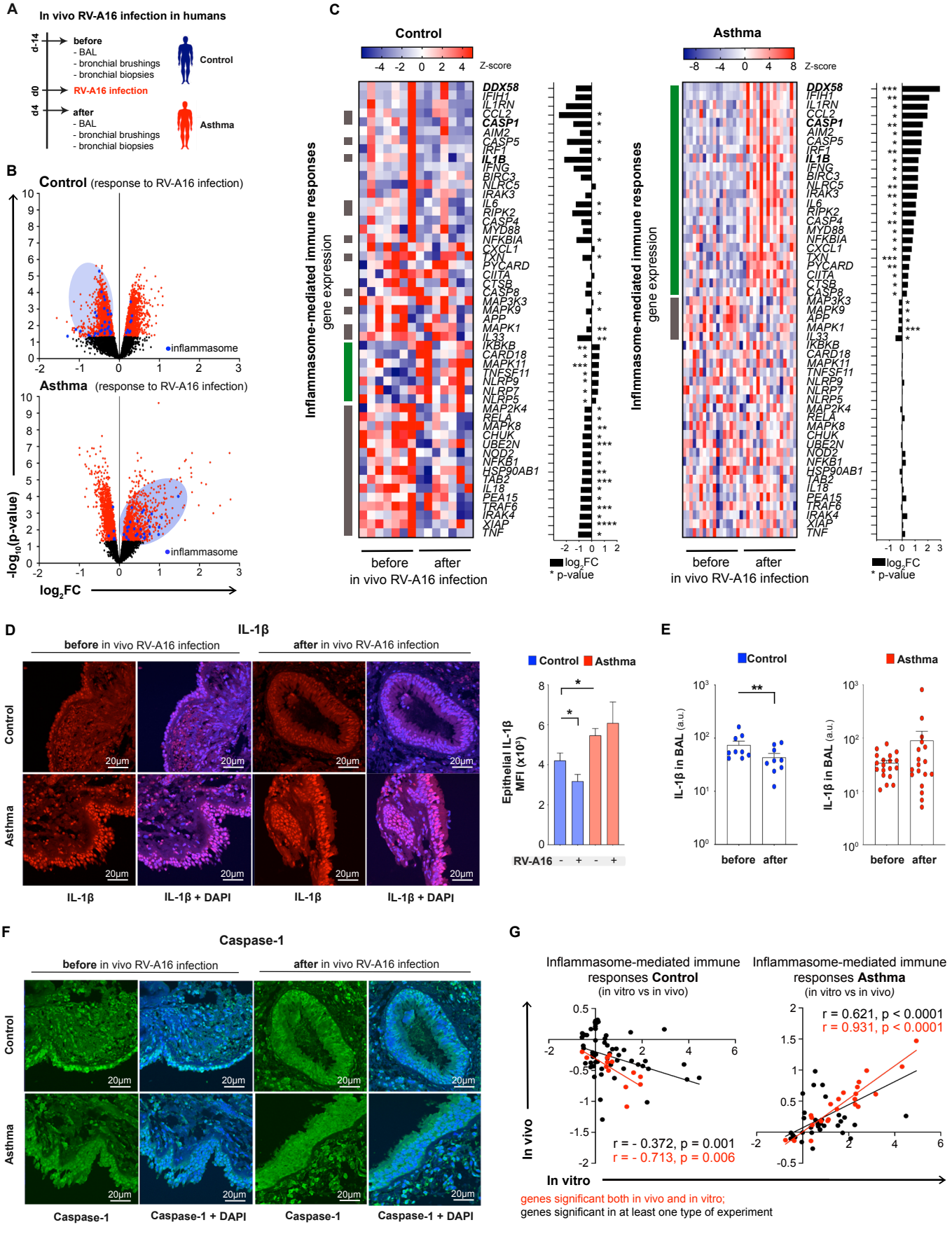
A
In vivo RV-A16 infection in humans
d-14
before
- BAL
- bronchial brushings
- bronchial biopsies
d0
RV-A16 infection
d4
after
- BAL
- bronchial brushings
- bronchial biopsies
Control
Asthma
B
Control (response to RV-A16 infection)
Asthma (response to RV-A16 infection)
inflammasome
-log10(p-value)
log2FC
C
Control
Asthma
Z-score
Inflammasome-mediated immune responses gene expression
DDX58
IFIH1
IL1RN
CCL2
CASP1
AIM2
CASP5
IRF1
IL1B
IFNG
BIRC3
NLRC5
IRAK3
IL6
RIPK2
CASP4
MYD88
NFKBIA
CXCL1
TXN
PYCARD
CIITA
CTSB
CASP8
MAP3K3
MAPK9
APP
MAPK1
IL33
IKBKB
CARD18
MAPK11
TNFSF11
NLRP9
NLRP7
NLRP5
MAP2K4
RELA
MAPK8
CHUK
UBE2N
NOD2
NFKB1
HSP90AB1
TAB2
IL18
PEA15
TRAF6
IRAK4
XIAP
TNF
before
after
in vivo RV-A16 infection
log2FC
* p-value
D
IL-1β
before in vivo RV-A16 infection
after in vivo RV-A16 infection
Control
Asthma
20μm
IL-1β
IL-1β + DAPI
Epithelial IL-1β MFI (x10³)
RV-A16
E
Control
Asthma
IL-1β in BAL (a.u.)
before
after
F
Caspase-1
Caspase-1 + DAPI
G
Inflammasome-mediated immune responses Control
(in vitro vs in vivo)
Inflammasome-mediated immune responses Asthma
(in vitro vs in vivo)
r = - 0.372, p = 0.001
r = - 0.713, p = 0.006
r = 0.621, p < 0.0001
r = 0.931, p < 0.0001
In vivo
In vitro
genes significant both in vivo and in vitro;
genes significant in at least one type of experiment

Figure 4

Sustained bronchial RIG-I inflammasome activation and inflammasome- mediated immune responses in asthma after rhinovirus infection in vivo in humans

A) Overview of the experimental RV-A16 infection in humans. Bronchoalveolar lavage (BAL) fluid, bronchial brushings, and bronchial biopsies from healthy controls and patients with asthma were collected two weeks before (day -14) and four days after (day 4) experimental infection with RV-A16 (100 $TCID_{50}$) on day 0 in vivo. **B)** Volcano plots of all (black), significant (red), and significant inflammasome-mediated immune response (blue) genes in bronchial brushings from controls (upper panel) and patients with asthma (lower panel) after experimental in vivo RV-A16 infection (control n=7, asthma n=17). X axis presents log_2 fold change (FC) of upregulated (right) and downregulated (left) genes. Y axis presents level of significance. **C)** Heatmap of genes encoding inflammasome-mediated immune responses after in vivo RV-A16 infection in controls (left panel) and patients with asthma (right panel) presented together with the corresponding log_2 fold change (FC) expression changes (black bars) (control n=7, asthma n=17). Green and grey left side color bars represent genes upregulated and downregulated, respectively. **D**) Representative confocal images of IL-1β in bronchial biopsies at baseline and after in vivo RV-A16 infection, scale bars: 20μm. Quantification based on the mean fluorescence intensity (MFI) $x10^3$ (10 equal epithelial areas from each biopsy of control subjects (n=3) and patients with asthma (n=3-4)). **E)** Secretion of IL-1β to BAL fluid before and after RV-A16 infection in vivo (control n=9, asthma n=18-19). Data are presented as arbitrary units (a.u.). **F)** Representative confocal images of caspase-1 in bronchial biopsies at baseline and after in vivo RV-A16 infection (control n=3, asthma n=3-4), scale bars: 20μm. **G)** Correlations of inflammasome-mediated immune response genes in in vitro and in vivo experiments of RV-A16 infection in controls (left panel), and patients with asthma (right panel). Red color represents genes significantly changed after RV-A16 infection vs before in both experiments. Black color represents genes significant in at least one of the experiments. In vitro: control n=6, asthma n=6. In vivo: control n=7, asthma n=17. (*) represents a significant difference between indicated conditions. Heatmap displays normalized gene expression across the groups (row normalization). Inflammasome-mediated immune responses gene set was curated based on databases and ontologies listed in the Molecular Signatures Database (MSigDB, Broad Institute, Cambridge). Bar graph data present mean ± SEM analyzed with one-way ANOVA (Kruskal-Wallis test), RM one-way ANOVA (Friedman test), mixed-effects model, or paired T-test or Wilcoxon test, as appropriate, depending on the data relation and distribution (if not mentioned differently), p-value: *<0.05; **<0.005; ***<0.0005, ****<0.00005. Correlations between in vitro and in vivo RV-A16-infection experiments were calculated with Pearson`s correlation coefficient, or Spearman`s rank correlation coefficient, depending on data distribution. *RV-A16*, rhinovirus A16; *BAL*, Bronchoalveolar lavage; *MFI*, mean fluorescence intensity*; a.u.*; arbitrary units; *$TCID_{50}$*, median tissue culture infectious dose.

Figure 5

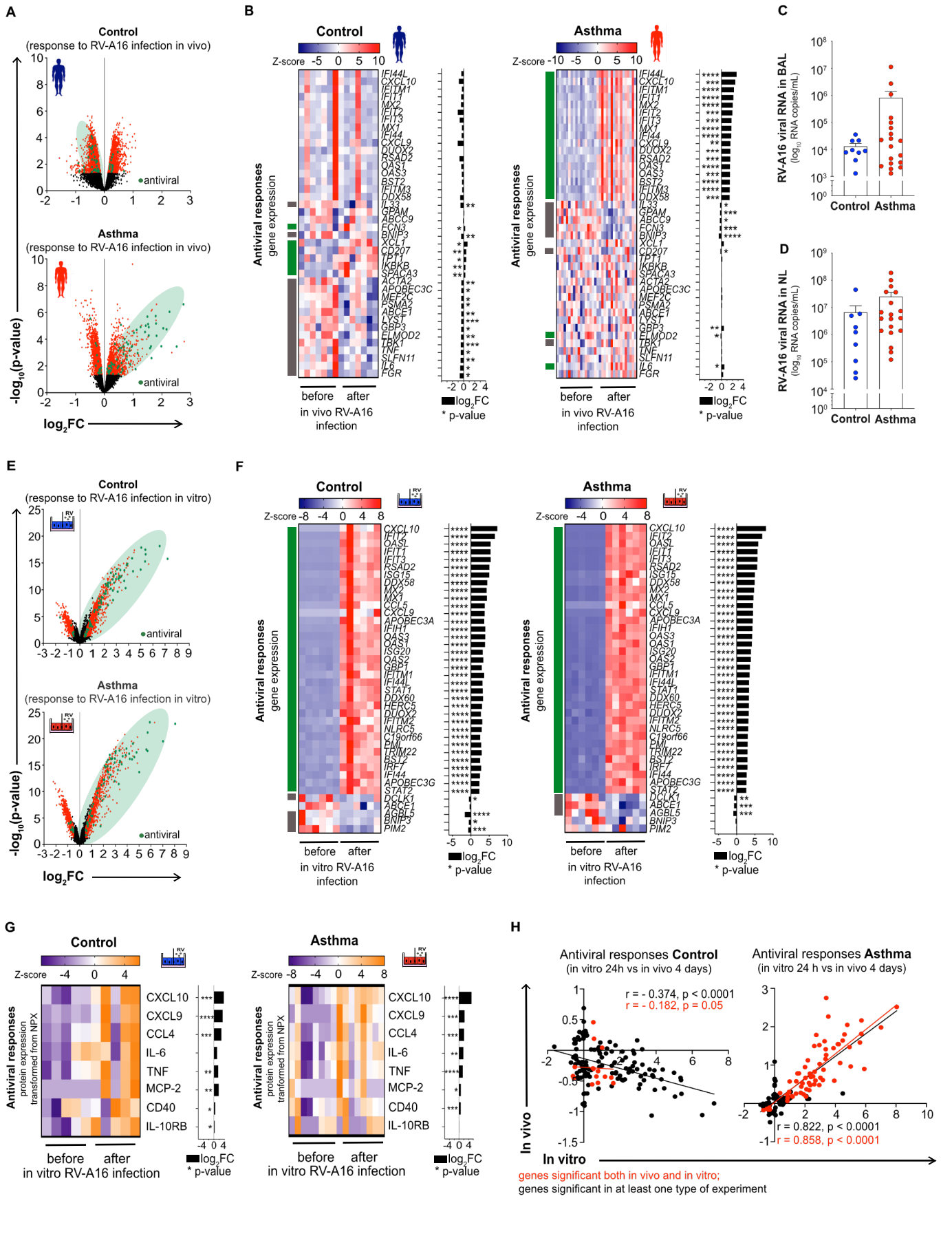
A
Control
(response to RV-A16 infection in vivo)
antiviral
Asthma
(response to RV-A16 infection in vivo)
antiviral
-log10(p-value)
log2FC
B
Control
Z-score -5 0 5 10
Asthma
Z-score -10 -5 0 5 10
Antiviral responses
gene expression
IFI44L
CXCL10
IFITM1
IFIT1
MX2
IFIT2
IFIT3
MX1
IFI44
CCL5
CXCL9
DUOX2
RSAD2
OAS1
OAS3
BST2
IFITM3
DDX58
IL33
GPAM
ABCC9
FCN3
BNIP3
XCL1
CD207
TPT1
IKBKB
SPACA3
ACTA2
APOBEC3C
MET2C
PSMA2
ABCE1
LYST
GBP3
FLMOD2
TBK1
TNF
SLFN11
IL6
FGR
before after
in vivo RV-A16 infection
log2FC
* p-value
C
RV-A16 viral RNA in BAL
(log10 RNA copies/mL)
Control Asthma
D
RV-A16 viral RNA in NL
(log10 RNA copies/mL)
Control Asthma
E
Control
(response to RV-A16 infection in vitro)
antiviral
Asthma
(response to RV-A16 infection in vitro)
antiviral
-log10(p-value)
log2FC
F
Control
Z-score -8 -4 0 4 8
Asthma
Z-score -4 0 4 8
Antiviral responses
gene expression
CXCL10
IFIT2
OASL
IFIT1
IFIT3
RSAD2
ISG15
DDX58
MX2
MX1
CCL5
CXCL9
APOBEC3A
IFIH1
OAS3
OAS1
ISG20
OAS2
GBP1
IFITM1
IFI44L
STAT1
DDX60
HERC5
DUOX2
IFITM2
NLRC5
C19orf66
PML
TRIM22
BST2
IRF7
IFI44
APOBEC3G
STAT2
DCLK1
ABCE1
AGBL5
BNIP3
PIM2
before after
in vitro RV-A16 infection
log2FC
* p-value
G
Control
Z-score -4 0 4
Asthma
Z-score -8 -4 0 4 8
Antiviral responses
protein expression
transformed from NPX
CXCL10
CXCL9
CCL4
IL-6
TNF
MCP-2
CD40
IL-10RB
before after
in vitro RV-A16 infection
log2FC
* p-value
H
Antiviral responses Control
(in vitro 24h vs in vivo 4 days)
r = - 0.374, p < 0.0001
r = - 0.182, p = 0.05
Antiviral responses Asthma
(in vitro 24 h vs in vivo 4 days)
r = 0.822, p < 0.0001
r = 0.858, p < 0.0001
In vivo
In vitro
genes significant both in vivo and in vitro;
genes significant in at least one type of experiment

Figure 5

Sustained rhinovirus infection and activation of antiviral responses in bronchial epithelium of patients with asthma in vivo

A) Volcano plots of all (black), significant (red), and significant antiviral (green) genes in bronchial brushings from controls (upper panel) and patients with asthma (lower panel) after experimental in vivo RV-A16 infection (control n=7, asthma n=17). X axis presents log_2 fold change (FC) of upregulated (right) and downregulated (left) genes. Y axis presents level of significance. **B**) Heatmap of antiviral genes significantly changed four days after experimental RV-A16 infection in healthy controls (left panel) and/or in patients with asthma (right panel) presented together with the log_2 fold change (FC) (black bars) (control n=7, asthma n=17). Green and grey left side color bars represent genes upregulated and downregulated, respectively. **C-D)** RV-A16 virus load in **C)** the bronchoalveolar lavage (BAL) fluid and **D)** the nasal lavage (NL) fluid in control individuals and patients with asthma four days after experimental RV-A16 infection (control n=9, asthma n=19). Data presented as log_{10} viral RNA copies per 1 mL of BAL/NL. **E)** Volcano plots of all (black), significant (red), and significant antiviral (green) genes in HBECs from control subjects (upper panel) and patients with asthma (lower panel) 24h after in vitro RV-A16 infection (control n=6, asthma n=6). X axis presents log_2 fold change (FC) of upregulated (right) and downregulated (left) genes. Y axis presents level of significance. **F)** Heatmap of antiviral genes significantly changed after in vitro RV-A16 infection in HBECs from control subjects (left panel) and/or patients with asthma (right panel) presented together with log_2 fold change (FC) (black bars) (control n=6, asthma n=6). Green and grey left side color bars represent genes upregulated and downregulated, respectively. **G**) Heatmap of proteins associated with the antiviral responses in HBECs from controls (left panel) and patients with asthma (right panel) 24h after in vitro RV-A16 infection, assessed by the PEA proteomics, transformed from the normalized protein expression (NPX), and demonstrated together with the log_2 fold change (FC) (black bars) (control n=5, asthma n=8). **H)** Correlations of antiviral response genes in in vitro and in vivo experiments of RV-A16 infection in controls (left panel), and patients with asthma (right panel). Red color represents genes significantly changed after RV-A16 infection vs before in both experiments. Black color represents genes significant in at least one of the experiments (in vitro: control n=6, asthma n=6; in vivo: control n=7, asthma n=17). HBECs from patients with asthma are presented in red, HBECs from controls are presented in blue. (*) represents a significant difference between indicated conditions. Bar graph data present mean $\pm$ SEM. Heatmap displays normalized gene expression across the groups (row normalization), p-value: *<0.05; **<0.005; ***<0.0005, ****<0.00005. Antiviral response gene set was curated based on databases and ontologies listed in the Molecular Signatures Database (MSigDB, Broad Institute, Cambridge). Data presented in E-F, H (in vitro): GSE61141. *HBECs*, differentiated human bronchial epithelial cells; *RV-A16*, rhinovirus A16; *NPX*, normalized protein expression; *BAL*, bronchoalveolar lavage; *NL*, nasal lavage.

Figure 6

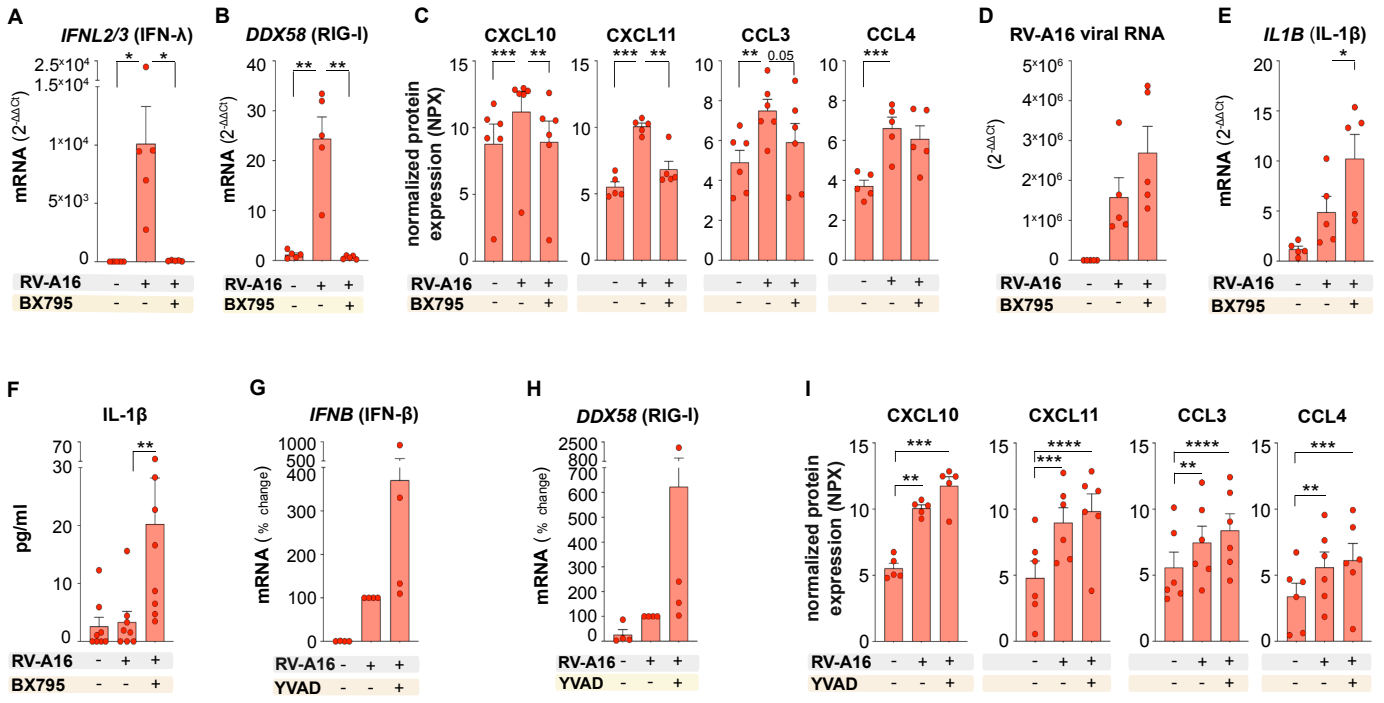
A
IFNL2/3 (IFN-λ)
mRNA (2-ΔΔCt)
RV-A16
BX795
B
DDX58 (RIG-I)
C
CXCL10
CXCL11
CCL3
CCL4
normalized protein expression (NPX)
0.05
D
RV-A16 viral RNA
E
IL1B (IL-1β)

F
IL-1β
pg/ml
G
IFNB (IFN-β)
mRNA (% change)
YVAD
H
DDX58 (RIG-I)
I
CXCL10
CXCL11
CCL3
CCL4
normalized protein expression (NPX)

Figure 6

Activation of the RIG-I inflammasome disturbed RIG-I dependent interferon signaling in bronchial epithelium of patients with asthma

A-F) HBECs from patients with asthma were infected with RV-A16 in the presence or absence of BX795, a chemical inhibitor of TBK1 and IKKε, or vehicle. mRNA expression of **A)** *IFNL2/3* (IFNλ) and **B)** *DDX58* (RIG-I) assessed using RT-PCR and presented as relative quantification ($RQ=2^{-\Delta\Delta Ct}$) as compared to the vehicle condition (n=5). **C)** Secretion of CXCL10, CXCL11, CCL3, and CCL4 proteins into the apical compartment assessed with the PEA targeted proteomics (n=6). Data are presented as normalized protein expression (NPX). Expression of **D)** *RV-A16 positive strand* (RV-A16 viral RNA) and **E)** *IL1B* (IL-1β) assessed using RT-PCR and presented as relative quantification ($RQ=2^{-\Delta\Delta Ct}$) (n=5). **F)** IL-1β release to the apical compartment assessed by ELISA (n=8). **G-I)** HBECs from patients with asthma were infected with RVA16 in the presence or absence of YVAD, a caspase-1 inhibitor or vehicle. mRNA expression of **G)** *IFNB* (IFNβ) and **H)** *DDX58* (RIG-I) (n=4). Data are demonstrated as the percentage of the expression normalized to the RV-A16 condition. **I)** Secretion of CXCL10, CXCL11, CCL3, and CCL4 into apical compartment assessed with the PEA proteomics (n=6). Data are presented as normalized protein expression (NPX). (*) represents a significant difference between indicated conditions. Graph data present mean ± SEM analyzed with one-way ANOVA (Kruskal-Wallis test), RM one-way ANOVA (Friedman test) or mixed-effects model, as appropriate, depending on the data relation and distribution, p-value: *<0.05; **<0.005; ***<0.0005, ****<0.00005. *HBECs*, differentiated human bronchial epithelial cells; *RV-A16*, rhinovirus A16; *NPX*, normalized protein expression; *YVAD*, ac-YVAD-cmk (caspase-1 inhibitor); *BX795,* TBK1/IKKε inhibitor.

Figure 7

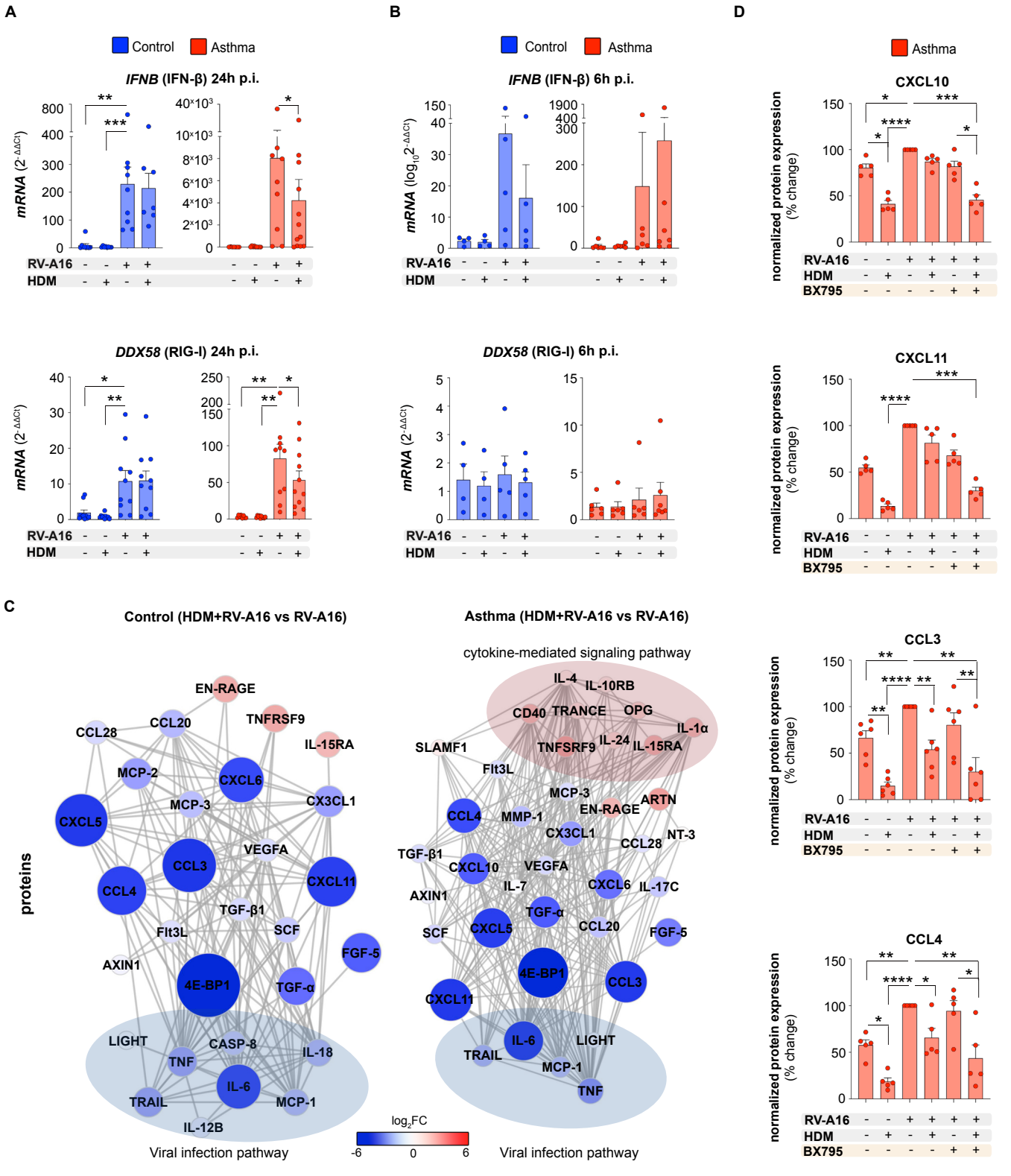
A
Control
Asthma
IFNB (IFN-β) 24h p.i.
mRNA (2-ΔΔCt)
RV-A16
HDM
DDX58 (RIG-I) 24h p.i.
B
IFNB (IFN-β) 6h p.i.
mRNA (log10 2-ΔΔCt)
DDX58 (RIG-I) 6h p.i.
D
CXCL10
CXCL11
CCL3
CCL4
normalized protein expression (% change)
BX795
C
Control (HDM+RV-A16 vs RV-A16)
Asthma (HDM+RV-A16 vs RV-A16)
cytokine-mediated signaling pathway
proteins
EN-RAGE
CCL28
CCL20
TNFRSF9
IL-15RA
MCP-2
CXCL6
MCP-3
CX3CL1
CXCL5
VEGFA
CCL3
CCL4
CXCL11
TGF-β1
Flt3L
SCF
FGF-5
AXIN1
4E-BP1
TGF-α
LIGHT
CASP-8
IL-18
TNF
IL-6
TRAIL
MCP-1
IL-12B
Viral infection pathway
log2FC
-6
0
6
IL-4
IL-10RB
CD40
TRANCE
OPG
IL-1α
SLAMF1
TNFSRF9
IL-24
IL-15RA
Flt3L
MCP-3
ARTN
CCL4
MMP-1
EN-RAGE
CX3CL1
NT-3
CCL28
TGF-β1
CXCL10
VEGFA
IL-7
CXCL6
IL-17C
AXIN1
TGF-α
SCF
CXCL5
CCL20
FGF-5
4E-BP1
CCL3
CXCL11
IL-6
LIGHT
TRAIL
MCP-1
TNF
Viral infection pathway

Figure 7

House dust mite impaired interferon responses in rhinovirus-infected bronchial epithelium of patients with asthma

A-C. Primary air liquid interface (ALI)-differentiated human bronchial epithelial cells (HBECs) from control individuals and patients with asthma were treated with house dust mite (HDM) (200 μg/mL) or vehicle 24h, followed by an infection with rhinovirus A16 (RV-A16) in the multiplicity of infection (MOI) 0.1 for 6h or 24h. mRNA expression of **A)** *IFNB* (IFN-β) (upper panel), and *DDX58* (RIG-I) (lower panel) (control n=7-9, asthma n=7-12) 24h p.i. **B)** *IFNB* (IFN-β) (upper panel), and *DDX58* (RIG-I) (lower panel) 6h p.i. (control n=4-5, asthma n=6-7) **C)** Visualization of interaction network of significant proteins secreted to the apical compartment from HBECs from control individuals (left panel) and patients with asthma (right panel) after in vitro treatment with HDM+RV-A16, when compared to RV-A16 infection alone assessed with PEA targeted proteomics (control n=5, asthma n=8). Network nodes represent log_2FC of significantly upregulated (red), and downregulated (blue) proteins; proteins not interacting with each other are not shown. Edges represent protein-protein interactions. Proteins enriched in viral infection or cytokine-mediated signaling pathway are marked with blue and red eclipses, respectively. Prepared with STRING (https://string-db.org) and Cytoscape (https://cytoscape.org). **D)** Expression of CXCL10, CXCL11, CCL3, and CCL4 in the apical compartment of HBECs from patients with asthma pre-treated with HDM or vehicle, followed by the infection with RV-A16 in the presence of BX795 or vehicle assessed with PEA proteomics (n=6). Data presented as the percentage of the response to the RV-A16 condition. (*) represents a significant difference between indicated conditions. Graph data present mean ± SEM analyzed with one-way ANOVA (Kruskal-Wallis test), RM one-way ANOVA (Friedman test) or mixed-effects model, as appropriate, depending on the data relation and distribution, *p-value≤0.05, **p-value≤0.01, ***p-value≤0.001, ****p-value≤0.0001. *HBECs*, differentiated human bronchial epithelial cells; *RV-A16*, rhinovirus A16; *p.i.*, post-infection; *HDM,* house dust mite; *BX795*, TBK1/IKKε inhibitor; *NPX*, normalized protein expression.

Figure 8

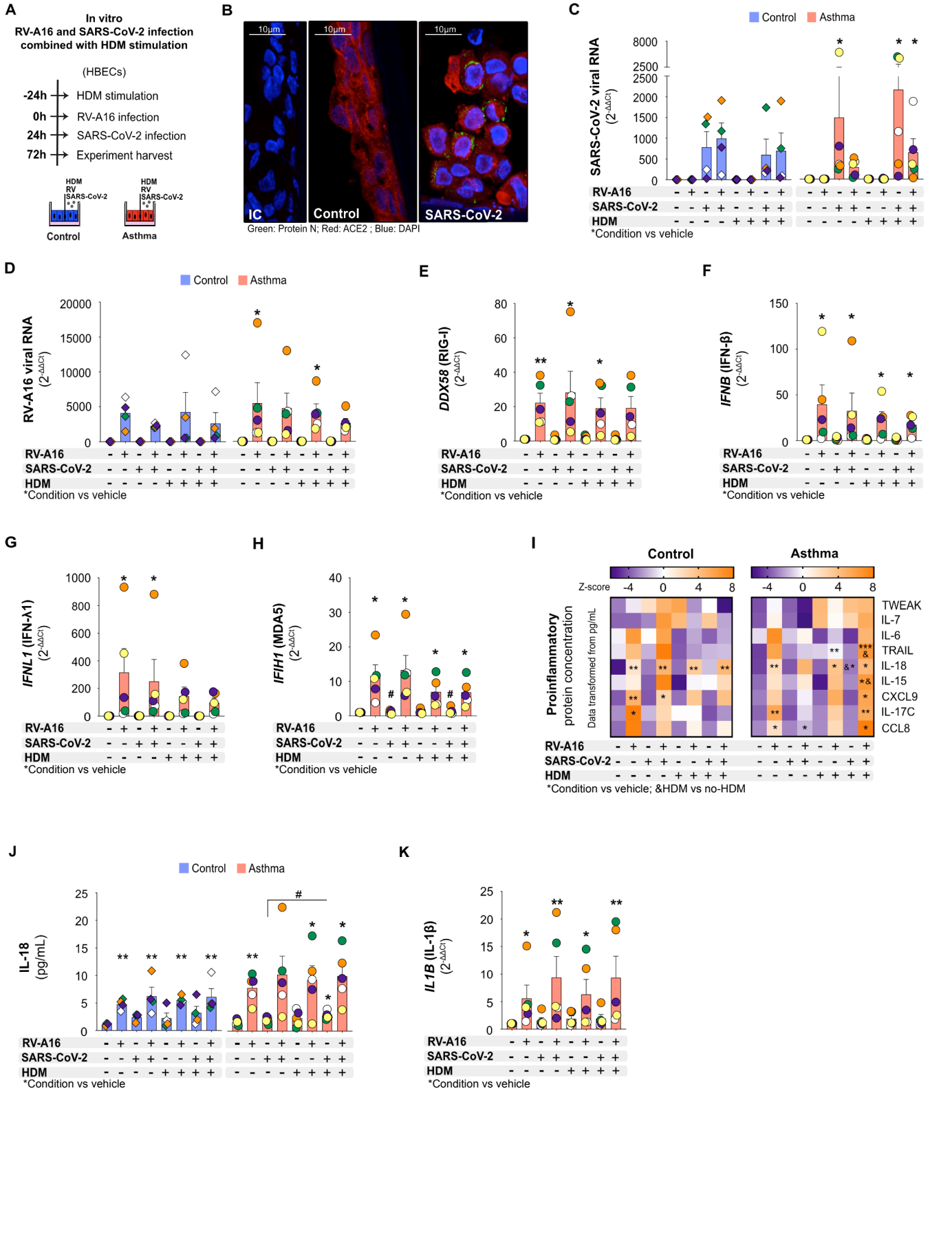
A
In vitro
RV-A16 and SARS-CoV-2 infection
combined with HDM stimulation
(HBECs)
-24h HDM stimulation
0h RV-A16 infection
24h SARS-CoV-2 infection
72h Experiment harvest
HDM RV SARS-CoV-2
Control
HDM RV SARS-CoV-2
Asthma
B
10µm
IC
Control
SARS-CoV-2
Green: Protein N; Red: ACE2 ; Blue: DAPI
C
Control
Asthma
SARS-CoV-2 viral RNA (2-ΔΔCt)
RV-A16
SARS-CoV-2
HDM
*Condition vs vehicle
D
RV-A16 viral RNA (2-ΔΔCt)
*Condition vs vehicle
E
DDX58 (RIG-I) (2-ΔΔCt)
*Condition vs vehicle
F
IFNB (IFN-β) (2-ΔΔCt)
*Condition vs vehicle
G
IFNL1 (IFN-λ1) (2-ΔΔCt)
*Condition vs vehicle
H
IFIH1 (MDA5) (2-ΔΔCt)
*Condition vs vehicle
I
Control
Asthma
Z-score
Proinflammatory protein concentration
Data transformed from pg/mL
TWEAK
IL-7
IL-6
TRAIL
IL-18
IL-15
CXCL9
IL-17C
CCL8
*Condition vs vehicle; &HDM vs no-HDM
J
Control
Asthma
IL-18 (pg/mL)
*Condition vs vehicle
K
IL1B (IL-1β) (2-ΔΔCt)
*Condition vs vehicle

Figure 8.

Pre-existing rhinovirus infection attenuated SARS-CoV-2 infection, but augmented epithelial inflammation in asthma

A) Overview of the experimental RV-A16 and severe acute respiratory syndrome coronavirus 2 (SARS-CoV-2) co-infection with/without HDM pre-treatment. Primary human bronchial epithelial cells (HBECs) from control subjects (n=4) and patients with asthma (n=5), differentiated in the Air-liquid Interface (ALI) conditions, were treated with house dust mite (HDM) (200 μg/mL) or vehicle for 24h, infected with rhinovirus A16 (RV-A16) in the multiplicity of infection (MOI) 0.1 for 24h, and then co-infected with SARS-CoV-2 in the MOI 0.1 for the following 48h. **B)** Representative confocal images of SARS-CoV-2 N protein and ACE2 in HBECs from patients with asthma after SARS-CoV-2 infection; scale bars: 10μm. Expression of **C)** SARS-CoV-2 virus load (average expression of *N protein*, *S protein* and *ORF1AB*) **D)** *RV-A16 positive strand* (RV-A16 viral RNA), **E)** *DDX58* (RIG-I), **F)** *IFNB* (IFN-β), **G)** *IFNL1* (IFN-λ1) **H)** *IFIH1* (MDA5) was assessed using RT-PCR and presented as relative quantification ($RQ=2^{-\Delta\Delta Ct}$) compared to medium condition separately for HBECs from controls and patients with asthma. **I)** Heatmap of proinflammatory proteins assessed in the apical compartments of HBECs from controls (left panel) and patients with asthma (right panel) after in vitro HDM pre-stimulation and RV-A16 and SARS-CoV-2 co-infection analyzed with the quantitative Proximity Extension Assay (PEA) targeted proteomics. Data are transformed from the concentrations in pg/mL. **J)** IL-18 secreted to the apical compartment analyzed with the quantitative PEA. Data are presented as pg/mL. **K)** mRNA expression of *IL1B* (IL-1β) in HBECs from patients with asthma. Patients with asthma are presented in transparent red, control individuals in transparent blue. (*) represents a significant difference as compared to the vehicle from the same group. (&) represents a significant difference between HDM-pre-treated and HDM-naïve condition. (#) represents significant difference as indicated. Bars depict the mean ± SEM, whereas color-coded diamonds (control subjects) or circles (patients with asthma) show individual data from the same donor. Data are present as mean analyzed with one-way ANOVA (Kruskal-Wallis test), RM one-way ANOVA (Friedman test) or mixed-effects model, as appropriate, depending on the data relation and distribution, *p-value≤0.05, **p-value≤0.01, ***p-value≤0.001. *RV-A16*, rhinovirus A16; *HDM*, House Dust Mite; *HBECs*, Human Bronchial Epithelial Cells; *SARS-CoV-2*, Severe Acute Respiratory Syndrome Coronavirus 2; *ALI*, air-liquid interface; *MOI*, multiplicity of infection.

Supplementary Figure S1

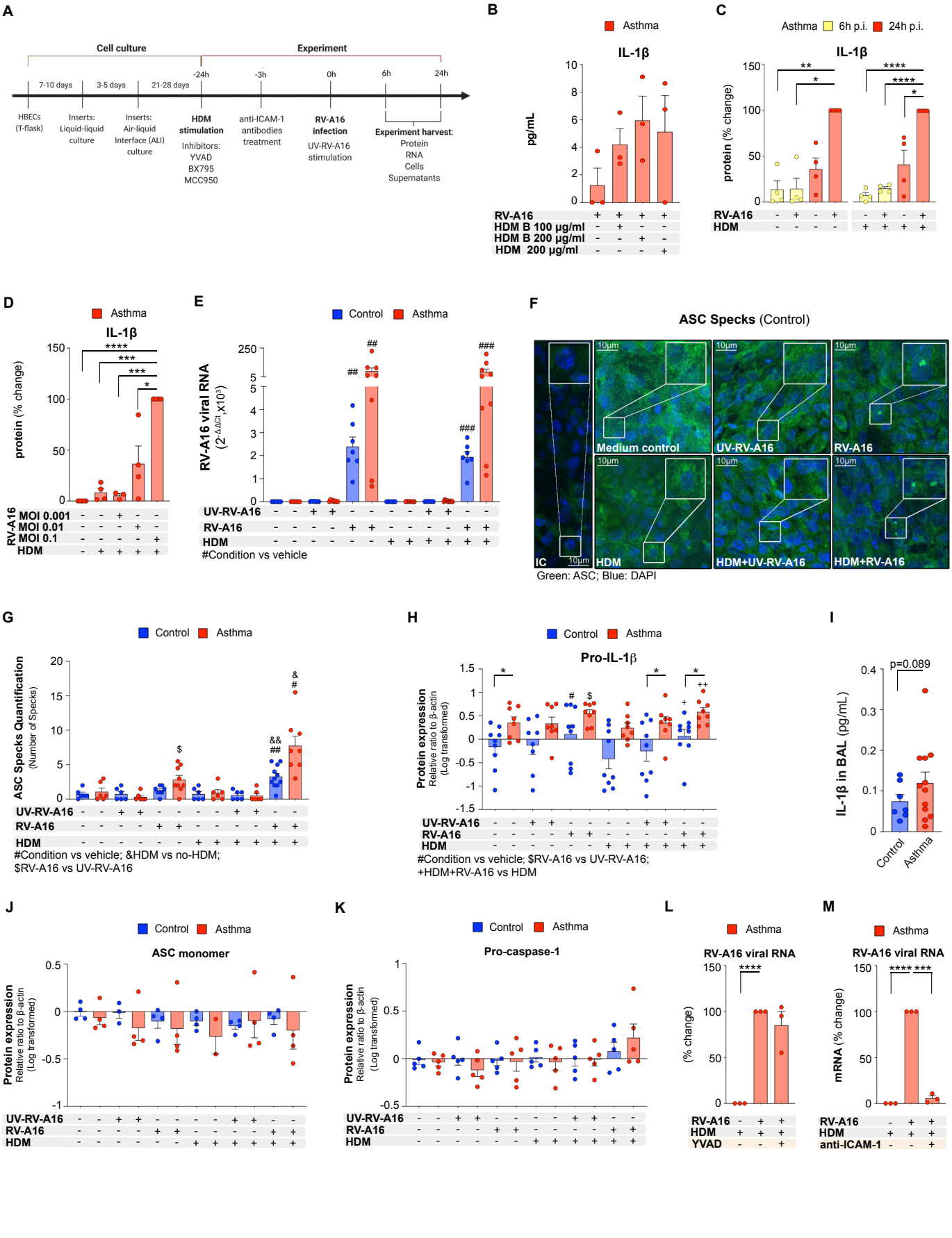

Supplementary Figure S1

House dust mite increased rhinovirus-induced inflammasome activation in human bronchial epithelium in asthma

A) Detailed experimental in vitro model overview. Primary human bronchial epithelial cells (HBECs) from control individuals (blue) or patients with asthma (red) were differentiated for 21-28 days in the Air-Liquid Interface (ALI) culture. 24h prior rhinovirus A16 (RV-A16) infection, cells were stimulated with house dust mite (HDM) (200μg/mL) and/or caspase-1 inhibitor (YVAD), TBK1/IKKε inhibitor (BX795) and NLRP3 inflammasome inhibitor (MCC950) or vehicle. To block cell entry of RV-A16, HBECs were incubated with anti-ICAM-1 antibodies 3h before the infection. Cells were infected with RV-A16 at the multiplicity of infection (MOI) 0.1, 0.01 and 0.001 or the respective UV-RV-A16 controls. Protein, RNA, cells, and supernatants were harvested at 6h and 24h after infection. **B-C)** IL-1β release to the apical compartment was assessed by ELISA **B)** two independent HDM extracts, HDM (the main one used in the manuscript) and HDM B (similar extract from a different company), were tested 24h after RV-A16 infection (n=3); and **C)** for 6h (yellow) and 24h p.i. (red) (n=4). Data are presented as the percentage of the response after 24h p.i. **D)** IL-1β release to the apical compartment assessed by ELISA 24h after RV-A16 infection in the MOI 0.1, 0.01, and 0.001, combined with HDM pre-stimulation (n=4). Data are presented as the percentage of the response after RV-A16 infection in the MOI 0.1. **E)** expression of *RV-A16 positive strand* (RV-A16 viral RNA) was assessed using RT-PCR, and presented as the relative quantification ($RQ=2^{-\Delta\Delta Ct}$) as compared to the vehicle condition in the HBECs from control individuals (control n=7, asthma n=7-9). **F)** Representative confocal images of ASC speck formation in the HBECs from control subjects (n=3); scale bars: 10μm. **G)** Quantification of ASC specks, presented as a number of specks (5-11 equal epithelial areas from control n=3, asthma n=3). **H)** Quantification of densitometry results of pro-IL-1β protein assessed by Western Blot, presented as a log-transformed ratio relative to β-actin and normalized to the vehicle condition in control individuals (control n=9, asthma n=8). **I)** IL-1β protein in the bronchoalveolar lavage (BAL) fluid of control subjects and patients with asthma (cohort SIBRO), assessed using the mesoscale platform and Welsh`s t-test. (control n=8, asthma n=12). **J-K)** Quantification of densitometry results from **J)** ASC and **K)** pro-caspase-1 protein expression assessed by Western Blot, presented as a log-transformed ratio relative to β-actin expression and normalized to the vehicle condition in the HBECs from the control individuals (ASC: control n=4, asthma n=4; caspase-1: control n=5, asthma n=5). **L-M)** expression of *RV-A16 positive strand* (RV-A16 viral RNA) in the HBECs from patients with asthma after **L)** YVAD treatment (n=3), and **M)** anti-ICAM-1 stimulation (n=3) was assessed using RT-PCR, and presented as a relative quantification ($RQ=2^{-\Delta\Delta Ct}$) as compared to the vehicle condition from patients with asthma (Fig. S1L) or control individuals (Fig. S1M). Data are presented as the percentage of the response after HDM+RV-A16 treatment. HBECs from patients with asthma are presented in red, HBECs from control individuals are presented in blue. (*) represents a significant difference as indicated. (#) represents a

significant difference of indicated condition as compared to the vehicle from the same group. (&) represents a significant difference upon HDM treatment when compared to the respective condition without HDM. ($) represents a significant difference between RV-A16 and UV-RV-A16 condition. (+) represents a significant difference between HDM+RV-A16 and HDM condition. Bar graph data show mean ± SEM analysed with one-way ANOVA (Kruskal-Wallis test), RM one-way ANOVA (Friedman test) or mixed-effects model, as appropriate, depending on the data relation (paired or unpaired) and distribution (if not mentioned differently), *p-value≤0.05, **p-value≤0.01, ***p-value≤0.001, ****p-value≤0.0001. Figure 1A was prepared with Biorender.com. *ALI*; Air-liquid interface cultures*; BAL*; Bronchoalveolar lavage, *HBECs*, differentiated human bronchial epithelial cells; *HDM*, house dust mite; *RV-A16*, rhinovirus A16; *UV-RV-A16*, UV-treated rhinovirus A16; *YVAD*, ac-YVAD-cmk (caspase-1 inhibitor); *anti-ICAM-1*, anti-ICAM-1 antibody; *BX795*, TBK1/IKKε inhibitor; *MCC950*, NLRP3 inflammasome inhibitor; *MOI*, multiplicity of infection; *p.i.*, post-infection.

Supplementary Figure S2

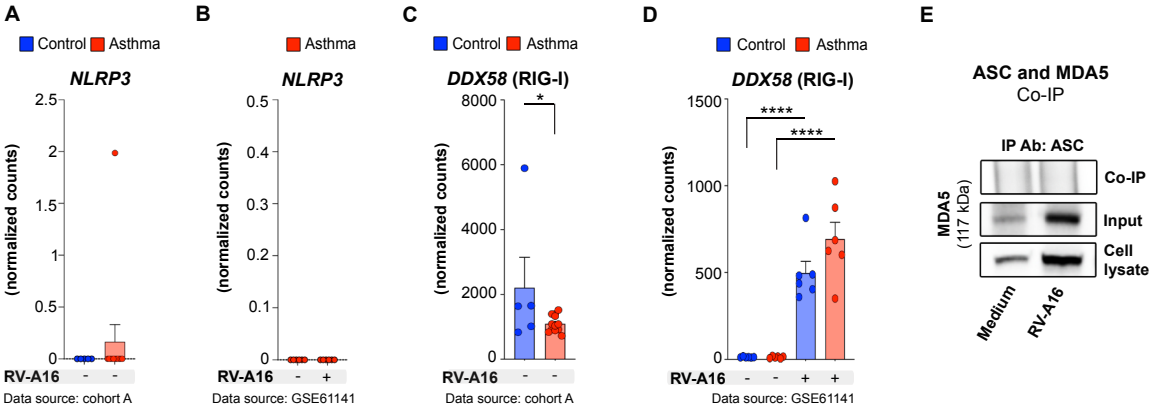

Supplementary Figure S2

Rhinovirus infection activated the RIG-I ASC inflammasome, but not NLRP3 or MDA5 inflammasomes in human airway epithelium

A-B) Expression of *NLRP3* in **A)** in HBECs at baseline (control n=5, asthma n=12), and **B)** HBECs from patients with asthma after RV-A16 infection (n=6). **C-D)** Expression of *DDX58* (RIG-I) in HBECs **C)** at baseline (control n=5, asthma n=12), and **D)** after RV-A16 infection (control n=6; asthma n=6). **D)** Co-immunoprecipitation (co-IP) of ASC/MDA5 complex using anti-ASC antibodies followed by MDA5 detection. HBECs from patients with asthma are presented in red, HBECs from control individuals are presented in blue. Transcriptome data are presented as normalized counts. (*) represents a significant difference between indicated conditions. Bar graph data present mean ± SEM, p-value: *<0.05; **<0.005; ***<0.0005, ****<0.00005. Data presented on the figure S2A and C: cohort A, S2B and D: GSE61141. *HBECs*, human bronchial epithelial cells; *RV-A16*, rhinovirus A16; *Co-IP*, Co-immunoprecipitation.

Supplemenary Figure S3

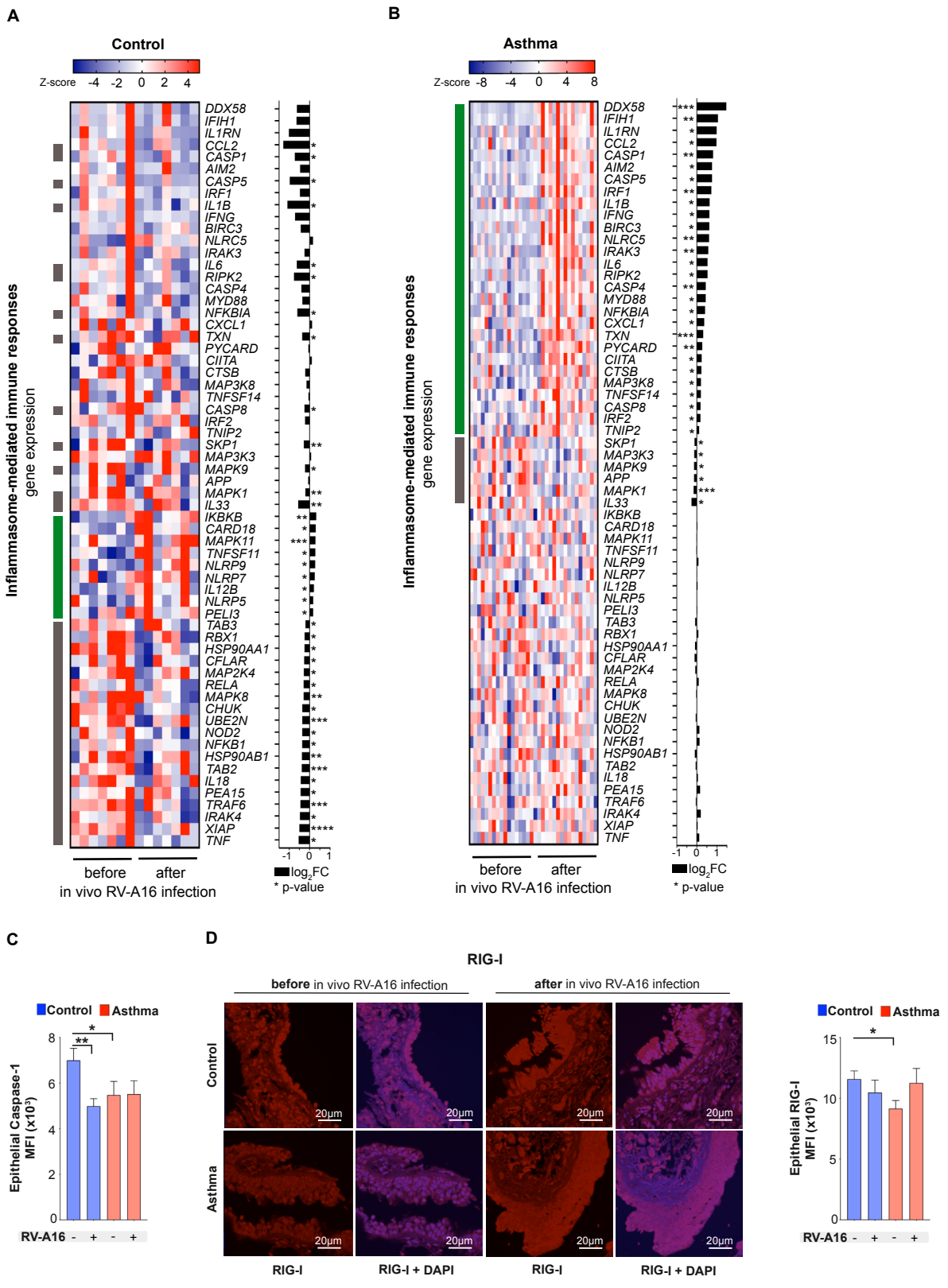

Supplementary Figure S3

Sustained bronchial RIG-I inflammasome activation and inflammasome- mediated immune responses in asthma after rhinovirus infection in vivo in humans

A-B) Full heatmap of genes encoding inflammasome-mediated immune responses after experimental RV-A16 infection in **A)** healthy controls and **B)** patients with asthma presented together with log_2 fold change (FC) expression changes (black bars) (control n=7, asthma n=17). Green and grey left side colour bars represent genes upregulated and downregulated, respectively. **C)** Quantification of confocal staining of caspase-1 in bronchial biopsies at baseline and after in vivo RV-A16 infection based on the mean fluorescence intensity (MFI) $x10^3$ (10 equal epithelial areas from each biopsy of control subjects (n=3) and patients with asthma (n=3-4)). **D**) Representative confocal images of RIG-I expression in bronchial biopsies at baseline and after experimental in vivo RV-A16 infection (control n=3, asthma n=3-4,), scale bars: 20μm. Quantification based on the mean fluorescence intensity (MFI) $x10^3$ (10 equal epithelial areas from each biopsy of control subjects (n=3) and patients with asthma (n=3-4)). Patients with asthma are presented in red, control individuals are presented in blue. Heatmap displays normalized gene expression across the groups (row normalization). Inflammasome-mediated immune responses gene set was curated based on databases and ontologies listed in the Molecular Signatures Database (MSigDB, Broad Institute, Cambridge). Bar graph data present mean ± SEM analysed with one-way ANOVA (Kruskal-Wallis test), RM one-way ANOVA (Friedman test) or mixed-effects model, as appropriate, depending on the data relation and distribution, p-value: *<0.05; *<0.005; ***<0.0005, ****<0.00005. *MFI*; mean fluorescent intensity; *RV-A16*, rhinovirus A16.

Supplementary Figure S4

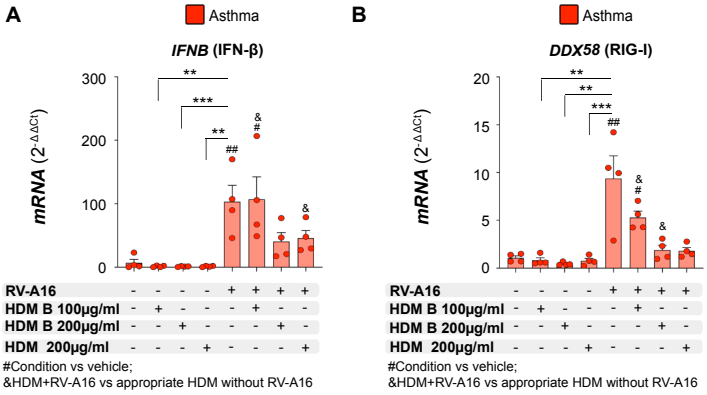

Supplementary Figure S4

House dust mite impaired interferon responses in rhinovirus-infected bronchial epithelium of patients with asthma

mRNA expression of **A)** *IFNB* (IFN-β) and **B)** *DDX58* (RIG-I) in HBECs from patients with asthma pre-treated with two HDM extracts from different manufacturers or vehicle for 24h followed by an infection with rhinovirus A16 (RV-A16) in the multiplicity of infection (MOI) 0.1, (n=4), assessed using RT-PCR. (*) represents a significant difference between indicated conditions. (#) represents a significant difference of indicated condition as compared to the vehicle. (&) represents a significant difference between HDM+RV-A16 treatment and HDM only. Graph data present mean ± SEM analysed with one-way ANOVA (Kruskal-Wallis test), RM one-way ANOVA (Friedman test) or mixed-effects model, as appropriate, depending on the data relation and distribution, *p-value≤0.05, **p-value≤0.01, ***p-value≤0.001. *HBECs*, differentiated human bronchial epithelial cells; *RV-A16*, rhinovirus A16; *HDM*, house dust mite.

Supplementary Figure S5

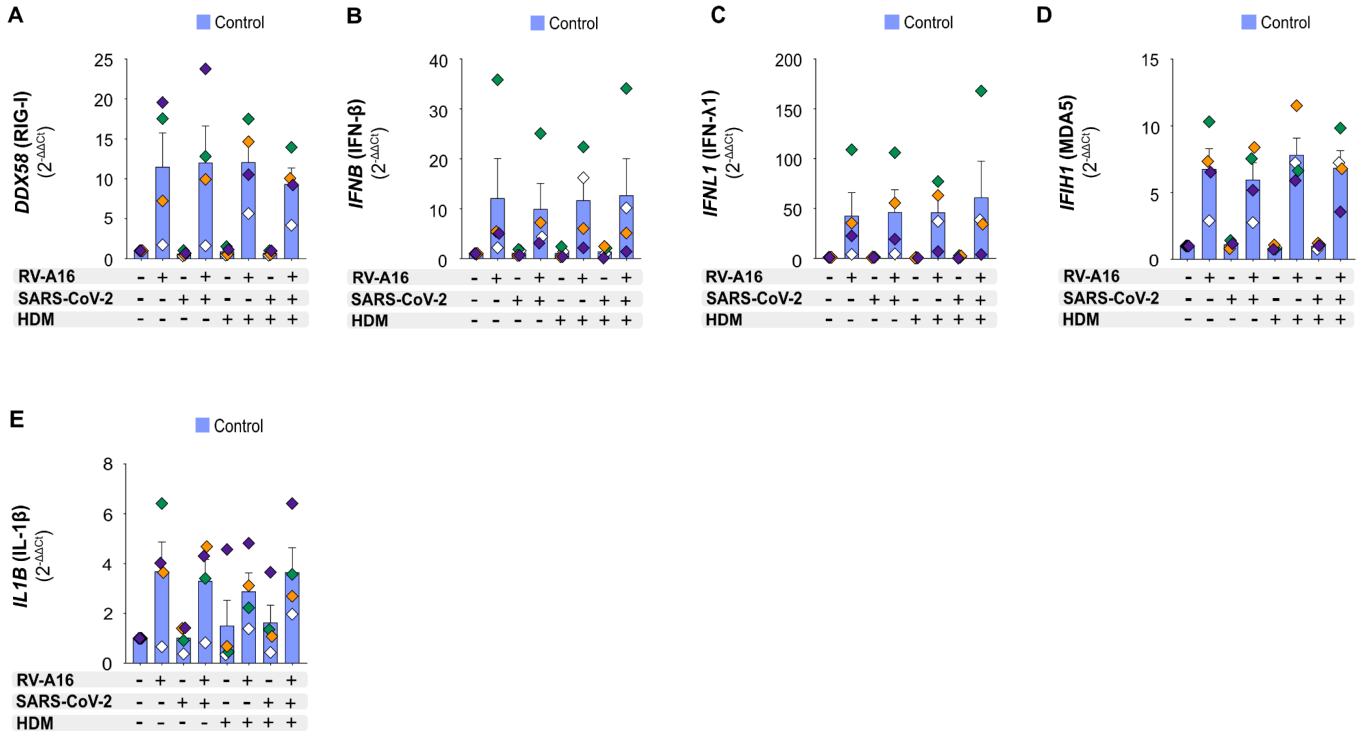

Supplementary Figure S5.

Pre-existing rhinovirus infection attenuated SARS-CoV-2 infection, but augmented epithelial inflammation in asthma

mRNA expression of **A)** *DDX58* (RIG-I), **B)** *IFNB* (IFN-β), **C)** *IFNL1* (IFN-λ1), **D)** *IFIH1* (MDA5), and **E)** *IL1B* (IL-1β) was assessed using RT-PCR and presented as relative quantification ($RQ=2^{-\Delta\Delta Ct}$) compared to vehicle condition (control: n=4). Data were analysed with Friedman's test. Bars depict the mean ± SEM, whereas color-coded diamonds (control subjects) show individual data from the same donor. *RV-A16*, rhinovirus A16; *HDM*, House Dust Mite; *HBECs*, Human Bronchial Epithelial Cells; *SARS-CoV-2*, Severe Acute Respiratory Syndrome Coronavirus

Supplementary Tables

Supplementary Table S1. Enrichment analysis of the ten most significant process networks in the top one hundred upregulated genes in human bronchial epithelial cells (HBECs) from control individuals and patients with asthma after rhinovirus A16 infection. Analyzed from GSE61141[66].

HBECs from control individuals					
	Networks	**Total**	**p-value**	**In data**	**Network objects from active data**
1	Inflammation_Interferon signaling	110	3.409E-37	27	IL29, PKR, CCL5, IFI17, IRF1, IL28A, MxB, ISG20, TAP1 (PSF1), IFI44, GBP1, I-TAC, Apo-2L(TNFSF10), STAT1/STAT2, SOCS1, IDO1, ISG54, STAT1, IRF7, MxA, IFP 35, IFI56, ISG15, IL28B, TLR3, PML, STAT2
2	Immune response_Innate immune response to RNA viral infection	83	1.840E-16	14	PKR, MDA-5, RIG-I, IP10, IRF1, I-TAC, WARS, 2'-5'-oligoadenylate synthetase, IDO1, STAT1, IRF7, MxA, TLR3, STAT2
3	Inflammation_Jak-STAT Pathway	185	4.596E-07	10	IL29, CCL5, IL28A, PLAUR (uPAR), LIFR, STAT1/STAT2, SOCS1, STAT1, IL28B, STAT2
4	Inflammation_IFN-gamma signaling	109	9.450E-06	7	PKR, CCL5, K12, IP10, IRF1, SOCS1, STAT1
5	Inflammation_Inflammasome	120	1.756E-04	6	PKR, MDA-5, RIG-I, IRF7, ISG15, TLR3
6	Chemotaxis	139	2.765E-03	5	CCL5, IP10, CX3CL1, PLAUR (uPAR), I-TAC
7	Inflammation_Innate inflammatory response	181	8.446E-03	5	APOBEC3G, IP10, I-TAC, IRF7, TLR3
8	Cell adhesion_Leucocyte chemotaxis	180	3.694E-02	4	CCL5, IP10, CX3CL1, I-TAC
9	Proliferation_Negative regulation of cell proliferation	183	3.889E-02	4	PKR, IFI17, WARS, STAT1
10	Immune response_Antigen presentation	194	4.655E-02	4	TAP1 (PSF1), STAT1, CEACAM1, STAT2

HBECs from patients with asthma					
	Networks	**Total**	**p-value**	**In data**	**Network objects from active data**
1	Inflammation_Interferon signaling	110	1.008E-32	25	IL29, CCL5, IFI17, IL28A, MxB, ISG20, TAP1 (PSF1), IFI44, GBP1, I-TAC, Caspase-1, Apo-2L(TNFSF10), MIG, STAT1/STAT2, IDO1, ISG54, STAT1, IRF7, MxA, IFP 35, IFI56, IL28B, TLR3, PML, STAT2
2	Immune response_Innate immune response to RNA viral infection	83	1.227E-14	13	MDA-5, RIG-I, IP10, IKK-epsilon, I-TAC, WARS, 2'-5'-oligoadenylate synthetase, IDO1, STAT1, IRF7, MxA, TLR3, STAT2
3	Inflammation_Jak-STAT Pathway	185	6.247E-06	9	IL29, IL-15RA, CCL5, IL28A, LIFR, STAT1/STAT2, STAT1, IL28B, STAT2
4	Inflammation_Inflammasome	120	2.189E-04	6	MDA-5, RIG-I, IKK-epsilon, Caspase-1, IRF7, TLR3
5	Inflammation_IFN-gamma signaling	109	1.126E-03	5	CCL5, K12, IP10, MIG, STAT1
6	Inflammation_Innate inflammatory response	181	1.918E-03	6	APOBEC3G, IP10, IKK-epsilon, I-TAC, IRF7, TLR3
7	Chemotaxis	139	3.287E-03	5	CCL5, IP10, I-TAC, IL-16, MIG
8	Immune response_Th17-derived cytokines	98	5.518E-03	4	MMP-13, I-TAC, MIG, STAT1
9	Inflammation_NK cell cytotoxicity	163	3.063E-02	4	IL-15RA, Apo-2L(TNFSF10), STAT1, STAT2
10	Cell adhesion_Platelet-endothelium-leucocyte interactions	174	3.063E-02	4	MMP-13, CCL5, STAT1, CD68

Supplementary Table S2. All antiviral response genes significantly changed after rhinovirus A16 (RV-A16) infection in bronchial brushings from control individuals and patients with asthma after in vivo RV-A16 infection or in differentiated human bronchial epithelial cells from control individuals and patients with asthma after in vitro RV-A16 infection (GSE61141)[66].

Bronchial brushings from control individuals in vivo		
Gene	**p-value**	**Log_2FC**
LYST	7.65E-05	-0.443907
IVNS1ABP	1.08E-04	-0.4197461
MAPK11	3.59E-04	0.28467409
BECN1	4.00E-04	-0.3110455
CCT5	4.43E-04	-0.412418
TBK1	4.93E-04	-0.5302973
ACTA2	5.67E-04	-0.4198554
ELMOD2	6.05E-04	-0.4646418
ABCE1	7.70E-04	-0.4356744
CD207	0.00120396	0.46706636
DNAJC3	0.00121386	-0.38085
BNIP3	0.00162649	-0.4523524
UNC93B1	0.00165717	0.29162879
SPACA3	0.00186858	0.29907682
IKBKB	0.00253497	0.31654719
IL33	0.00257272	-0.5662286
IFNAR1	0.00277058	-0.3379496
SLFN11	0.00304737	-0.5547823
IRF3	0.00309228	0.26590699
APOBEC3C	0.00450924	-0.4267123
CHRM2	0.00499786	0.2406417
IFNAR2	0.00502243	-0.3416906
CXADR	0.00512015	-0.2713458
MAPK14	0.00614791	-0.2494267
HSPB1	0.00753452	-0.2903693
CXCR4	0.00848183	-0.9033424
KCNJ8	0.01022031	0.19106938
CCDC130	0.01152673	0.26813823
POLR3G	0.01328435	0.29856694
DDX1	0.01405911	-0.2643058
RELA	0.01479098	-0.2935714
TRIM56	0.01547338	0.1881259
TLR8	0.01552932	-0.7104081
PSMA2	0.01595628	-0.4307298
CHUK	0.01748839	-0.3588789
FCN3	0.0184118	0.27715324
IL12B	0.0188253	0.208578
POLR3F	0.02210039	-0.2253792
HYAL2	0.02246593	0.1740213
CFL1	0.02444936	-0.3017413
IFNGR2	0.02559222	-0.3396424
UNC93B1	0.02568665	0.28795446
FGR	0.02652297	-0.7025369
DDX21	0.02830701	-0.3674024
RNASEL	0.02979535	-0.1934832
PTPRC	0.03030047	-0.8586604
DHX36	0.03121596	-0.3011299
TNF	0.0315715	-0.5356796
TPT1	0.0326018	0.45659592
DDX3X	0.033224	-0.2460331
XCL1	0.03392249	0.68704931
MICA	0.03469049	0.24172981
BANF1	0.03533612	0.21109478
MEF2C	0.03647154	-0.4306598
CD86	0.03691275	-0.8744841
CYP1A1	0.03713228	0.25314154
BANF1	0.03814064	-0.2129742
CCL4	0.04035564	-0.703145
CDK6	0.04161901	-0.1921755
PRKRA	0.04265319	-0.1935144
IL6	0.044015	-0.6248495

BNIP3L	0.0445931	-0.2107504
GBP3	0.0463936	-0.4441241

Bronchial brushings from patients with asthma in vivo		
Gene	**p-value**	**Log_2FC**
IFI44L	2.7513864	2.44E-07
IFITM1	2.26654724	8.93E-07
IFI44	1.78485617	1.86E-06
IFITM3	1.49792001	2.05E-06
BNIP3	-0.4879504	2.91E-06
MX1	1.79778192	6.72E-06
BST2	1.5213133	7.38E-06
IRF9	0.5769468	8.53E-06
OAS2	1.44133293	9.67E-06
STAT1	1.26202938	1.22E-05
OAS1	1.54613253	1.25E-05
MX2	2.04970628	1.52E-05
IFIT1	2.16478729	1.85E-05
PLSCR1	1.12390665	2.00E-05
DDX60	1.41443322	2.87E-05
TRIM22	1.02773215	3.26E-05
OAS3	1.54432653	5.23E-05
IFIT3	1.81597424	5.49E-05
DHX58	0.70446222	9.76E-05
DDX58	1.47047202	9.79E-05
EIF2AK	0.7781584	1.71E-04
FCN3	-0.3050202	1.99E-04
IKBKE	0.36925583	2.21E-04
STAT2	0.82594415	2.36E-04
GPAM	-0.2662866	2.96E-04
IFI16	0.66718059	3.25E-04
ISG15	0.96431722	3.28E-04
IFIT2	1.98331393	3.34E-04
DUOX2	1.62111069	3.40E-04
CXCL10	2.51578782	3.53E-04
PSMB9	0.94885053	3.74E-04
ISG20	0.59236245	4.44E-04
ADAR	0.52414375	4.48E-04
RSAD2	1.58864248	4.60E-04
NLRC5	0.61071381	6.45E-04
TRIM5	0.68854983	6.60E-04
IFITM2	0.87811185	7.01E-04
IRF7	0.47976395	7.04E-04
IRAK3	0.5721565	8.88E-04
HERC5	1.15893187	0.00107361
PML	0.66965248	0.00129139
CLU	-0.2599909	0.00156214
IFIT5	0.78368937	0.0017862
IFIH1	1.05426744	0.00181852
CXCL9	1.63985158	0.00260229
IRF1	0.72633033	0.00279675
PMAIP1	0.78214465	0.003265
GBP3	0.43999573	0.00331372
PYCARD	0.26990835	0.00334091
ZNF175	-0.2148014	0.00442761
CCL22	0.23745083	0.00563918
CCL19	0.24199143	0.0057422
APOBEC3G	0.59811982	0.00594614
ZC3H12A	0.27829253	0.00721255
OASL	0.89995485	0.00761047
APOBEC3F	0.34347153	0.0082971
IL6	0.53328796	0.00912099
ENO1	0.23331382	0.00934609
ABCC9	-0.2962732	0.00937097
BATF3	0.20857068	0.00957246
FOSL1	0.17740254	0.00977377
LGALS9	0.49906318	0.009962
HYAL1	0.15341526	0.0102313
APOBEC3H	0.21874676	0.01147115
TLR3	0.47466227	0.01234421

SERINC3	-0.1090338	0.01379487
SAMHD1	0.25655864	0.0140242
TLR8	0.46085583	0.01454437
PTPRC	0.62254589	0.01553325
TRIM11	0.10106083	0.01588222
CCL8	1.08815918	0.01736971
BNIP3L	-0.1621839	0.01771446
DCLK1	-0.1757575	0.01996567
LILRB1	0.63895374	0.02009985
CXADR	-0.1408438	0.02034223
F2RL1	0.20734859	0.02125084
TICAM1	0.18010247	0.02131712
APOBEC3D	0.22884253	0.02143983
IL33	-0.2644045	0.02260751
MST1R	0.19118748	0.02307895
HMGA1	0.13802169	0.02337107
ATG7	0.19313255	0.02563914
CDK6	0.13288052	0.02909091
CD86	0.5879905	0.02938831
HNRNPUL1	-0.1108471	0.03039986
CD207	-0.188618	0.03084029
IFNG	0.62195628	0.03202974
AGBL4	-0.2163882	0.03219032
IFNE	0.16956428	0.03676611
PRF1	0.4861052	0.04035228
CD40	0.30119882	0.0404023
ELMOD2	-0.1612959	0.04506776
SRC	0.13429267	0.04968988

Human bronchial epithelial cells from control individuals in vitro		
Gene	**p-value**	**Log_2FC**
IFIT2	7.149E-19	6.556
RSAD2	1.321E-18	5.049
OASL	3.391E-18	5.383
DDX58	1.106E-17	4.451
IFIT3	2.416E-17	5.408
MX2	1.33E-16	4.293
IFIH1	1.62E-16	3.93
CXCL10	1.72E-16	7.211
IFIT1	5.28E-16	5.359
OAS3	1.49E-15	3.911
OAS1	2.49E-15	3.849
CCL5	7.93E-15	3.8
HERC5	1.40E-14	3.05
ISG15	1.77E-14	4.998
DDX60	2.11E-14	3.328
APOBEC3A	2.28E-14	3.66
MX1	3.55E-14	4.369
C19orf66	6.97E-14	2.55
TRIM22	1.05E-13	2.948
IRF7	2.27E-13	2.788
ISG20	2.99E-13	3.233
OAS2	3.19E-13	3.4
STAT1	5.49E-13	3.245
IFI44L	9.02E-13	3.161
GBP1	1.03E-12	2.973
LGALS9	1.14E-12	2.699
NLRC5	1.88E-12	2.954
IFITM1	2.24E-12	3.642
STAT2	4.70E-12	2.322
PML	4.98E-12	2.81
IFI44	5.01E-12	2.485
TLR3	8.37E-12	2.098
TRIM25	9.38E-12	2.307
IRF1	9.84E-12	2.275
EIF2AK2	1.68E-11	2.167
APOBEC3G	2.40E-11	2.338
CXCL9	4.86E-11	3.759
BST2	5.97E-11	2.546
IFITM3	1.34E-10	2.711

DHX58	1.63E-10	2.137
IFITM2	2.30E-10	3.114
TRIM5	4.98E-10	2.133
PLSCR1	5.15E-10	2.003
TNF	7.26E-10	1.634
ZC3HAV1	2.38E-09	1.784
PSMB9	2.94E-09	1.885
TICAM1	4.18E-09	1.55
DUOX2	8.29E-09	2.733
APOBEC3F	8.74E-09	1.714
IKBKE	1.91E-08	1.756
IFIT5	2.91E-08	1.548
IFI16	3.20E-08	1.766
APOBEC3B	7.72E-08	2.314
CCL22	1.51E-07	1.697
ADAR	1.67E-07	1.552
PMAIP1	2.48E-07	1.58
IRF9	5.61E-07	1.231
IL23A	6.12E-07	1.446
PSMA2	1.28E-06	1.173
GBP3	3.34E-06	1.523
AGBL5	1.41E-05	-1.63
BCL3	2.21E-05	1.001
IRAK3	2.73E-05	1.001
ZC3H12A	5.23E-05	1.283
TBK1	5.63E-05	0.781
APOBEC3D	7.83E-05	0.8212
SRC	0.000167	0.8428
MST1R	0.0002878	0.9134
SAMHD1	0.0003501	0.8651
UNC13D	0.0003652	0.8952
PIM2	0.0004463	-0.7108
IFNGR2	0.0004815	0.79
HMGA1	0.0005404	0.8514
FOSL1	0.000623	0.7987
UNC93B1	0.0007337	1.011
TRIM56	0.002255	0.5678
APOBEC3C	0.002863	0.6992
GTF2F1	0.007381	0.5849
MAVS	0.007572	-0.5188
DHX36	0.00758	0.535
RELA	0.007593	0.5051
IVNS1ABP	0.01132	-0.5954
EIF2AK4	0.01289	-0.4502
HNRNPUL1	0.0142	-0.5764
STMN1	0.01626	-0.4616
TRIM34	0.01815	0.4168
BCL2L1	0.01992	-0.5224
BNIP3	0.021	-0.554
IKBKG	0.0211	0.4076
CXADR	0.02114	-0.4977
SERINC5	0.02395	-0.4672
TPT1	0.02416	0.53
LSM14A	0.03128	-0.4094
SLFN11	0.0375	0.4628
ILF3	0.03774	-0.4139
DCLK1	0.03914	-0.5191
CD40	0.04965	0.412

Human bronchial epithelial cells from patients with asthma in vitro		
Gene	**p-value**	**Log_2FC**
OASL	7.85E-24	5.906
CXCL10	1.53E-23	8.047
IFIT1	6.74E-22	5.723
IFIT2	3.04E-20	7.015
CXCL9	8.69E-20	4.486
IFIH1	2.55E-19	4.319
ISG20	7.46E-19	3.936
DDX58	1.02E-18	4.937
RSAD2	1.12E-18	5.618

HERC5	1.69E-18	3.359
IFIT3	2.12E-18	5.715
C19orf66	2.33E-18	3.042
MX2	3.91E-18	4.787
PML	5.07E-18	3.02
OAS1	6.75E-18	4.169
DHX58	1.16E-17	2.529
OAS2	1.38E-17	3.88
NLRC5	1.54E-17	3.176
CCL5	1.91E-17	4.491
GBP1	2.11E-17	3.626
MX1	2.96E-17	4.603
STAT2	5.46E-17	2.636
IFI44	5.47E-17	2.745
TRIM22	5.79E-17	2.969
APOBEC3G	6.16E-17	2.688
OAS3	6.39E-17	4.22
APOBEC3A	7.85E-17	4.408
TRIM5	1.06E-16	2.389
STAT1	1.50E-16	3.396
IFI44L	1.91E-16	3.4
APOBEC3F	2.71E-16	2.283
DDX60	3.08E-16	3.367
IRF7	3.30E-16	2.946
IFITM1	6.70E-16	3.543
IKBKE	1.36E-15	2.104
TLR3	1.49E-15	2.351
LGALS9	2.32E-15	2.614
PLSCR1	2.52E-15	2.191
IRF1	5.70E-15	2.376
IFITM2	8.08E-15	3.223
EIF2AK2	1.37E-14	2.326
ISG15	2.03E-14	5.013
TRIM25	2.11E-14	2.397
IFITM3	7.08E-14	2.617
APOBEC3B	2.09E-13	2.488
TICAM1	5.63E-13	2.069
PSMB9	5.84E-13	2
ZC3HAV1	6.16E-13	2.085
BST2	1.05E-12	2.952
IFI16	2.85E-12	2.035
TNF	3.32E-12	2.265
DUOX2	3.70E-12	3.288
ADAR	5.35E-12	1.839
IFIT5	2.19E-11	1.601
IRF9	3.05E-11	1.428
PMAIP1	1.83E-10	1.51
IL23A	8.16E-10	2.161
SAMHD1	1.19E-09	1.413
ZC3H12A	2.16E-09	1.723
CCL22	4.67E-09	1.918
MST1R	2.12E-08	1.137
BCL3	6.60E-08	1.057
CD40	3.82E-07	0.9531
SRC	8.37E-07	0.8584
IL6	1.11E-06	2.266
TRIM34	1.49E-06	0.8456
APOBEC3C	3.56E-06	0.9637
UNC93B1	4.02E-06	1.062
IRAK3	1.09E-05	0.9916
PSMA2	1.76E-05	0.8836
HMGA1	2.06E-05	0.8408
APOBEC3D	3.79E-05	0.8388
RELA	4.69E-05	0.6723
EIF2AK4	5.24E-05	-0.734
TRIM56	6.39E-05	0.6574
ABCE1	8.10E-05	-0.7558
AGBL5	0.0001097	-0.926
IFNGR2	0.0001243	0.6204
RNASEL	0.0001512	0.6969

FOSL1	0.0001995	1.182
GBP3	0.0003406	1.763
UNC13D	0.0003743	0.6806
BANF1	0.0005562	-0.618
SERINC5	0.001265	-0.5607
POLR3E	0.001463	-0.5625
GTF2F1	0.00148	0.5035
DCLK1	0.001586	-0.7357
STMN1	0.001603	-0.6112
CXADR	0.001645	-0.5167
BCL2L1	0.002159	-0.5074
DDX3X	0.002533	0.4623
IRF5	0.002761	0.5806
BAD	0.004124	-0.543
MAVS	0.00597	-0.4032
TBK1	0.006174	0.4936
FAM111A	0.009602	0.4343
LSM14A	0.01183	-0.4332
IKBKG	0.01247	0.3916
ILF3	0.01367	-0.3934
SPON2	0.01699	0.53
DDX21	0.0178	-0.3879
IFNAR1	0.01898	-0.3322
IVNS1ABP	0.02507	-0.3771
XPR1	0.02681	0.4449
ELMOD2	0.02688	-0.4107
PYCARD	0.03129	0.3599
LYST	0.03498	0.351
HNRNPUL1	0.03777	-0.3541
PRKRA	0.0379	-0.3664
BNIP3L	0.04307	-0.319
DHX36	0.0456	0.3483
TMEM173	0.04837	0.3204

Supplementary Table S3. KEGG pathways enriched in significantly changed proteins secreted from the human bronchial epithelial cells of control subjects and patients with asthma after house dust mite stimulation and rhinovirus A16 (RV-A16) infection, as compared to RV-A16 infection alone.

KEGG pathways downregulated (controls)						
#term ID	term description	observed gene count	background gene count	strength	false discovery rate	matching proteins in your network (labels)
map04060	Cytokine-cytokine receptor interaction	21	143	0.79	0.0000000000139	CX3CL1, TGFB1, CCL2, CXCL6, KITLG, IL12B, TNFSF10, IL18, CXCL5, CXCL11, CCL20, CCL28, CCL7, CCL8, IL6, TNF, TNFSF14, FLT3LG, CCL3, VEGFA, CCL4
map04062	Chemokine signaling pathway	11	40	1.06	0.000000202	CX3CL1, CCL2, CXCL6, CXCL5, CXCL11, CCL20, CCL28, CCL7, CCL8, CCL3, CCL4
map05323	Rheumatoid arthritis	10	36	1.06	0.000000784	TGFB1, CCL2, CXCL6, IL18, CXCL5, CCL20, IL6, TNF, CCL3, VEGFA
map04620	Toll-like receptor signaling pathway	7	22	1.12	0.0000553	IL12B, CXCL11, CASP8, IL6, TNF, CCL3, CCL4
map04657	IL-17 signaling pathway	8	36	0.97	0.0000725	CCL2, CXCL6, CXCL5, CASP8, CCL20, CCL7, IL6, TNF
map05142	Chagas disease (American trypanosomiasis)	7	28	1.02	0.00014	TGFB1, CCL2, IL12B, CASP8, IL6, TNF, CCL3
map04668	TNF signaling pathway	7	31	0.97	0.00022	CX3CL1, CCL2, CXCL5, CASP8, CCL20, IL6, TNF
map05134	Legionellosis	5	12	1.24	0.00036	IL12B, IL18, CASP8, IL6, TNF
map05200	Pathways in cancer	10	98	0.63	0.001	TGFB1, KITLG, IL12B, AXIN1, TGFA, FGF5, CASP8, IL6, FLT3LG, VEGFA
map05168	Herpes simplex infection	6	31	0.91	0.0015	CCL2, IL12B, CASP8, IL6, TNF, TNFSF14
map05164	Influenza A	6	33	0.88	0.0019	CCL2, IL12B, TNFSF10, IL18, IL6, TNF
map04621	NOD-like receptor signaling pathway	5	21	1	0.0022	CCL2, IL18, CASP8, IL6, TNF
map05133	Pertussis	5	21	1	0.0022	CXCL6, IL12B, CXCL5, IL6, TNF
map05152	Tuberculosis	6	36	0.84	0.0023	TGFB1, IL12B, IL18, CASP8, IL6, TNF
map05321	Inflammatory bowel disease (IBD)	5	23	0.96	0.0025	TGFB1, IL12B, IL18, IL6, TNF
map04933	AGE-RAGE signaling pathway in diabetic complications	5	25	0.92	0.0033	TGFB1, CCL2, IL6, TNF, VEGFA
map05144	Malaria	5	26	0.9	0.0037	TGFB1, CCL2, IL18, IL6, TNF
map05132	Salmonella infection	4	14	1.08	0.0038	IL18, IL6, CCL3, CCL4
map05143	African trypanosomiasis	4	15	1.05	0.0044	IL12B, IL18, IL6, TNF
map04010	MAPK signaling pathway	7	71	0.61	0.0086	TGFB1, KITLG, TGFA, FGF5, TNF, FLT3LG, VEGFA
map04932	Non-alcoholic fatty liver disease (NAFLD)	4	19	0.94	0.0086	TGFB1, CASP8, IL6, TNF
map05161	Hepatitis B	4	20	0.92	0.0097	TGFB1, CASP8, IL6, TNF
map04623	Cytosolic DNA-sensing pathway	3	9	1.14	0.0109	IL18, IL6, CCL4
map05146	Amoebiasis	4	22	0.88	0.0121	TGFB1, IL12B, IL6, TNF
map05145	Toxoplasmosis	4	24	0.84	0.0154	TGFB1, IL12B, CASP8, TNF
map04622	RIG-I-like receptor signaling pathway	3	11	1.06	0.0155	IL12B, CASP8, TNF
map05212	Pancreatic cancer	3	11	1.06	0.0155	TGFB1, TGFA, VEGFA
map01521	EGF5R tyrosine kinas5e inhibitor resistance	4	26	0.81	0.0177	TGFA, EIF4EBP1, IL6, VEGFA
map05211	Renal cell carcinoma	3	12	1.02	0.0177	TGFB1, TGFA, VEGFA
map04014	Ras signaling pathway	5	45	0.67	0.0189	KITLG, TGFA, FGF5, FLT3LG, VEGFA

map05165	Human papillomavirus infection	5	46	0.66	0.02	AXIN1, EIF4EBP1, CASP8, TNF, VEGFA
map04151	PI3K-Akt signaling pathway	7	92	0.5	0.0215	KITLG, TGFA, FGF5, EIF4EBP1, IL6, FLT3LG, VEGFA
map05210	Colorectal cancer	3	14	0.95	0.0218	TGFB1, AXIN1, TGFA
map05225	Hepatocellular carcinoma	3	14	0.95	0.0218	TGFB1, AXIN1, TGFA
map05410	Hypertrophic cardiomyopathy (HCM)	3	14	0.95	0.0218	TGFB1, IL6, TNF
map04068	FoxO signaling pathway	3	17	0.87	0.0319	TGFB1, TNFSF10, IL6
map04218	Cellular senescence	3	19	0.82	0.0407	TGFB1, EIF4EBP1, IL6
map01523	Antifolate resistance	2	6	1.14	0.0408	IL6, TNF
map04672	Intestinal immune network for IgA production	3	21	0.77	0.0492	TGFB1, CCL28, IL6
map05140	Leishmaniasis	3	21	0.77	0.0492	TGFB1, IL12B, TNF
map05226	Gastric cancer	3	21	0.77	0.0492	TGFB1, AXIN1, FGF5

Pathways marked in red demonstrate proteins included in viral infection pathway on the Figure 7C

KEGG pathways upregulated (controls)
No significant enrichment

KEGG pathways downregulated (asthma)						
#term ID	**term description**	**observed gene count**	**background gene count**	**strength**	**false discovery rate**	**matching proteins in your network (labels)**
map04060	Cytokine-cytokine receptor interaction	21	143	0.79	0.0000000000132	CX3CL1, TGFB1, CCL2, CXCL6, KITLG, TNFSF10, IL17C, IL7, CXCL5, CXCL10, CXCL11, CCL20, CCL28, CCL7, IL6, TNF, TNFSF14, FLT3LG, CCL3, VEGFA, CCL4
map04062	Chemokine signaling pathway	11	40	1.06	0.000000192	CX3CL1, CCL2, CXCL6, CXCL5, CXCL10, CXCL11, CCL20, CCL28, CCL7, CCL3, CCL4
map04657	IL-17 signaling pathway	10	36	1.06	0.000000742	CCL2, CXCL6, IL17C, CXCL5, CXCL10, MMP1, CCL20, CCL7, IL6, TNF
map05323	Rheumatoid arthritis	10	36	1.06	0.000000742	TGFB1, CCL2, CXCL6, CXCL5, MMP1, CCL20, IL6, TNF, CCL3, VEGFA
map04668	TNF signaling pathway	7	31	0.97	0.00029	CX3CL1, CCL2, CXCL5, CXCL10, CCL20, IL6, TNF
map04620	Toll-like receptor signaling pathway	6	22	1.06	0.00045	CXCL10, CXCL11, IL6, TNF, CCL3, CCL4
map05200	Pathways in cancer	10	98	0.63	0.0012	TGFB1, KITLG, AXIN1, IL7, TGFA, FGF5, MMP1, IL6, FLT3LG, VEGFA
map04933	AGE-RAGE signaling pathway in diabetic complications	5	25	0.92	0.0063	TGFB1, CCL2, IL6, TNF, VEGFA
map05142	Chagas disease (American trypanosomiasis)	5	28	0.87	0.0088	TGFB1, CCL2, IL6, TNF, CCL3
map04010	MAPK signaling pathway	7	71	0.61	0.015	TGFB1, KITLG, TGFA, FGF5, TNF, FLT3LG, VEGFA
map04151	PI3K-Akt signaling pathway	8	92	0.56	0.015	KITLG, IL7, TGFA, FGF5, EIF4EBP1, IL6, FLT3LG, VEGFA
map05164	Influenza A	5	33	0.8	0.015	CCL2, TNFSF10, CXCL10, IL6, TNF
map04623	Cytosolic DNA-sensing pathway	3	9	1.14	0.0181	CXCL10, IL6, CCL4
map05133	Pertussis	4	21	0.9	0.0181	CXCL6, CXCL5, IL6, TNF
map04640	Hematopoietic cell lineage	5	41	0.71	0.0248	KITLG, IL7, IL6, TNF, FLT3LG
map05212	Pancreatic cancer	3	11	1.06	0.0248	TGFB1, TGFA, VEGFA
map01521	EGFR tyrosine kinase inhibitor resistance	4	26	0.81	0.0277	TGFA, EIF4EBP1, IL6, VEGFA
map04014	Ras signaling pathway	5	45	0.67	0.0277	KITLG, TGFA, FGF5, FLT3LG, VEGFA

map04926	Relaxin signaling pathway	3	13	0.98	0.0277	TGFB1, MMP1, VEGFA
map05144	Malaria	4	26	0.81	0.0277	TGFB1, CCL2, IL6, TNF
map05211	Renal cell carcinoma	3	12	1.02	0.0277	TGFB1, CCL2, IL6, TNF
map05132	Salmonella infection	3	14	0.95	0.031	IL6, CCL3, CCL4
map05210	Colorectal cancer	3	14	0.95	0.031	TGFB1, AXIN1, TGFA
map05225	Hepatocellular carcinoma	3	14	0.95	0.031	TGFB1, AXIN1, TGFA
map05410	Hypertrophic cardiomyopathy (HCM)	3	14	0.95	0.031	TGFB1, IL6, TNF
map05168	Herpes simplex infection	4	31	0.73	0.0319	CCL2, IL6, TNF, TNFSF14
map04068	FoxO signaling pathway	3	17	0.87	0.0403	TGFB1, TNFSF10, IL6

Pathways marked in red demonstrate proteins included in viral infection pathway on the Figure 7C

KEGG pathways upregulated (asthma)						
#term ID	**term description**	**observed gene count**	**background gene count**	**strength**	**false discovery rate**	**matching proteins in your network (labels)**
map04060	Cytokine-cytokine receptor interaction	8	143	0.7	0.0021	IL4, IL1A, IL10RB, TNFRSF11B, CD40, IL24, TNFSF11, TNFRSF9

Pathways marked in red demonstrate proteins included in cytokine-mediated signaling pathway on the Figure 7C

Supplementary Table S4. Protein concentrations in apical compartment of human bronchial epithelial cells from control individuals and patients with asthma in indicated conditions.

Control (n=4)	**Medium**	**RV-A16**	**SARS-CoV-2**	**RV-A16 + SARS-CoV-2**	**HDM**	**HDM+ RV-A16**	**HDM + SARS-CoV-2**	**HDM+RV-A16+ SARS-CoV-2**
TWEAK, pg/mL (mean, SEM)	70.61 (10.11)	81.12 (25.90)	91.16 (30.74)	103.3 (24.18)	106.9 (31.01)	72.73(17.71)	83.42 (24.71)	58.33 (10.82)
IL-7, pg/mL (mean, SEM)	11.67 (4.517)	11.68 (0.4573)	12.33 (2.145)	20.02 (9.446)	18.29 (8.381)	13.35 (4.343)	17.52 (7.691)	12.91 (3.969)
IL-6, pg/mL (mean, SEM)	838.9 (461.0)	1603 (761.4)	895.8 (503.8)	1542 (837.9)	411.5 (182.0)	637.9 (395.5)	447.2 (271.5)	642.7 (332.4)
TRAIL, pg/mL (mean, SEM)	1246 (279.0)	1879 (276.4)	1089 (439.8)	2416 (923.1)	806.8 (162.3)	1012 (253.8)	1106 (442.6)	1122 (306.4)
IL-18, pg/mL (mean, SEM)	1.13 (0.09892)	4.767 (0.4784)	2.427 (0.3510)	6.238 (1.634)	2.261 (0.9410)	5.52 (0.4008)	3.224 (1.174)	6.117 (1.489)
IL-15, pg/mL (mean, SEM)	13.64 (3.601)	14.61 (2.332)	11.81 (3.049)	18.45 (4.596)	10.66 (1.038)	13.91 (2.131)	14.02 (2.787)	15.36 (2.302)
CXCL9, pg/mL (mean, SEM)	26.57 (5.050)	75.36 (5.172)	26.41 (5.236)	64.17 (12.07)	29.64 (6.358)	68.07 (26.22)	28.67 (4.519)	70.48 (34.03)
IL-17C, pg/mL (mean, SEM)	57.13 (14.14)	131.7 (65.29)	63.66 (35.79)	91.39 (30.62)	75.52 (30.22)	75.64 (25.73)	47.46 (8.440)	57.80 (8.351)
CCL8, pg/mL (mean, SEM)	0.2323 (0.02910)	5.146 (2.076)	0.4479 (0.1871)	3.085 (1.220)	0.3860 (0.1017)	2.052 (1.083)	0.4622 (0.2222)	2.112 (0.5764)

RV-A16, rhinovirus A16; *SARS-CoV-2*, severe acute respiratory syndrome coronavirus 2; *HDM*, house dust mite

Asthma (n=5)	**Medium**	**RV-A16**	**SARS-CoV-2**	**RV-A16 + SARS-CoV-2**	**HDM**	**HDM+ RV-A16**	**HDM + SARS-CoV-2**	**HDM+RV-A16+ SARS-CoV-2**
TWEAK, pg/mL (mean, SEM)	59.38 (16.12)	99.62 (35.25)	62.92 (13.09)	43.90 (7.524)	148.0 (57.71)	108.3 (35.22)	143.5 (60.21)	148.7 (55.08)
IL-7, pg/mL (mean, SEM)	13.36 (3.353)	21.49 (9.893)	14.12 (3.772)	9.822 (2.986)	27.67 (14.72)	20.58 (9.203)	24.80 (14.36)	29.50 (15.03)
IL-6, pg/mL (mean, SEM)	1004 (323.7)	1795 (558.7)	959.6 (280.9)	1147 (392.5)	658.3 (255.2)	953.3 (406.1)	625.9 (250.9)	1558 (604.9)
TRAIL, pg/mL (mean, SEM)	724.6 (59.55)	2069 (520.7)	945.7 (179.2)	1144 (238.4)	1153 (360.4)	1266 (136.6)	941.0 (256.9)	2167 (177.7)
IL-18, pg/mL (mean, SEM)	1.603 (0.2176)	7.817 (1.117)	2.076 (0.2509)	10.25 (3.334)	2.336 (0.6292)	9.263 (2.571)	2.825 (0.3171)	9.956 (2.112)
IL-15, pg/mL (mean, SEM)	10.32 (1.243)	16.20 (1.749)	11.94 (1.113)	15.80 (1.542)	7.976 (1.722)	18.68 (3.937)	11.13 (1.307)	21.62 (1.733)
CXCL9, pg/mL (mean, SEM)	22.10 (7.700)	53.18 (12.46)	20.93 (5.088)	35.83 (10.81)	19.97 (6.450)	64.72 (27.70)	17.19 (4.945)	67.16 (26.03)
IL-17C, pg/mL (mean, SEM)	53.18 (26.43)	196.5 (103.5)	45.89 (17.83)	94.16 (28.81)	66.09 (25.44)	156.8 (74.68)	64.77 (30.70)	195.0 (110.2)
CCL8, pg/mL (mean, SEM)	0.4266 (0.1867)	6.139 (4.612)	0.3114 (0.1229)	1.687 (0.5324)	0.4799 (0.1937)	6.693 (5.944)	0.3721 (0.1516)	14.40 (12.91)

RV-A16, rhinovirus A16; *SARS-CoV-2*, severe acute respiratory syndrome coronavirus 2; *HDM*, house dust mite

Supplementary Table S5. House dust mite extracts characteristics.

	HDM extract (Allergopharma)	**HDM extract B (Citeq)**
Protein content	0.525 mg protein/mg extract	0.216 mg protein/ mg extract
Endotoxin content	6.27 EU/mg extract	51 EU/mg extract
Der p 1	46.66 µg/mg extract	21 µg/mg extract
Der p 2	-	2.9 µg/mg extract

EU, endotoxin units, *Der p 1*, house dust mite Der p1 allergen; *Der p 2*, house dust Mite Der p 2 allergen.

Supplementary Table S6. Commercially available reagents used in the study.

Reagent	Catalog number	Company
Human Bronchial Epithelial cells	EP51AB	Epithelix
Human Bronchial Epithelial cells	CC-2540	Lonza
THP-1 cells	thpx-sp	Invivogen
House dust mite extract	02.01.64	Citeq
Human Rhinovirus A16	C1404B	Virapur
Ac-YVAD-cmk caspase-1 inhibitor	inh-yvad	Invivogen
MCC950, NLRP3 inflammasome inhibitor	AV02509	Avistron
TBK1/IKKε inhibitor BX795	702675-74-9	Sigma-Aldrich
LPS	tlrl-3pelps	Invivogen
ATP	tlrl-atp	Invivogen
BEGM Bronchial Epithelial Growth Medium BulletKit	CC3171+CC-4175	Lonza
DMEM	41965-039	Gibco
MucilAir Medium	EP03MD	Epithelix
RPMI-1640	R8758-500ml	Sigma-Aldrich
Opti-MEM® I Reduced Serum Medium	31985070	LifeTechnologies
Corning Inserts in 24-well culture plates, sterile	3470-COR	Corning
Retinoic Acid	R2625-50mg	Sigma-Aldrich
Trypsin-EDTA (0.5%)	15400-054	Thermofisher Scientific
Human IL1B/IL-1F2 duo set	DY201	R&D systems
TMB Substrate Reagent Kit	555214	BD
V-Plex Human IL1B kit	K151QPD-1	MSD
RIPA Lysis and Extraction Buffer	89901	ThermoFisher Scientific
cOmplete™, Mini, EDTA-free Protease Inhibitor Cocktail	4693159001	Merc (Roche)
Pierce BCA Protein Assay Kit	23225	ThermoFisher Scientific
4–20% Mini-PROTEAN® TGX™ Precast Protein Gels, 10-well, 50 µl	4561094	Biorad
Trans-Blot® Turbo™ Mini Nitrocellulose Transfer Packs	1704158	Biorad
10x Tris/Glycine/SDS Running Buffer	161-0772	Biorad
SurePAGE™, Bis-Tris, 10x8, 4-20%, 12 wells	M00656	GenScript
Nitrocellulose Transfer Membrane, 0.22um	L-08006-001	Advansta
WesternBright Sirius HRP substrate	K-12043-C20	Advansta
Restore™ PLUS Western Blot Stripping Buffer	46428	ThermoFisher Scientific
SuperSignal West Femto Maximum Sensitivity Substrate	34095	ThermoFisher Scientific
2-mercaptoetanol	63689-100ml-F	Sigma-Aldrich
RNAeasy Plus Micro Kit	74034	Qiagen
RevertAid RT Reverse Transcription Kit	K1691	ThermoFisher Scientific
Maxima SYBR Green/ROX qPCR Master Mix (2X)	K0221	ThermoFisher Scientific
RNAlater Stabilization Solution	1018087	Qiagen
SuperScript IV VILO Master Mix	11756050	ThermoFisher Scientific
RecoverAll	AM1975	ThermoFisher Scientific
FSC22 Frozen Section Media	3801480	Leica
ProLong Diamond Antifade Mountant with DAPI	P36962	ThermoFisher Scientific
TaqMan™ 2019-nCoV Assay Kit v1*	A47532	ThermoFisher Scientific
RV_20f2 TaqMan Assay - Vi99990017_po	A41333	ThermoFisher Scientific
Western Blot analyses		
Mouse anti-NLRP3	AG-20B-0014-C100	Adipogen
Goat anti-IL1B	AF-201-NA	R&D systems
Mouse anti-ASC	sc-514414	Santa Cruz Biotechnology
Rabbit anti-Caspase-1	2225	Cell Signaling
Goat anti-RIG-I	sc-48929	Santa Cruz Biotechnology

HRP Goat Anti Mouse IgG	111-035-146	Jackson Laboratory
HRP Mouse anti-goat IgG	sc2354	Santa Cruz Biotechnology
HRP AffiniPure Goat Anti Rabbit IgG	111-035-003	Jackson Laboratory
HRP Anti-beta Actin	ab49900	Abcam
Co-immunoprecipitation analyses		
Rabbit anti-ASC	sc22514-R	Santa Cruz Biotechnology
Protein A Beads	161-0413	Biorad
Mouse anti-RIG-I	sc376845	Santa Cruz Biotechnology
Rabbit anti-MDA5	ab126630	Abcam
HRP Goat Anti Mouse IgG	115-035-146	Jackson Laboratory
HRP AffiniPure Goat Anti Rabbit IgG	111-035-003	Jackson Laboratory
Western Blot from apical compartments analyses		
Goat anti-IL1B	AF-201-NA	R&D systems
HRP Mouse anti-goat IgG	sc2354	Santa Cruz Biotechnology
Confocal staining in HBECs		
Mouse IgG1 anti-IL1B	ab156791	Abcam
Mouse IgG1 anti-RIG-I	sc-376845	Santa Cruz Biotechnology
Mouse IgG1 anti-ASC	sc-514414	Santa Cruz Biotechnology
Goat anti-mouse IgG, Alexa Fluor 546	A11003	Invitrogen
Goat anti-mouse IgG, Alexa Fluor 488	A11001	Invitrogen
Mouse IgG1 Control	X0931	Dako
Goat serum (Normal)	X0907	Dako
Confocal staining in bronchial brushings		
Rabbit anti-Caspase-1	2225	Cell Signalling
Mouse IgG1 anti-IL1B	ab156791	Abcam
Mouse IgG1 anti-RIG-I	sc-376845	Santa Cruz Biotechnology
Goat anti-Rabbit IgG, Alexa Fluor 488	A11034	Invitrogen
Goat anti-mouse IgG, Alexa Fluor 546	A11003	Invitrogen
Goat anti-mouse IgG, Alexa Fluor 546	A11003	Invitrogen
Rabbit Immunoglobin Fraction	X0936	Dako
Mouse IgG1 Control	X0931	Dako
Goat Serum (Normal)	X0907	Dako
Confocal staining for NLRP3 and SARS-CoV-2 experiment		
Anti ACE2	ab15348	Abcam
Anti NLRP3	AG-20B-0014-C100	Adipogen
Anti Occludin	OC-3F10	ThermoFisher
Anti N-Protein	MA1-7404	ThermoFisher
Rabbit Ig Fraction	X0936	DAKO
Mouse IgG1	X0931	DAKO
Mouse IgG2b	X0944	DAKO
Goat anti-Mouse IgG Alexa 488	A11001	Invitrogen
Goat anti-Rabbit IgG Alexa 546	A11010	Invitrogen
Goat anti mouse IgG2b	A21143	Invitrogen
DAPI	10236276001	Sigma Aldrich

Supplementary Table S7. Clinical characteristics of study participants. In vivo and in vitro cohorts.

In vivo RV-A16 infection cohort									
Condition	**Gina status**	**ACQ status at baseline[$]**	**Age (years, age range)**	**Gender**	**Drugs**	**FeV1 (%) day 0 (% predicted)**	**Total serum IgE (IU/mL)**	**Total SPT weal size (mm)**	**HDM SPT weal size (mm)**
Control	Healthy	Healthy	21-25	Male	na	113	22	0	0
Control	Healthy	Healthy	21-25	Male	na	97	16	0	0
Control	Healthy	Healthy	21-25	Male	na	97	16	0	0
Control	Healthy	Healthy	46-50	Female	na	88	19	0	0
Control	Healthy	Healthy	31-35	Female	na	103	13	0	0
Control	Healthy	Healthy	26-30	Male	na	105	3	0	0
Control	Healthy	Healthy	26-30	Female	na	105	38	0	0
Control	Healthy	Healthy	51-55	Male	na	105	16	0	0
Control	Healthy	Healthy	16-20	Male	na	100	14	0	0
Asthma	mild	well	26-30	Female	SABA	113	207	5	0
Asthma	moderate	poor	31-35	Male	ICS	70	870	11	3
Asthma	mild	well	21-25	Male	SABA	91	121	14	4
Asthma	moderate	well	16-20	Female	ICS	92	64	16	0
Asthma	moderate	well	46-50	Female	ICS	88	57	8	0
Asthma	mild	partial	31-35	Male	SABA	79	806	13	5
Asthma	moderate	partial	31-35	Female	ICS	65	507	8	0
Asthma	moderate	poor	31-35	Male	ICS	84	146	12	3
Asthma	moderate	partial	46-50	Male	SABA	73	1204	7	4
Asthma	mild	partial	31-35	Female	SABA	78	119	6	6
Asthma	moderate	poor	26-30	Male	SABA	73	19	11	4
Asthma	moderate	poor	51-55	Male	ICS	83	157	26	5
Asthma	moderate	partial	31-35	Female	ICS	77	67	7	0
Asthma	moderate	poor	41-45	Female	ICS	68	1593	3	4
Asthma	mild	well	21-25	Female	SABA	115	213	10	4
Asthma	moderate	poor	41-45	Male	ICS	74	228	17	0
Asthma	moderate	well	46-50	Male	ICS	81	87	9	3
Asthma	moderate	partial	46-50	Female	ICS	82	2106	29	9
Asthma	mild	well	51-55	female	SABA	101	69	14	5

RV-A16; rhinovirus A16*; GINA*; global initiative for asthma; *ACQ*, asthma control questionnaire; *FeV1*, forced expiratory volume in 1 second; *IgE*, immunoglobulin E; *SPT*, skin prick test; *HDM*, house dust mite; *na*, not applicable; *SABA*, short acting beta agonists; *ICS*, inhaled corticosteroids. $ Well controlled=ACQ score ≤0.75, partially controlled=ACQ score 0.76-1.49, poorly controlled=ACQ score ≥1.50, *=summation of all positive individual allergen weal sizes

Cohort SIBRO (In vitro)				
Obesity Status	**Asthma Status**	**Age (years, age range)**	**Gender**	**BMI (kg/m^2)**
Non-Obese	Non-asthma	41-45	Male	24.61
Non-Obese	Non-asthma	26-30	Male	21.62
Non-Obese	Non-asthma	26-30	Female	21.01
Non-Obese	Non-asthma	46-50	Male	23.57
Non-Obese	Non-asthma	41-45	Male	22.86
Non-Obese	Non-asthma	41-45	Female	22.21
Non-Obese	Non-asthma	51-55	Female	24.14
Non-Obese	Asthma	31-35	Male	21.74
Non-Obese	Asthma	26-30	Female	24.8
Non-Obese	Asthma	21-25	Male	23.94
Non-Obese	Asthma	26-30	Male	22.69
Non-Obese	Asthma	51-55	Female	21.56
Non-Obese	Asthma	36-40	Female	19.92
Non-Obese	Asthma	46-50	Female	21.1
Non-Obese	Asthma	46-50	Female	23.42
Non-Obese	Asthma	41-45	Male	25.21
Non-Obese	Asthma	51-55	Female	21.56
Non-Obese	Asthma	51-55	Female	21.83
Non-Obese	Asthma	56-60	Female	24.68

BMI, body max index.

Cohort A (In vitro)		
Diagnosis	**Gender**	**Age (years, age range)**
Control	Female	26-30
Control	Male	26-30
Control	Male	61-65
Control	Male	41-45
Control	Female	31-35
Asthma	Female	26-30
Asthma	Female	61-65
Asthma	Female	26-30
Asthma	Female	61-65
Asthma	Female	51-55
Asthma	Female	41-45
Asthma	Female	36-40
Asthma	Female	61-65

Asthma	Male	51-55
Asthma	Male	56-60
Asthma	Male	31-35
Asthma	Male	51-55

Supplementary Table S8. Primary human bronchial epithelial cells (HBECs) used in the study. Commercially available and obtained from the study subjects.

HBECs source	Condition	Age (years, age range)	Gender	Smoker
Epithelix	Healthy	71-75	Male	No
Epithelix	Healthy	51-55	Male	No
Epithelix	Healthy	76-80	Male	No
Epithelix	Healthy	51-55	Male	No
Epithelix	Healthy	61-65	Male	No
Epithelix	Healthy	56-61	Male	No
Lonza	Healthy	66-70	Female	No
Lonza	Healthy	21-25	Female	No
Epithelix	Healthy	51-55	Female	No
Epithelix	Healthy	16-20	Male	No
Epithelix	Healthy	61-65	Female	No
Epithelix	Healthy	16-20	Male	No
Epithelix	Asthma	36-40	Male	No
Epithelix	Asthma	51-55	Male	No
Epithelix	Asthma	41-45	Male	No
Epithelix	Asthma	56-60	Male	No
Lonza	Asthma	66-70	Male	No
Lonza	Asthma	61-65	Female	No
Lonza	Asthma	11-15	Female	No
Lonza	Asthma	21-25	Male	No
Epithelix	Asthma	16-20	Female	No
Epithelix	Asthma	46-50	Male	No
Epithelix	Asthma	76-80	Female	No
Epithelix	Asthma	51-55	Female	No
Epithelix	Asthma	46-50	Female	No

Cell source	Condition	Age (years, age range)	Gender
Cohort A	Control	51-55	Female
Cohort A	Control	71-75	Male
Cohort SIBRO	Non-asthma	31-35	Female
Cohort A	Asthma	46-50	Female
Cohort A	Asthma	36-40	Female
Cohort A	Asthma	51-55	Male
Cohort A	Asthma	61-65	Male
Cohort A	Asthma	46-50	Female
Cohort A	Asthma	36-40	Male
Cohort A	Asthma	21-25	Female
Cohort A	Asthma	61-65	Female
Cohort A	Asthma	26-30	Female
Cohort A	Asthma	66-70	Female
Cohort A	Asthma	61-65	Female
Cohort A	Asthma	51-55	Female
Cohort SIBRO	Asthma	41-45	Male
Cohort SIBRO	Asthma	31-35	Male
Cohort SIBRO	Asthma	51-55	Male

Supplementary Table S9. Sequences of the primers used in the study.

Gene	Forward primer sequence	Reverse primer sequence
IL1B	CTCTTCGAGGCACAAGGCA	GGCTGCTTCAGACACTTGAG
RV-A16 POSITIVE STRAND	CGGGACTGCAAACACTACCT	CACCACGTGTGTCCCTAACA
DDX58	TGATTGCCACCTCAGTTGCT	TCCTCTGCCTCTGGTTTGGA
NLRC5	GCTGGAGGAGGTCAGTTTGC	TGTTTCGGCTCAGGTCAAGT
IFIH1	AGATGCAACCAGAGAAGATCCA	TGGCCCATTGTTCATAGGGT
CASP1	GCCCACCACTGAAAGAGTGA	TTCACTTCCTGCCCACAGAC
IFNL2/3	CTGGGAGACAGCCCAGTTCA	AGAAGCGACTCTTCTAAGGCATCTT
IFNB1.1	CGCCGCATTGACCATCTA	GACATTAGCCAGGAGGTTCTC
IFNB1.2	AGGCCAAGGAGTACAGTCAC	GAGGTAACCTGTAAGTCTGTTAATG
EEFA1	TGAAGTCTGGTGATGCTGCC	CAAAGCGACCCAAAGGTGGA
Gene	**Primer pair ID**	**Company**
IFNL1	H_IL29_1	Sigma Aldrich

Supplementary Table S10. List of genes included in inflammasome-mediated immune responses and antiviral responses gene sets. Curated from the gene sets available at the GSEA and MSigDB Databases.

Inflammasome-mediated immune responses	TXNIP, NLRP3, NLRP1, PANX1, PYCARD, HSP90AB1, APP, MEFV, P2RX7, NLRC4, BCL2, BCL2L1, TXN, CASP1, PSTPIP1, AIM2, CASP4, CASP5, CASP8, NLRC5, DDX58, IFIH1, IL18, NLRP7, NOD1, TAB1, IRAK3, CHUK, MAP3K8, TAB2, PELI3, TAB3, IKBKB, IL1A, IL1B, IL1R1, IL1RAP, IL1RN, IRAK1, IRAK2, TMEM189-UBE2V1, MAP3K3, MYD88, IRAK4, TOLLIP, MAP2K1, MAP2K6, PELI2, PELI1, MAP2K4, SKP1, MAP3K7, TRAF6, UBE2N, IL1R2, TNIP2, CUL1, IKBKG, RIPK2, SQSTM1, BTRC, RBX1, NAIP, CARD18, CD40LG, CTSB, HSP90AA1, HSP90B1, PYDC1, SUGT1, TNF, TNFSF11, TNFSF14, TNFSF4, IFNG, IL12A, IL12B, IL33, IRF1, TIRAP, CIITA, NLRP12, NLRP4, NLRP5, NLRP6, NLRP9, NLRX1, BIRC2, BIRC3, CARD6, CCL2, CCL5, CCL7, CFLAR, CXCL1, CXCL2, FADD, IFNB1, IL6, IRF2, MAPK1, MAPK11, MAPK12, MAPK13, MAPK3, MAPK8, MAPK9, NFKB1, NFKBIA, NFKBIB, PEA15, RELA, XIAP, NOD2.
Antiviral responses	ABCC9, ABCE1, ABCF3, ACTA2, ADAR, ADARB1, AGBL4, AGBL5, AIMP1, AP1S1, APOB, APOBEC1, APOBEC3A, APOBEC3B, APOBEC3C, APOBEC3D, APOBEC3F, APOBEC3G, APOBEC3H, ATG7, AZU1, BAD, BANF1, BATF3, BCL2, BCL2L1, BCL2L11, BCL3, BECN1, BNIP3, BNIP3L, BST2, BTBD17, C17orf85, C19orf2, C19orf66, CARD9, CCDC130, CCL11, CCL19, CCL22, CCL4, CCL5, CCL8, CCT5, CD207, CD40, CD86, CD8A, CDK6, CFL1, CHRM2, CHUK, CLU, CRCP, CREBZF, CXADR, CXCL10, CXCL12, CXCL9, CXCR4, CYP1A1, DCLK1, DDIT4, DDX1, DDX21, DDX3X, DDX41, DDX58, DDX60, DEFA1, DEFA1B, DEFA3, DHX36, DHX58, DMBT1, DNAJC3, DUOX2, EEF1G, EIF2AK2, EIF2AK4, ELMOD2, ENO1, EXOSC4, EXOSC5, F2RL1, FADD, FAM111A, FCN3, FGR, FOSL1, FOXP3, GATA3, GBP1, GBP3, GLI2, GPAM, GTF2F1, HBXIP, HERC5, HMGA1, HMGA2, HNRNPUL1, HSPB1, HYAL1, HYAL2, HYAL3, IFI16, IFI44, IFI44L, IFIH1, IFIT1, IFIT1B, IFIT2, IFIT3, IFIT5, IFITM1, IFITM2, IFITM3, IFNA1, IFNA10, IFNA13, IFNA14, IFNA16, IFNA17, IFNA2, IFNA21, IFNA4, IFNA5, IFNA6, IFNA8, IFNAR1, IFNAR2, IFNB1, IFNE, IFNG, IFNGR1, IFNGR2, IFNK, IFNW1, IKBKB, IKBKE, IKBKG, IL10RB, IL12A, IL12B, IL23A, IL28A, IL28B, IL28RA, IL29, IL33, IL6, ILF3, IRAK3, IRF1, IRF3, IRF5, IRF7, IRF9, ISG15, ISG20, ITCH, IVNS1ABP, KCNJ8, LGALS9, LILRB1, LSM14A, LYST, MAPK11, MAPK14, MAVS, MB21D1, MEF2C, MICA, MST1R, MX1, MX2, NLRC5, NLRP3, NPC2, OAS1, OAS2, OAS3, OASL, ODC1, OPRK1, PCBP2, PENK, PIM2, PLSCR1, PMAIP1, PML, POLR3A, POLR3B, POLR3C, POLR3D, POLR3E, POLR3F, POLR3G, POLR3H, POLR3K, PRF1, PRKRA, PSMA2, PSMB9, PTPRC, PYCARD, RELA, RNASEL, RPS15A, RSAD2, SAMHD1, SERINC3, SERINC5, SLFN11, SPACA3, SPON2, SRC, STAT1, STAT2, STMN1, TBK1, TBX21, TICAM1, TLR3, TLR7, TLR8, TMEM173, TNF, TNFSF4, TPT1, TRIM11, TRIM22, TRIM25, TRIM34, TRIM5, TRIM56, TRIM6, UNC13D, UNC93B1, XCL1, XPR1, ZC3H12A, ZC3HAV1, ZNF175.

Supplementary Table S11. All proteins available for PEA measurements used as statistical background for STRING analyses of targeted proteomics data.

UniprotID
P03950, Q9Y5C1, O95445, Q96KN2, P15907, P12830, P00915, P07451, P22748, Q9NQ79, P49747, Q16627, P55774, P13501, P13987, P08709, P03951, P39060, Q9BXJ1, P06681, Q9BXR6, P20023, P01034, P27487, Q12805, P17813, Q9UGM5, Q15485, Q16769, P22749, Q14393, P08581, P0DOY2, P17936, P24592, P11215, P05362, P32942, P16871, Q14767, Q8NHL6, Q8N423, O75023, P05451, P23141, P12318, O75015, P14151, Q9Y5Y7, P42785, P11226, P10721, P15529, Q16853, P01033, Q13361, Q9H1U4, P13591, O00533, P46531, O14786, P59665, P80188, P14543, Q99650, P19021, P55058, P05154, P07359, Q13093, O15031, Q15113, Q12884, Q13332, Q06141, P35542, Q14515, P00441, Q96H15, P24821, P22105, P35443, P05543, P20062, Q03167, Q15582, P07478, P35590, P07911, P19320, Q6EMK4, P04070, Q86SJ2, Q7Z5R6, Q8TD06, P15848, P08237, O43521, Q02742, P21810, Q06520, P11274, Q8N5S9, Q9BQT9, Q9NX58, P04637, Q49AH0, P02462, O43186, P0CG37, Q9UBG0, Q8WYN0, P16562, Q9UK85, P25685, P52564, Q13561, P22681, Q01543, P47929, A4D1B5, Q9NS71, O00451, P01275, P01242, Q9Y662, O60243, O75054, Q9NRM6, Q9UKR0, Q96I82, Q6UXK5, Q8N2G4, Q12912, Q6UB28, Q16653, O94760, O00221, Q969V3, Q92982, O95644, P23515, Q9UBM4, P30041, Q9NZ53, Q10471, Q96SM3, P58294, Q9HCU5, Q7Z5A7, O14904, O14917, Q13576, P57771, Q07960, Q9NZN5, Q6UXD5, Q9C0C4, O96013, Q96LC7, O43699, Q9P0V8, Q9H156, Q9H5Y7, Q86WV1, O14662, O43752, O95988, Q9Y6A5, Q9Y2W6, P09758, O95183, Q92558, Q9UPY6, Q96PQ0, Q13105, Q16698, Q76LX8, P35318, O00253, P35475, Q9BYF1, P22004, P35218, P31997, P07711, Q99895, O94907, P12104, P19883, P27352, P51161, P01241, Q9UK05, P04792, Q9UJM8, P18510, Q9HB29, Q8TAD2, Q8NEV9, Q14213, P24394, Q04760, P78380, P41159, P06858, P31994, P47992, Q9UEW3, Q9UKP3, P16860, Q9Y6K9, Q8IYS5, Q13219, P26022, P09874, P01833, Q99075, Q14005, P51888, Q16651, P02760, P25116, P21980, P12931, Q14242, Q15109, P00797, Q9BQR3, Q13043, Q8IW75, Q9UIB8, Q9NQ25, Q99523, Q9BUD6, P04179, P07204, P40225, P40225, P13726, O14763, Q9Y6Q6, O14836, Q12866, Q96IQ7, Q9BWV1, O00220, O43915, Q15389, Q02763, Q92583, P29965, P07585, O00182, P09601, P39900, P09237, P01127, Q9BQ51, P01730, P49763, Q96D42, P15144, P20160, Q13867, P33151, P15085, P15086, P42574, P07339, Q9UBR2, Q16663, O15467, O00175, Q13740, P36222, Q13231, P02452, Q9NPY3, Q12860, Q9H2A7, P04080, P19957, P54760, P00533, P16422, P16581, P15090, P17931, P56470, P28799, Q99988, Q9HCN6, P08833, P18065, Q16270, P05107, P13598, P14778, P27930, Q96F46, O95998, P01589, P08887, Q9Y624, Q92876, P01130, P36941, Q9NQ76, P08253, P08254, P14780, Q99727, P24158, P05164, P02144, Q9UM47, P10451, Q15166, O75594, P98160, P05121, P16284, P04085, Q8NBP7, P80370, P16109, P35247, Q9HD89, Q99969, Q86VB7, Q96PL1, Q9HCB6, Q01638, P13686, P10646, P00750, P02786, Q07654, Q5T2D2, Q9Y275, P19438, P20333, O14798, Q92956, P25445, P30530, P78324, Q03405, P04275, P16860, Q10588, Q9UKK9, P16112, P05067, Q9BY76, P15289, P50895, P15291, O43505, P08236, P08118, P00918, P23280, Q9UBX1, P11717, Q6YHK3, Q8N6Q3, Q9NNX6, P48960, Q8TCZ2, Q4KMG0, Q6UXG3, O43405, Q5KU26, Q8IWV2, P24387, Q9Y240, Q86T13, Q15828, Q9NZV1, Q6UXH1, P47712, Q02487, Q9UBP4, Q14118, Q07108, Q13822, Q96AP7, Q96RD9, P30043, O95633, P21217, Q11128, P01215, P55808, Q8TDQ0, P04233, Q6UXH9, P55103, P08648, P05556, P78552, O43278, O43291, Q08431, Q16363, Q14696, Q99538, Q6GTX8, P06734, P19256, P14174, O00339, Q99972, Q14112, Q99983, Q9UKJ1, P23284, P30086, Q5VY43, P09619, Q99497, P07237, P48745, P10586, Q9Y6N7, Q14162, Q96QR1, O75326, O43464, P00995, Q9NQ38, O00241, P31948, O95721, P63313, P04066, O14773, Q969Z4, P29350, Q8TEU8, Q9Y279, Q01151, P09038, P42701, P18627, Q9UQV4, O76036, Q13241, P48061, P10747, O15123, P05089, P40933, Q9Y653, P43629, P29474, P21246, Q15116, Q8WXI7, Q5T4W7, O15169, O15444, Q9NRJ3, Q9H5V8, P80162, P28325, Q8NFT8, Q13541, O95750, P12034, P49771, Q13651, Q08334, P29460, Q13261, Q16552, Q9P0M4, Q13478, P14784, Q9NYY1, Q9UHF4, Q8N6P7, Q13007, P15018, P42702, P03956, P09238, P20783, Q99748, P13725, P80511, Q13291, Q8IXJ6, O95630, P50225, P30203, Q969D9, P01374, O14788, Q9GZV9, Q9NSA1, P10147, Q14116, P21583, O00300, P00749, P13500, P00813, Q14790, Q99731, P78556, P55773, P13236, P25942, P02778, O14625, P42830, Q07325, P78423, P01579, P01583, P35225, P60568, O95760, P05112, P13232, P10145, P01137, P09603, P80075, P80098, Q99616, Q9BZW8, Q9NZQ7, P06127, P01732, O43508, P01375, O43557, Q07011, P22301, P05113, P51671, P01138, P39905, P01135, P50591, P05231, P14210, P15692, P09341, Q7Z6M3, P27540, Q13490, P16278, P78410, Q9UHC6, Q15517, P28845, P78310, Q9UMR7, Q8WTT0, Q8WXI8, Q6UXB4, Q6EIG7, Q9BXN2, Q07065, Q13574, O00273, Q9UN19, Q14203, P19474, Q9GZT9, Q04637, P63241, Q96P31, Q6DN72, Q96DB9, P14317, P50135, P52294, Q8N608, O43736, Q9UKX5, P23229, P18564, Q8IU57, Q00978, P51617, Q9NWZ3, Q05084, P08727, Q8NHJ6, O60449, P48740, P35240, P16455, Q96SB3, P34130, Q12968, Q03431, O75475, Q06830, P30044, Q6ZUJ8, Q9HCM2, Q14435, O95786, P58499, O94992, Q04759, O43597, Q9Y2J8, O60880, Q9UQQ2, Q9Y3P8, P78362, P52823, P30048, Q12933, Q92844, O14867, Q9NP99, Q9C035, Q15661, Q9UNE0, Q96PD2, P05412, Q05516, P23526, Q9UHX3, Q8IZP9, P51693, O95841, O43827, P50995, P09525, Q9UBU3, P20711, P40259, P19022, Q9HBB8, Q9H4D0, Q8N1Q1, P21964, P43234, Q9Y5K6, Q6WN34, Q15846, Q76M96, P46109, Q9NY25, Q9H6B4, Q9NR28, P09417, Q9UHL4, P98082, P27695, O75356, Q6UWV6, P12724, Q96LA6, P09467, P22466, P09104, P35754, O75791, P51858, Q01973, Q8WX77, P26010, O43240, Q16773, P46379, Q96JA1, A6NI73, Q86VZ4, Q9NPH0, Q16820, Q641Q3, Q8NI22, O95544, Q92692, Q9NQX5, O95502, Q15155, Q9UKJ0, Q02790, Q9NWQ8, P09668, Q92520, P41236, P25815, Q9BYZ8, Q9BZR6, P00352, P16083, Q8WTU2, Q9BQB4, Q13275, P35237, P50452, Q9Y286, Q04900, Q8WVQ1, Q8NBJ7, O00161, P31431, P29017, P52888, Q8NBS9, P19971, P01222, Q03403, Q9GZM7, Q06418, P40818, P13611, P28907, P30533, Q16620, P12644, Q96GW7, Q2TAL6, P22223, P55285, P48052, P14384, P25774, Q8N126, Q8TD46, Q8TDQ1, Q08708, O94779, Q9P126, Q8IUN9, Q9UBT3, P53634, Q9P0K1, O75077, Q8NBI3, O15197, P52798, Q08345, P15311, Q96LA5, O00214, P56159, O60609, P78333, P09919, P15509, O14793, Q16775, Q01344, P57087, Q16719, Q9BS40, Q6UX15, O43155, Q6ISS4, O43561, Q14108, P21757, Q8NFP4, O15232, P55145, P10636, Q02083, P08473, O95185, P41271, O14594, Q92823, O60462, Q9NR71, Q9HAN9, Q9BZM5, Q16288, P41217, P16234, O43157, Q9ULL4, P15151, Q2VWP7, Q96B86, Q6NW40, Q9HCK4, Q2MKA7, Q6ZMJ2, Q96GP6, Q92765, P37023, Q9Y336, Q9BZZ2, Q9H3U7, P17405, Q92752, Q08629, P04216, Q9H3S3, Q9HAV5, Q96NZ8, P29460, P29459, O95727, P12544, Q9NP84, O75509, Q03393, O60242, Q9BTE6, Q9BYC5, P19801, Q9UJ72, P07306, O15263, Q86Z14, P49789, Q10589, P55291, Q12864, P63098, Q9Y2V2, O94985, P40198, Q16619, Q9Y4X3, Q8IX05, P08962, P41208, Q9Y5P4, P52943, P78560, P32926, P16444, Q9H4A9, Q13444, P51452, Q96EP0, P14625, P42892, Q5JZY3, P23588, P21802, P13284, O76070, P36269, P09211, P09466, O15496, P32456, P30519, P24071, Q6UXK2, Q9UK53, P29218, Q9H0C8, Q8IU54, P26951, P24001, Q96EK5, P43628, Q6UWL6, Q9NS15, P48357, Q9Y6D9, P20138, P41227, O00308, Q969M7, P58417, P07196, P06748, Q13451, Q9Y680, Q8TCT1, Q15126, Q9NRG1, Q9UHV9, P11464, O14944, Q96B36, Q06323, Q96IU4, Q92597, Q9H477, P23443, Q8N474, P37108, Q9H4F8, P13385, Q9BW30, Q99426, Q96RJ3, P18031, Q6UX27, Q16864, Q9UKS7, Q9P0J1, Q9Y478, P30838, O95994, O95831, Q8NDB2, P55957, Q13145, P01258, P27797, O43570, Q9ULX7, P48730, Q9HAW4, Q11201, O00748, Q02246, P06850, Q8NC01, P23582, Q86SJ6, P42658, Q02880, Q9Y5L3, O43854, P98073, Q9UHF1, Q96RT1, P01588, Q0Z7S8, Q12778, Q9NQ88, O60760, Q13308, O14713, O75569, P09960, Q9GZY6, P01229, Q7L5Y9, P40121, Q9Y5V3, P53582, Q03426, Q9Y4K4, Q15797, Q9NXA8, Q9Y5A7, P19878, O60934, P80303, P20472, P49023, P68106, O60240, O15357, Q9NRA1, Q8IUK5, Q86SR1, P35070, Q07954, P25786, Q9BXJ7, Q8N8S7, P53539, P61244, O75688, P50749, P20936, Q12913, O75787, Q9UKL0, P49788, Q7LG56, Q86WD7, Q15165, Q9UNK0, O00186, P19429, P07332, P09769, P07947, Q7L8A9, P42768, O75354, P21589, Q8TE58, P40222, P04083, P16870, P06731, P13688, O60911, O95971, P09326, Q9UBG3, Q9UJ71, P38936, O00548, P78325, Q9NQ30, P29317, Q13158, 6BAA4, Q14512, P15328, P41439, P09958, P35052, P08069, P06756, P18084, P15260, Q9UBX7, Q9UKR3, Q9P0G3, O60259, O95274, Q16674, Q13421, P50579, P21741, Q99717, Q96NY8, P01298, O00592, O00622, P31949, P26447, P07949, P04626, P21860, Q15303, Q9BXY4, O14828, Q9BYH1, P09486, P18827, P56279, P37173, P48307, Q9HBG7, O15455, O75888, Q9NS68, O95407, P00519, P07948, Q14508, P35916, Q6UXB2, P08670, Q9Y5W5, O95388, O43895, P15514, Q14956, Q16790, P26842, P32970, O43927, P48023, P09382, P10144, P20718, O75144, Q29983, Q29980, P01133, P43489, P35968, O00233, Q9UJY5, P15121, P05187, P55008, O43707, P02771, Q12904, P20273, Q9Y644, P06865, Q9BYE9, Q9P1Z2, Q9UDT6, P42575, P30260, Q99795, Q9NTU7, P0DN86, Q496F6, P20849, P02745, O95715, P28838, Q9H0P0, Q9H773, P55039, Q14241, Q9BS26, Q53H82, P55789, O60907, O43524, O60763, Q9HD26, Q14353, O14558, P09105, P13747, P01591, P49441, Q14773, Q9UMF0, P38484, P01584, Q96PD4, Q9Y5K2, P33241, Q9H8J5, Q86SF2, P32004, P62166, P43490, P09110, O60542, P08397, Q9H3G5, P12872, P01303, Q8WUW1, Q9Y2B0, Q92832, Q96FQ6, Q93096, O75695, Q08174, Q8IWL2, P20340, P36888, P28827, P42331, P35637, O76038, P13521, Q96I15, Q9UHD8, O60575, Q99536, P48643, P51580, Q96J42, P13693, O95379, Q9BSL1, Q13459, Q8NEZ2, Q5VIR6, P17948, Q7Z5L0, Q6PCB0, Q9Y5K8, Q7Z739.